UNIVERSITY OF LIVERPOOL

Development and biological assessment of prednisolone solid drug nanoparticles

Thesis submitted in accordance with requirements of the University of Liverpool for the degree of Doctor of Philosophy

Louise R. I. L. Tidbury

January 2018

DECLARATION

This thesis is the result of my own work. The material contained within the thesis has not been presented, either wholly or in part, for any other degree or qualification.

Louise R. I. L. Tidbury

This research was carried out in:

Department of Molecular and Clinical Pharmacology, University of Liverpool

Department of Chemistry, University of Liverpool

Department of Women's and Children's Health, University of Liverpool

CONTENTS

ACKNOWLEDGEMENTS

Thank you to my supervisors Brian Flanagan, Andrew Owen, Steve Rannard and Paul McNamara for giving me the opportunity to carry out this PhD project and for all your expert guidance along the way. Particular thanks to my primary supervisor Brian for keeping us all in line and for your constant encouragement throughout lab work and writing up. Thank you to the Alder Hey Children's Charity and the Institute of Translational Medicine for funding this project.

Thanks to all the other staff and students who have trained and advised me over the years. Special thanks to Lee Tatham for kindly and patiently teaching me all the pharmacology techniques and statistical methods since I was an undergraduate student, right through my MRes and this PhD - I really appreciate all the help and time you have given me. Big thanks also to Marco Giardiello for teaching me everything on the formulation and characterisation side, especially for your help with the XRD and SEM. Thank you so much to Rachel Corkhill for making me feel at home in the Alder Hey labs, looking after my cells and helping me set up experiments. Thanks also to: Jo Sharp and Ana Jimenez-Valverde for their invaluable help with *in vivo* work; Marco Siccardi for help with HPLC; Paul Curley for help with radiation and advice on in vivo work; Helen Cauldbeck and Mark Long for help with radiation in Chemistry, Andy Dwyer for help with NMR spectra; and Christina Chan for sharing the journey with me since undergrad.

I'm immensely grateful to my family, especially my parents for their support, encouragement and advice during the PhD and always. Thank you Mum, Dad, Poh Poh and Grandad for teaching me to study hard and do my best. Thanks to Laurence and Niki for setting a good example as Dr Tidburys. Huge thanks to Jay who has tirelessly provided all kinds of encouragement, advice, assistance, cheering up, expertly cooked dinners and everything I needed to survive this PhD, and of course all your help in the lab over the years.

COMMUNICATIONS

Production, Characterisation and In Vitro Assessment of Steroid Nanoparticles.

L. Tidbury, P. McNamara, B. Flanagan, A. Owen and S. Rannard.

1. Institute of Translational Medicine Research Day, University of Liverpool, July 2015

2. British Society for Nanomedicine Early Career Researchers Meeting, University of Liverpool, August 2015

ABBREVIATIONS

11β-HSD	11β-hydroxysteroid dehydrogenase
^{14}C	carbon-14 radioactive isotope
^{1}H-NMR	proton nuclear magnetic resonance
^{3}H-PRD	tritiated prednisolone
A → B	apical to basolateral
ACN	acetonitrile
ACTH	adrenocorticotrophic hormone
AOT	dioctyl sulphosuccinate sodium salt
AP-1	activator protein-1
ATP	adenosine triphosphate
AUC	area under curve
B → A	basolateral to apical
BSA	bovine serum albumin
BW	beeswax
CC_{50}	cytotoxic concentration causing 50% cell death
C_{max}	maximum concentration
CNS	central nervous system
CO_2	carbon dioxide
CremEL	cremopor EL
CRF	corticotrophin releasing factor
CTAB	cetyl trimethylammonium bromide
CYP3A4	cytochrome P450 3A4
DCM	dichloromethane
DEX	dexamethasone
dH_2O	de-ionised water

DLS	dynamic light scattering
DMARD	disease modifying anti-rheumatic drug
DMEM	Dulbecco's Modified Eagles Media
DMF	dimethylformamide
DMSO	dimethyl sulfoxide
DNP	2,4-dinitrophenol
DUSP-1	dual specificity phosphate-1
D_z	hydrodynamic diameter
EDTA	ethylenediaminetetraacetic acid
ELISA	enzyme-linked immunosorbent assay
EPR	enhanced permeability and retention
ES-MS	electrospray mass spectrometry
ETFD	emulsion-templated freeze-drying
F127	Pluronic F-127
F68	Pluronic F-68
FaSSGF	fasted-state simulated gastric fluid
FaSSIF	fasted-state simulated intestinal fluid
FBS	fetal bovine serum
FDA	US Food and Drug Administration
FeSSGF	fed-state simulated gastric fluid
FeSSIF	fed-state simulated intestinal fluid
FRET	fluorescence (Förster) resonance energy transfer
G6Pase	glucose-6-phosphatase
GC	glucocorticoid
GI	gastrointestinal
GILZ	glucocorticoid inducible leucine zipper
GMP	good manufacturing practice

GR	glucocorticoid receptor
GRE	glucocorticoid response elements
H_2O_2	hydrogen peroxide
H_2SO_4	sulphuric acid
HBSS	Hanks buffered saline solution
HEPES	4-(2-Hydroxyethyl)piperazine-1-ethanesulphonic acid
HGel	hydrolysed gelatin
HIV	human immunodeficiency virus
HPA	hypothalamic-pituitary-adrenal
HPC	hydroxypropyl cellulose
HPLC	high-performance liquid chromatography
HPMC	(hydroxypropyl)methyl cellulose
HRP	horseradish peroxidase
ICH	International Conference for Harmonisation
IgE	immunoglobulin E
IID	Inactive Ingredient Database
IL	interleukin
IRS-1	insulin receptor substrate-1
IV	intravenous
LDH	lactase dehydrogenase
LPS	lipopolysaccharide
MAPK	mitogen-activated protein kinase
MC	mineralocorticoid
MR	mineralocorticoid receptor
MRI	magnetic resonance imaging
MS	mass spectrometry
MSNP	mesoporous silica nanoparticle

MTT	3-(4, 5-Dimethylthiazol-2-yl)-2, 5-diphenyltetrazolium bromide
Na^+	sodium
NaA	sodium alginate
NaC	sodium caprylate
NAD(P)H	reduced nicotinamide adenine dinucleotide (phosphate)
NaM	sodium myristate
NDC	sodium deoxycholate
NF-κB	nuclear factor- κB
NLC	nanostructured lipid nanocarrier
O/W	oil/water
P	polymer
P_{app}	apparent permeability
PBMC	peripheral blood mononuclear cell
PBS	phosphate buffered saline
PdI	polydispersity index
PEG 1K	polyethylene glycol 1000
PEG 600	polyethylene glycol 600
PEPCK	phosphoenolpyruvate carboxykinase
P-gp	P-glyoprotein
PI3-K	phosphatidylinositol 3-kinase
PK	pharmacokinetics
PKB	protein kinase B
PMA	phorbol 12-myristate 13-acetate
PRD	prednisolone
PVA	polyvinyl alcohol 80% hydrolysed
PVP	polyvinylpyrrolidone K 30
pXRD	powder X-ray diffraction

RBL	rat basophilic leukemia
ROS	reactive oxygen species
RPMI	Roswell Park Memorial Institute cell culture medium
S	surfactant
SD	standard deviation
SDN	solid drug nanoparticle
SDS	sodium dodecyl sulphate
SEM	scanning electron microscopy
SLN	solid lipid nanoparticle
$t_{1/2}$	half life
T20	Tween 20
T80	Tween 80
TEER	trans-epithelial electrical resistance
Th2	T helper cell type 2
T_{max}	time to maximum concentration
TMB	3,3',5,5'-Tetramethylbenzidine
TNF-α	tumour necrosis factor-α
TPGS	D-α-Tocopherol polyethylene glycol 1000 succinate
wt%	weight percentage
ζ	zeta potential

ABSTRACT

Prednisolone (PRD) is a highly useful and effective glucocorticoid drug used to treat many inflammatory conditions such as asthma, nephrotic syndrome, rheumatoid arthritis and systemic lupus erythematosus. Unfortunately, the benefits of prednisolone and other glucocorticoid drugs are limited by many, often serious, adverse effects including osteoporosis, diabetes, skin and muscle atrophy and behavioural and mood impairment that present particular risk during prolonged, high dose or paediatric use. To overcome these negative effects, the reformulation of existing glucocorticoids could improve their physicochemical properties. Nanoformulations in particular offer the potential to improve drug delivery through several mechanisms including targeting of specific cells or local conditions, increased absorption and bioavailability, prolonged duration of action and reduced inactivation by metabolism.

Emulsion-templated freeze-drying offers a method of producing solid drug nanoparticles (SDNs) well suited to high-throughput screening and the production of a large library of candidates. PRD was screened with a range of polymer and surfactant excipients and two lead candidates were chosen based on size and reproducibility. Drug stability was confirmed by mass spectrometry and nuclear magnetic resonance spectroscopy. SDNs were characterised by powder X-ray diffraction and electron microscopy. Short term stability of dispersed SDNs was confirmed in several bio-relevant fluids over six hours, including simulated gastro-intestinal fluids.

The two lead SDNs were assessed *in vitro* to determine cytotoxicity in Caco-2 and A549 cell lines. A decrease in cell viability was observed in Caco-2 cells treated with SDNs 1 and 2 when assessed by MTT assay, but not when assessed with CellTiter-Glo assay. The inverse was found in A549 cells treated with SDNs 1 and 2. SDN permeation of a Caco-2 cell monolayer was determined as a model of intestinal absorption. Compromised monolayers as demonstrated by mannitol permeation indicated that SDN apparent permeability data were unreliable. Efficacy of SDN inhibition of cytokine production was assessed in A549 cells and primary human lymphocytes and found to be equivalent to inhibition by aqueous PRD.

SDN pharmacokinetics and biodistribution were assessed *in vivo* in CD-1 mice. When administered orally, SDNs 1 and 2 demonstrated a longer half-life and higher exposure (area under curve) compared to aqueous PRD. Also following oral administration, SDNs 1 and 2 demonstrated longer half-life and higher exposure (area under curve) in the kidneys compared to aqueous PRD. Accumulation in all other tissues was comparable for SDNs and aqueous PRD. This selective accumulation of PRD SDNs in kidneys could serve as a targeting mechanism for treatment of inflammatory kidney disorders. Overall, the data reported here supports the potential use of PRD SDNs as a safe, efficacious oral formulation as an alternative to conventional unformulated PRD.

CHAPTER 1

GENERAL INTRODUCTION

CONTENTS

1.1 Glucocorticoids

1.1.1 Class of drugs

Corticosteroids are a class of steroid, which in humans are endogenous hormones synthesised in the adrenal glands but can also refer to synthetic analogues of these. The class is further divided into glucocorticoids, which are secreted by the zona fasciculata cells situated in the adrenal cortex, and mineralocorticoids, secreted by the zona glomerulosa of the adrenal cortex [1]. Glucocorticoids (GCs) have roles in metabolic and immune functions whereas mineralocorticoids (MCs) primarily regulate water and electrolyte balance [2, 3]. The main endogenous GC in humans is hydrocortisone (also called cortisol), which is synthesised from its precursor cholesterol in a multi-step pathway (Fig. 1.1). This synthesis is regulated by the HPA (hypothalamic-pituitary-adrenal) axis, the interaction between hormones released from the hypothalamus, anterior pituitary gland and adrenal cortex. CRF (corticotrophin releasing factor) released from the hypothalamus regulates release of ACTH (adrenocorticotrophic hormone) from the anterior pituitary [4]. In turn, ACTH regulates GC synthesis and release from the adrenal cortex by inducing the conversion of cholesterol to pregnenolone, the rate limiting step in GC synthesis. Negative feedback through glucocorticoids in the blood inhibits CRF and ACTH release [5].

GCs and MCs can have overlapping activity due to the similarity in their steroidal structures, but synthetic GCs have been developed by modifying the structures to tailor their uses more specifically [6]. The most commonly used of these are prednisolone (and its derivatives prednisone, methyl prednisolone and prednisolone phosphate), dexamethasone and betamethasone, as well as

budesonide and fluticasone propionate which are administered by inhalation [7-9].

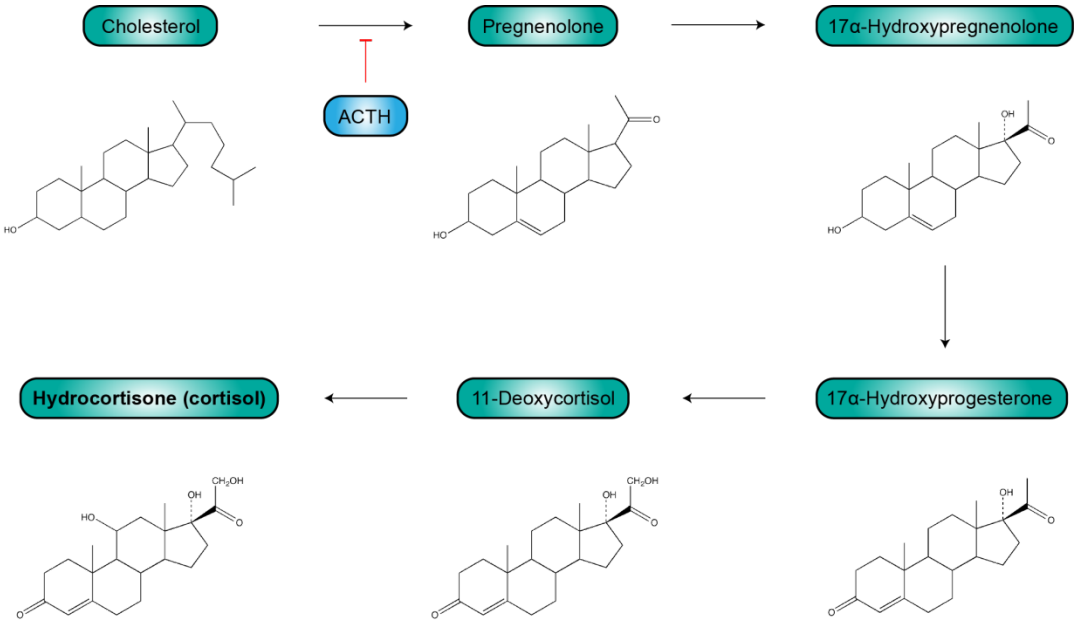

Figure 1.1 Synthesis of endogenous glucocorticoids from cholesterol. Adrenocorticotrophic hormone (ACTH) inhibits the conversion of cholesterol to pregnenolone, the rate limiting step in glucocorticoid synthesis. Adapted from [10].

1.1.2 Prednisolone

Prednisolone (PRD) is one of the most commonly used synthetic GCs, with many indications including asthma, rheumatoid arthritis, organ transplantation, systemic lupus erythematosus, nephrotic syndrome and multiple sclerosis. It is interconvertible with inactive prednisone through the action of the endogenous enzymes 11β-hydroxysteroid dehydrogenase (11β-HSD) type 1 and 2 (Fig. 1.2) which have a physiological role in the conversion between endogenous hydrocortisone and inactive cortisone, particularly important in mineralocorticoid-sensitive tissues (see section 1.1.4)[11].

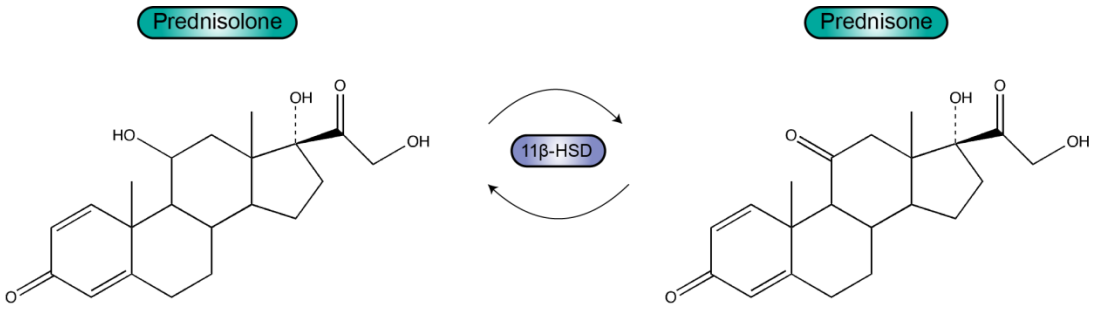

Figure 1.2 The interconversion of prednisolone and prednisone, catalysed by endogenous enzyme 11β-hydroxysteroid dehydrogenase (11β-HSD).

Following oral administration, PRD is extensively absorbed from the gastrointestinal (GI) tract and reaches peak plasma concentrations within 1-3 hours [12]. Plasma albumin has a high capacity and low affinity for PRD; inversely, transcortin (human corticosteroid binding protein) has a low capacity and high affinity for prednisolone [13]. The fraction of protein bound prednisolone decreases with increased concentrations non-linearly as a result of saturable transcortin binding and competition for binding with endogenous cortisol [14]. PRD is cleared by hepatic metabolism involving phase I hydroxylation and reduction followed by phase II conjugation to glucuronide or sulphate [13]. The kidney excretes the conjugated or unconjugated metabolites as well as up to 20% unchanged PRD and around 5% prednisone [15].

1.1.3 Uses in disease treatment

Both synthetic and naturally occurring GCs are used as therapeutic drugs mostly for their anti-inflammatory and immunosuppressive properties, with the exception of replacement therapy. Replacement therapy is necessary in cases where the adrenal glands do not produce enough endogenous steroid hormones (i.e. Addison's disease) and is treated with several daily doses of hydrocortisone

[16]. GCs are one of the most widely used and effective classes of drug employed for the treatment of a wide range of chronic and acute inflammatory disorders as well as immunosuppression following transplantation.

PRD is the standard oral GC used for the treatment of acute and severe asthma. The British Thoracic Society's British Guidelines on the Management of Asthma recommends giving PRD as soon as possible following the onset of an acute exacerbation, with daily doses of 40-50 mg for adults continued for five days or until recovery, or lower doses of 10-40 mg in children depending on age for three days or until recovery [17]. Oral PRD is also used to treat adults and children with severe asthma that cannot be controlled with inhaled steroids and/or long-acting β-agonists, and it is these cases where the necessity of long term oral GC therapy leads to occurrence of adverse effects (discussed in section 1.1.5) [18].

GCs are important components of treatment of early rheumatoid arthritis, where they are used alongside disease modifying anti-rheumatic drugs (DMARDs) such as methotrexate to achieve rapid relief of symptoms and reduced progression of joint damage. It is recommended that the initial treatment for rheumatoid arthritis should consist of a low dose of a GC such as PRD alongside the DMARD methotrexate, to be tapered off by 6 months but may be reinstated thereafter as a short course to treat disease flares as required [19].

Some conditions, such as nephrotic syndrome, rely primarily on GCs for treatment. Clinical features of nephrotic syndrome include oedema, abdominal pain, proteinuria and hypoproteinemia [20]. The condition may be idiopathic, as in the case of minimal change disease, or caused by kidney injury as a result of a systemic disease such as diabetes. The pathogenesis of nephrotic syndrome,

although not fully understood, is thought to originate from abnormalitites of podocytes – foot-like kidney epithelial cells which form part of the glomerular filtration barrier [21]. Evidence suggests the involvement of immune cell cytokine production in altering normal glomerular filtration, and this correlates with the high response rate of most patients to the immunosuppressive action of GCs [22]. Although most cases of nephrotic syndrome are responsive to steroid therapy, around 90% of these will have one or more relapse [21]. Those with frequent relapses are at risk of adverse effects from prolonged GC use, but alternate-day dosing and corticosteroid-sparing agents such as cyclophosphamide may help to minimise this [23].

1.1.4 Mechanisms of action

The effects of GCs are primarily mediated by interaction with the glucocorticoid receptor (GR), an intracellular nuclear receptor located in the cytoplasm of most cell types. Cortisol also has high affinity for mineralocorticoid receptors (MR) but is prevented from binding in mineralocorticoid-sensitive tissues, such as the kidney, by the enzyme 11β-HSD which converts it to inactive cortisone [24]. In its unliganded state, the GR exists as a complex with several heat-shock proteins and co-chaperones [25]. GCs enter the cell, probably by passive diffusion through the plasma membrane due to their lipophilicity, and bind with high affinity to the GR [2]. The receptor dissociates from chaperone proteins and undergoes a conformational change to reveal the DNA-binding domain. The resulting GC/GR complex forms homodimers and translocates to the nucleus where they bind to glucocorticoid response elements (GREs) in the promoter region of target genes [26]. This initiates regulation of gene transcription by

several mechanisms (Figure 1.3). Transactivation occurs when binding of the receptor complex to positive GREs induces gene transcription (Figure 1.3, A). Transrepression occurs when the GC/GR complex down-regulates transcription of pro-inflammatory genes. The GC/GR complex may bind directly to negative GREs, blocking the binding of essential transcription factors (Figure 1.3, B) [27]. Additionally, the GC/GR complex may inhibit expression of inflammatory genes regulated by transcription factors such as activator protein-1 (AP-1) and nuclear factor-κB (NF-κB), by direct interaction with the transcription factor to prevent response element binding or through competition for co-activators (Figure 1.3, C) [8].

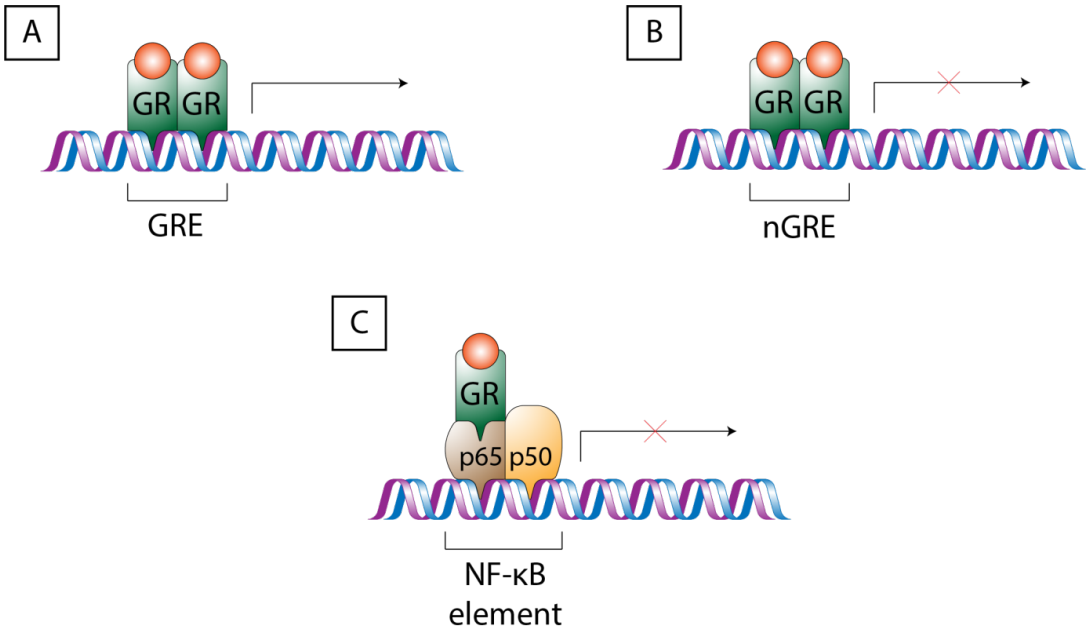

Figure 1.3 Transcriptional mechanisms of glucocorticoids. A: Direct binding of glucocorticoid (red) on glucocorticoid receptor (green) complex homodimer to positive glucocorticoid response element (GRE) induces gene expression. B: Direct binding of glucocorticoid receptor complex to negative GRE inhibits gene expression. C: Indirect inhibition of gene transcription: interaction of glucocorticoid receptor complex with transcription factors inhibits their activity. Adapted from [8].

The therapeutic effects of GCs are mediated by transactivation or transrepression. Transcription of genes that encode anti-inflammatory proteins is induced, leading to increased expression of factors such as interleukin (IL)-10 and annexin-1. IL-10 targets macrophages and dendritic cells where binding to the IL-10 receptor activates the JAK1-STAT3 signalling pathway, resulting in inhibition of pro-inflammatory cytokine production [28, 29]. Annexin-1 inhibits cytosolic phospholipase $A_2\alpha$, an enzyme which hydrolyses phospholipids to arachidonic acid, consequently preventing the conversion of arachidonic acid into prostaglandins and leukotrienes [30]. On the other hand, transrepression of genes by GCs decreases expression of pro-inflammatory proteins. AP-1 and NF-κB regulate genes for many cytokines (e.g. IL-1, 2, 3, 4, 5, 6, 9, 11, 12, 13, 16, 17 and 18 and TNF-α) chemokines (e.g. IL-8) and cell adhesion molecules involved in inflammation [31], and inhibition of AP-1 and NF-κB by the GR complex is a major mechanism by which GCs exert their anti-inflammatory effects [32].

GCs also play a role in pro-inflammatory responses to danger and stress signals involved in innate immunity. It has been demonstrated that GCs enhance the expression of NLRP3, a component of the inflammasome, in macrophages resulting in enhanced secretion of pro-inflammatory molecules including IL-1*β,* TNF- α and IL-6 [33].

1.1.5 Adverse effects

Although GCs are highly effective and useful in treating a wide variety of diseases, their use is limited by adverse effects associated with large doses, prolonged use or systemic administration. The metabolic effects of GCs are

considered to be unwanted side effects when used as anti-inflammatory or immunosuppressive therapeutic agents. These side effects range in severity up to serious and life threatening and therefore the risk-benefit ratio of using GCs must be considered.

Adrenal insufficiency is one of the most common adverse effects associated with long-term GC use and becomes apparent following cessation of GC treatment. This occurs as a result of GC negative feedback on the HPA axis which suppresses CRF and ACTH release, and therefore decreased production of endogenous steroid hormones [34]. Gradual recovery of the HPA axis can be achieved by phased withdrawal of GC.

The role of endogenous GCs in bone development and structure involves regulation of osteoblast maturation during bone growth [35]. However, a common side effect of prolonged GC therapy is osteoporosis and increased risk of fractures as a consequence [36]. The mechanisms leading to this include reduced calcium absorption from the gut and increased renal calcium excretion, and direct action on bone cells. In osteoblasts, the cell responsible for producing the bone matrix, GCs enhance expression of dickkopf-1, an antagonist of the Wnt signalling pathway which promotes osteoblastogenesis [37]. GCs also act on mature osteoblasts by inhibiting the synthesis of collagen and enhancing apoptosis by activation of caspase 3 [38]. Conversely, osteoclasts resorb mineralised bone matrix and their activity is increased by GCs. By enhancing IL-6 expression, which mediates osteoclastogenesis, and inhibiting expression of interferon-β, which inhibits osteoclastogenesis, GCs upregulate formation of osteoclasts and therefore increased bone resorption [39]. Loss of bone density

caused by GCs can be reversed or prevented by co-administering bisphosphonates and vitamin D [40].

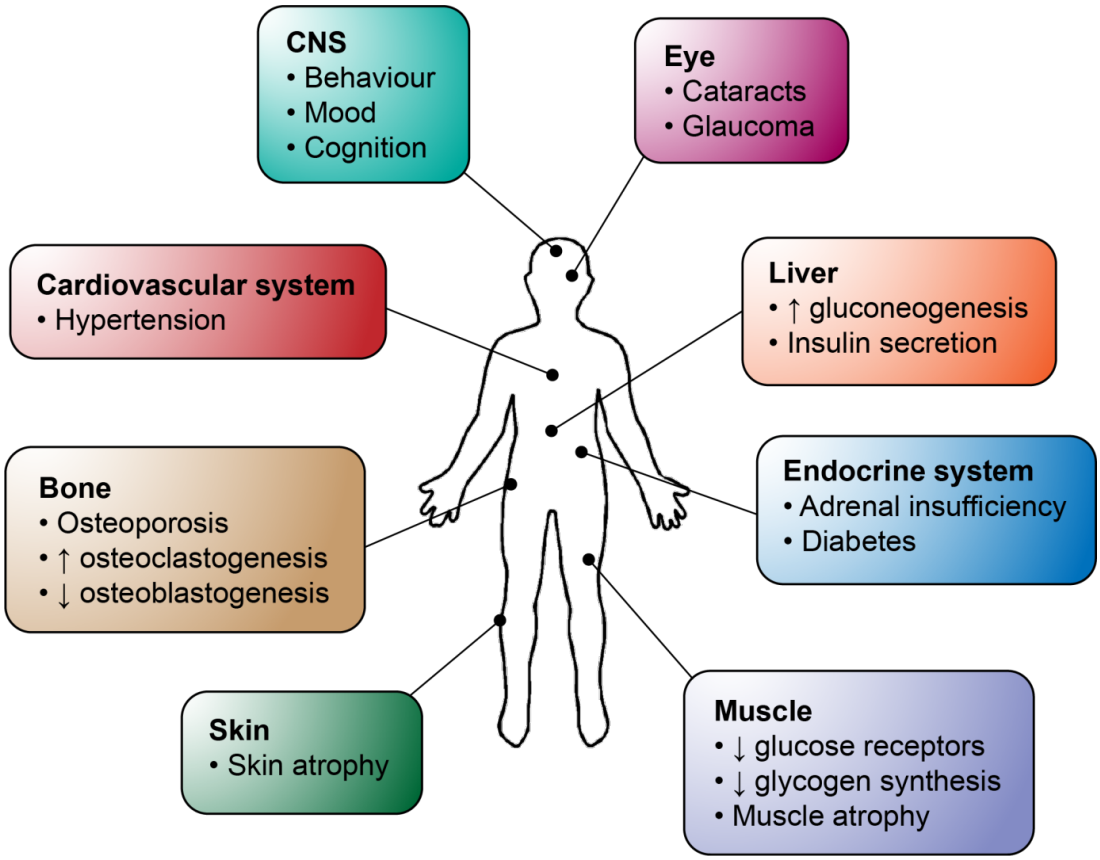

Figure 1.4 Overview of main adverse effects of glucocorticoids

Hyperglycaemia is a major side effect associated with high dose or chronic GC therapy. It can lead to steroid-induced diabetes, or in patients with pre-existing diabetes can worsen glycaemic control [41]. GCs at supra-physiological concentrations (i.e. above endogenous GC concentrations as with therapeutic GC use) interfere with normal glucose metabolism through mechanisms in several tissues. Skeletal muscle is particularly important for glucose metabolism as it accounts for around 80% of glucose uptake and storage as glycogen. This uptake is dependent on insulin, therefore any interference in insulin signalling will have a negative effect on glucose metabolism. GCs have been shown to reduce

expression of the insulin signalling molecules insulin receptor substrate (IRS)-1, phosphatidylinositol 3-kinase (PI3-K) and protein kinase B (PKB)/Akt, resulting in reduced cell surface expression of the glucose receptor as well as reduced glycogen synthesis [42]. Another adverse effect of GCs on skeletal muscle is muscle atrophy as a result of protein degradation. GCs upregulate expression of atrogin-1 and MuRF-1, proteins involved in the ubiquitin-proteasome system, leading to increased muscle proteolysis [43]. Altered insulin signalling also contributes to muscle atrophy through GC inhibition of insulin and insulin-like growth factor 1 which are required for protein synthesis [44].

GCs also exert negative effects on glucose metabolism through mechanisms in the liver. As a consequence of skeletal muscle proteolysis described above, the liver is supplied with an increased supply of substrates for gluconeogenesis. GCs also directly affect hepatic glucose production by inducing expression of phosphoenolpyruvate carboxykinase (PEPCK) and glucose-6-phosphatase (G6Pase), enzymes involved in gluconeogenesis [45].

GC effects on insulin secretion by pancreatic β-cells is an important component in GC-induced diabetes but the mechanisms are not well established. Effects observed in various *in vitro* and *in vivo* studies in rodent cells, healthy rodents, rodent models of obesity or insulin resistance, healthy human subjects or GC-treated patients can appear contradictory. The effects observed vary depending on duration of exposure and susceptibility of the patient, for example those with existing insulin sensitivity or with close relatives with type 2 diabetes [44]. With single dose GC treatment β-cell insulin secretion is inhibited [46], but in longer term treatment of several days, hyperinsulinaemia develops from enhanced β-cell

function as a compensatory response to GC-induced insulin resistance [47]. However, chronic treatment with GCs over months or years is associated with the development of diabetes so it is likely that this β-cell compensation eventually fails or an inhibitory mechanism develops with prolonged exposure [41].

GC receptors are densely expressed in areas of the brain related to behaviour, memory and mood. As such, the central nervous system (CNS) is another important physiological system where GCs exert adverse effects. Psychiatric symptoms are frequently associated with GC treatment and can be grouped into behavioural, mood and cognitive effects. Behavioural effects include increased appetite, insomnia, irritability and aggression, factors which can be particularly problematic in children receiving long term GC treatment as disruptions in behaviour are likely to impact negatively on parental care and schooling [48]. Changes in mood appear to be related to length of treatment, with elevated mood and mania common in acute therapy and depression becoming more prevalent with prolonged treatment [49]. Frequent cognitive effects exhibited include deficits of memory, concentration and attention. In adults, these effects are mostly reversible following discontinuation of GCs but children may not recover as fully [50]. This could be a result of dysfunction of the hippocampus, an area of the brain important in declarative memory. Prolonged exposure to glucocorticoids has been associated with smaller hippocampal volume [51].

Cutaneous effects can occur with topical and systemic administration of GCs, a principal example of which is skin atrophy. Skin atrophy is characterised by thinning of the skin layers and increased fragility and susceptibility to physical

damage. GCs affect both the epidermal and dermal layers of the skin by suppressing proliferation of keratinocytes and fibroblasts, resulting in thinning of these layers, reduced strength and elasticity and increased trans-epidermal water loss. The molecular mechanisms involved in these effects include dysregulation of proteins (collagen, elastin) and lipids (ceramide, cholesterol) critical for skin function [52].

GC therapy can be associated with adverse effects of the eyes, following both topical and systemic application. High dose, chronic GC treatment is a risk factor for developing steroid-induced cataracts [53]. GCs mediate the development of cataracts possibly by altering the levels of growth factor in the aqueous humour, which prevents the differentiation of lens epithelial cells, leading to their migration and accumulation into light-scattering clumps [54]. Increased incidence of glaucoma is also associated with GC treatment. GCs may reduce drainage through the trabecular meshwork of the eye, leading to increased ocular pressure which, if unresolved, can lead to damage of the optic nerve [55].

Hypertension is one of the main adverse effects of GCs on the cardiovascular system, and is itself a risk factor for atherosclerosis and coronary artery disease. GCs contribute to hypertension by interfering with sodium (Na^+) regulation, possibly by activating MRs in the distal convoluted tubules of the kidney resulting in enhanced Na^+ reabsorption [24].

1.1.6 Limitations of glucocorticoid therapy

The extensive side effects of GCs in many cases limit the use of these otherwise comprehensively useful and potent drugs. The development of a novel drug

which could selectively mediate the powerful therapeutic effect of GCs but not the adverse effects would be invaluable, particularly for patients who require chronic anti-inflammatory treatment. The hypothesis that the effects of GCs can be separated according to their mode of action, such that therapeutic effects are brought about through transrepression of target genes and adverse effects are a result of transactivation of genes, emerged in the late 1990s in response to experiments performed by Heck, Reichardt and other groups. They found that mutations in the D-loop of the GR resulted in impaired gene activation but did not inhibit AP-1 or NFκB mediated anti-inflammatory effects, and in a mouse model with mutated GR dexamethasone (DEX) retained its anti-inflammatory effects but did not activate several genes involved in gluconeogenesis [56]. From this work, the notion that GC effects could be uncoupled according to transactivation or transrepression led researchers to pursue the possibility of discovering a novel GC ligand with mainly transrepression mediated mechanisms and greatly reduced transactivational activity.

More recent evidence implies that this is an overly simplistic and idealistic hypothesis on which to pin hopes of improved GC therapy, and both therapeutic and adverse effects are likely to be the result of both activation and inhibition of a large number of genes [57]. Rather than only having adverse effects, GC transactivation results in transcription of genes that are beneficial to inhibition of inflammation, including IL-10, annexin-1 (described in 1.1.3), dual specificity phosphate-1 (DUSP-1) and GC inducible leucine zipper (GILZ). DEX activates expression of DUSP-1 in a variety of cell types including mast cells, macrophages and lymphocytes where it inhibits mitogen-activated protein kinase (MAPK) activation of transcription, stabilisation and translation of inflammatory

gene mRNA such as that of IL-8 [58]. GILZ is another GC-inducible gene which mediates anti-inflammatory effects. GILZ can bind to transcription factors such as NF-κB, c-Jun and c-Fos, inhibiting their transactivational activity on pro-inflammatory genes [59].

An alternative approach to improved therapeutic index of GCs would be to alter them in such a way that would allow selective targeting of inflamed tissues, therefore enhancing the ratio of therapeutic effect to adverse outcomes. Potential methods of altering the biodistribution of GCs include conjugation to other molecules [60], encapsulation in liposomal drug delivery vehicles [61] or formulation as nanoparticles [62]. Nanoformulation of GCs is the key concept of this thesis and is discussed further in the following sections.

1.2 Nanomedicine

Nanomedicine is a generalised term used to describe the broad and diverse field of research that has emerged through a convergence of scientific disciplines focused on the application of nanoscale materials to improved health care. The definition of nanomaterials varies between sources and there is no single global definition. In the US, the National Nanotechnology Institute defines nanotechnology as the study of materials between 1 and 100 nm [63], whereas the European Technology Platform on Nanomedicine more broadly defines materials at the nanometric scale [64] and the European Medicines Agency includes materials with at least one component of nano-scale size [65]. In reality, the entire nanometric range of 1 – 1000 nm is typically considered relevant to materials for nanomedicine, as demonstrated by a number of licensed nanomedicines across this range [66]. The umbrella of nanomedicine covers three separate areas: diagnostics (including theranostic and imaging purposes), regenerative medicine and therapeutics. This thesis will focus on therapeutic applications of nanomedicine, under the definition of submicron materials used for pharmacologic effect.

1.2.1 Drug delivery systems

Exploiting the properties of nanoscale materials offers an approach to enhancing several aspects of pharmaceutical use. Issues associated with pharmaceuticals are often a result of inappropriate distribution or poor absorption, such as low bioavailability of poorly soluble drug, toxicity associated with chronic or high doses and penetration into non-target tissues, and limited circulatory time due to rapid metabolism and elimination. These shortcomings in drug therapy are

particularly detrimental to the quality of life of patients with chronic diseases where frequency of administration and occurrence of adverse effects inevitably reduce adherence to dosing regimens, ultimately resulting in worsening of disease state or development of drug resistance. Nanoformulation can modify the physicochemical properties of drugs and consequently how they are perceived by and interact with the GI, circulatory and immune systems as well as the target tissue.

As such, nanomedicine offers the potential to improve drug delivery through several mechanisms including targeting of specific cells or local conditions, increased absorption and bioavailability, prolonged circulation time and reduced inactivation by metabolism.

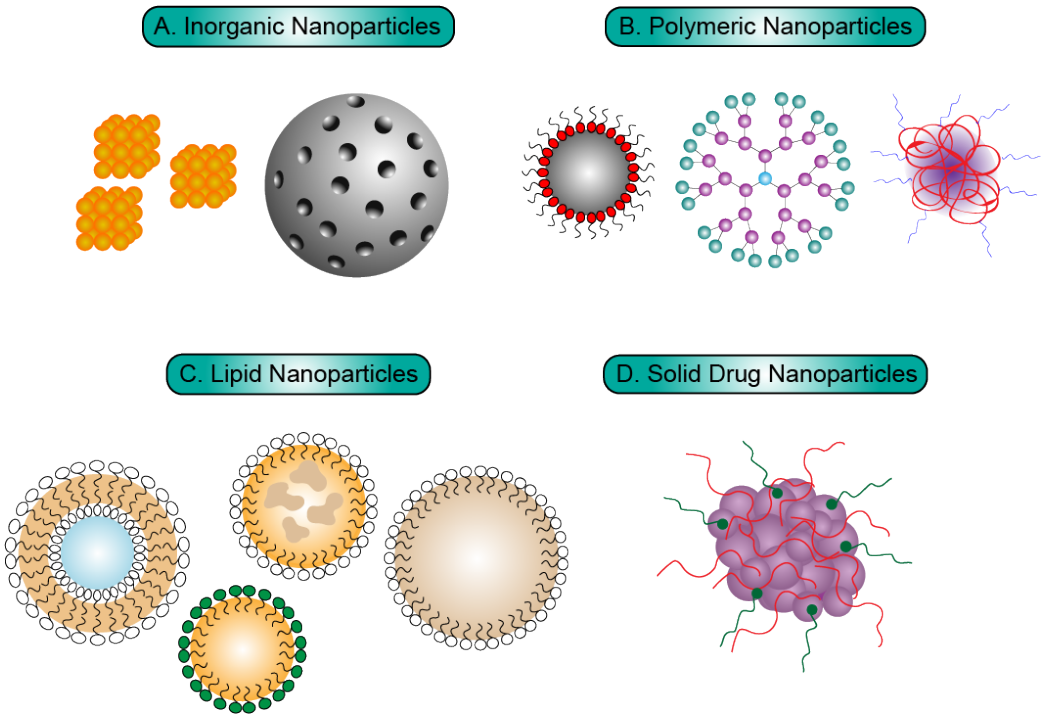

Figure 1.5 The main classes of nanoparticles applicable to drug delivery. A: inorganic nanoparticles (gold nanoparticles, silica nanoparticles), B: polymeric nanoparticles (polymeric micelles, dendrimers, PEGylated polymeric nanoparticles), C: lipid

nanoparticles (liposomes, nanoemulsions, nanostructured lipid carriers, solid lipid nanoparticles) and D: solid drug nanoparticles.

1.2.1.1 Inorganic Nanoparticles

Materials classed as inorganic nanoparticles include carbon structures such as nanotubes and fullerenes, silica nanoparticles and metal nanoparticles such as iron oxide and gold (Fig. 1.5, A). Metal nanoparticles in particular have a large range of potential applications, from the use of the optical and thermal properties of gold nanoparticles for imaging and targeted hyperthermic tumour treatment, to the addition of antimicrobial silver nanoparticles to products such as wound dressings [67, 68].

Mesoporous silica nanoparticles (MSNPs) are an interesting platform for drug delivery. Referred to as insulator nanoparticles, silica nanoparticles are chemically and thermally stable, and their inert surfaces may be functionalised to target specific cell environments [69]. Mesoporous refers to a material with pore sizes of 2-50 nm, and it is this property which lends itself well to drug loading within the pores. MSNPs can be engineered to be stimuli-responsive by capping pore openings with molecules which detach or are decomposed in response to certain triggers such as pH, temperature or enzymatic activity, and the encapsulated drug may therefore be released specifically at the target tissue [70]. As such, MSNPs are an attractive platform for the selective delivery of anti-cancer agents to tumours. Fernando *et al.* reported their development of doxorubicin-loaded MSNPs gated with acidic and esterase- sensitive β-amino ester polymers, and demonstrated the triggered release of doxorubicin in human breast cancer cells *in vitro* [71]. Silica materials may have toxic effects due to

NLRP3 inflammasome activation and silanol-mediated membranolysis but reduced toxicity is observed with MSNPs, possibly as a result of their porosity decreasing the area through which membrane interactions may occur [72, 73].

1.2.1.2 Polymeric Nanoparticles

Polymeric nanoparticles constitute a significant portion of nanomedicine research due to their great diversity and potential for drug delivery. By mimicking naturally occurring biomacromolecules, polymer nanoparticles can enhance delivery of therapeutics by protecting them from degradation, prolonging circulation half-life, and targeting therapeutic sites [74]. Natural or biodegradable synthetic polymers may be used to produce nanoparticles and drug can be incorporated by encapsulation or adsorption. Depending on the intended function, polymeric nanoparticles can be designed to control drug release in response to specific stimuli such as pH, temperature and magnetic fields [75]. Different routes of synthesis can produce a variety of particle architecture including micelles, nanospheres and dendrimers (Fig. 1.5, B) [76, 77].

Dendrimers are polymeric macromolecules with a highly branched structure consisting of a core, branches (the repeating monomer unit) which extend from the core, and an outer surface formed by functional groups at the terminus of branches. The layers of branching units are termed generations and determine the size of the dendrimer [78].

Dendrimers are a product of multiple-step organic synthesis. As a result of this, dendrimers could be single chemical entities rather than products of various molecular weights as produced by traditional polymer synthesis. This unique characteristic of dendrimers makes them very attractive targets in the field of

nanomedicine and drug delivery [79], as having low dispersity and a defined and controlled number of surface groups should allow for the rational and tuneable design to deliver different drugs in different environments [80]. Variability in size and shape has been shown to be an important property of nanosized drug carriers with regards to active and passive targeting to specific tissues [81].

To make a successful drug delivery system for use *in vivo*, a dendrimer may be modified to allow tissue targeting and needs to allow adequate biodistribution of the drug without increasing its toxicity and immunogenicity [82]. PEGylation of various materials has been found to reduce adverse effects such as cytotoxicity and rapid clearance and is a method that can be applied to dendrimers by integration of polyethylene glycol (PEG) within the structure, particularly on the surface [83-85]. However, PEG may actually be immunogenic and anti-PEG antibodies can induce rapid clearance of PEG-conjugated therapeutics, reducing their circulation time and efficacy [86, 87]. Dendrimer-based pharmaceutical products in clinical use include VivaGel® (Starpharma Holdings), a microbicidal gel which inhibits infection with sexually transmitted infections such as human immunodeficiency virus (HIV) and herpes simplex virus [88].

1.2.1.3 Lipid based Nanoparticles

The bioavailability of many drugs is limited by their poor water solubility. Some hydrophobic drugs are also lipophilic and these represent good candidates for encapsulation in lipid-based drug delivery systems. Existing lipid-based nanomaterials include solid lipid nanoparticles (SLNs), which utilise lipids with relatively high melting points as this confers stability at body temperature [89], and nanostructured lipid carriers (NLCs) (Fig. 1.5, C), which are formulated with

a mixture of solid and liquid lipids to create a solid nanocarrier with greater drug loading capacity than SLNs due to their less ordered and crystalline structures [90].

The tendency of phospholipids to form bilayers in aqueous surroundings led to the use of nanoscale liposomes, vesicles with a lipid bilayer membrane surrounding an aqueous core, as drug delivery vehicles. By merit of possessing both aqueous and lipidic environments, liposomes are commonly employed in nanomedicine research as they have the potential to carry both hydrophobic and hydrophilic drugs, within the aqueous core or lipid membrane respectively [91]. Doxil® is a liposome-encapsulated form of doxorubicin which is often referred to as the "first nanodrug" since its approval in 1995. Despite improvements regarding circulation time and passive tumour targeting, Doxil® can cause adverse effects such as palmar plantar erythrodysesthesia and complement activation-related pseudo-allergy, an immune effect also known to be caused by other nanomaterials [92]. PEGylated liposomes loaded with methylprednisolone hemisuccinate have been developed by Moallem *et al.* who demonstrated that these materials show improved therapeutic efficacy compared to unformulated drug in a murine model of systemic lupus erythematous, qualified by reduced kidney glomerulonephritis, spleen size and anti-dsDNA antibody levels [93]. Lobatto *et al.* also reported optimised anti-inflammatory effects achieved by their PEGylated prednisolone phosphate liposomes in a rabbit model of atherosclerosis [94].

Nanoemulsions are another example of a lipid-based drug delivery system. Oil-in-water nanoemulsions are suitable for encapsulation of lipophilic drugs, and are

formed by the emulsification of an aqueous phase, oil (containing dissolved drug) and stabiliser mixture, either spontaneously or through high-energy homogenisation, to produce stabilised, nanosized droplets of oil containing the drug suspended in the aqueous phase [95]. The surface of nanoemulsion droplets may be adapted to create targeted drug delivery vehicles, for example, Chuan *et al.* described a method of adsorbing bovine serum albumin (BSA) to peptides stabilising the surface of curcumin nanoemulsion droplets with the potential to selectively deliver the drug to antigen presenting cells and inhibit antigen-specific NF-κB-mediated inflammation [96].

1.2.2 Solid Drug Nanoparticles

Although nanocarriers offer many benefits, as described above, the process of encapsulating drug within other materials reduces the maximum achievable loading of drug within the particle. As opposed to the encapsulation of drug in various nanocarriers, nanoparticles may be constructed from the drug itself (Fig. 1.5, D). Due to the absence of carrier systems which may be sensitive to gut conditions, solid drug nanoparticles (SDNs) are suitable for oral administration, and are therefore an appropriate method for reformulating drugs which were previously unsuitable as or had limitations as orally-delivered formulations. This has implications for existing parenterally-administered drugs or high pill burden regimens for chronic conditions, in which cases patient adherence may be poor and therefore detrimental to disease control [97]. In the case of poorly water soluble drugs, formulation as SDNs is particularly pertinent, and has demonstrated success through a number of approved medicines [98]. It has been estimated that 39% of marketed drugs and 60% of new molecular entities in the

drug development pipeline intended for oral immediate release are classed by the Biopharmaceutics Classification System as Class II or IV compounds, due to their poor solubility [99]. As such, there is much potential for technology such as SDN re-formulation to provide a solution to the solubility issues of this large pool of drugs.

Several processes exist by which SDNs can be made; attrition methods including milling and homogenisation involve forming small particles from larger ones. These approaches have their limitations, in that they are unsuitable for amorphous and low melting point drugs and impurities may occur in the product [100]. An alternative bottom-up method for producing SDNs was developed to resolve these issues, which consists of emulsion-templated freeze-drying (ETFD) [101].

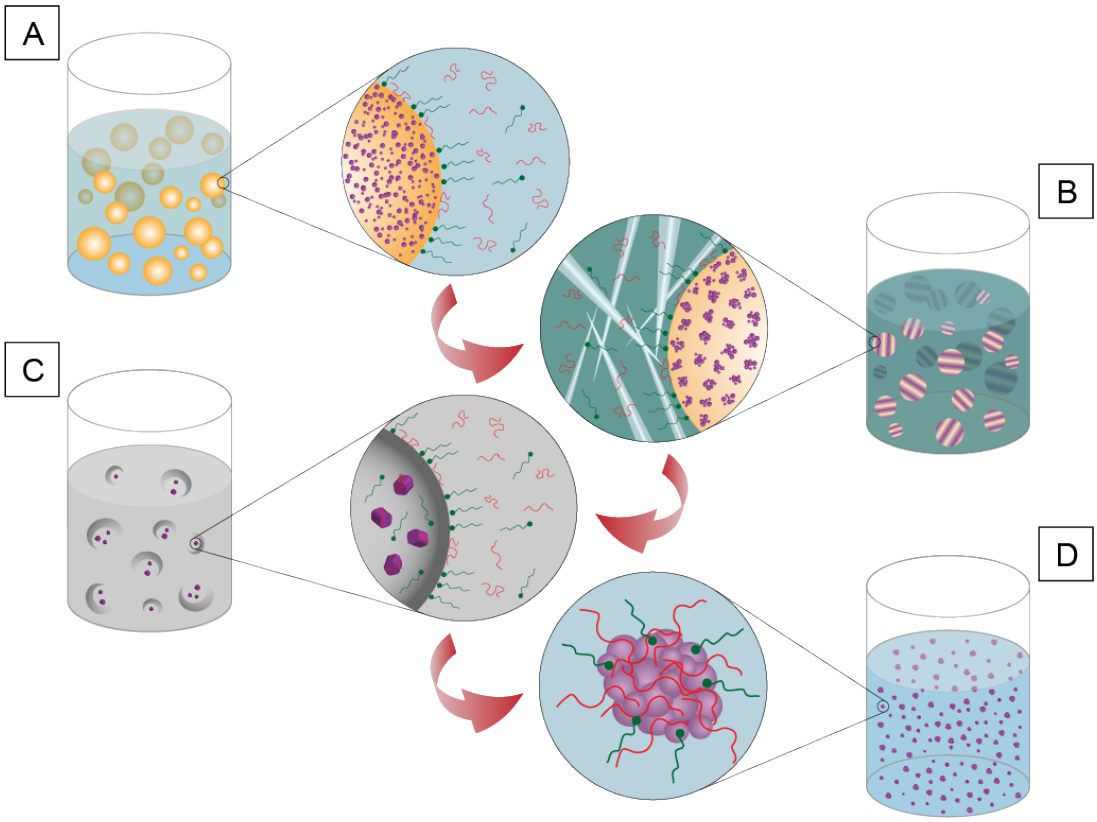

Figure 1.6 Production of solid drug nanoparticles by emulsion-templated freeze-drying. A: formation of an oil-in-water emulsion by mixing a solution of hydrophobic material (purple) in an oil phase (yellow) with a solution of polymer (red) and surfactant (green) in water (blue). B: Freezing the emulsion leads to supersaturation and phase separation of solutes. C: Sublimation of solvents during freeze drying forms a solid, porous monolith of excipients containing dispersed hydrophobic material. D: Addition of water releases the hydrophobic material as dispersed nanoparticles stabilised with excipients. Figure adapted from [102]

An emulsion is first formed by mixing an oil phase, in which a hydrophobic compound is dissolved, with aqueous polymer and surfactant stabilisers (Fig. 1.6, A), followed by rapid cooling (Fig. 1.6, B) and freeze-drying (Fig. 1.6, C). When water is added to the resulting solid monolith, a dispersion of excipient-stabilised nanoparticles is formed (Fig.1.6, D).

By screening one drug with multiple polymers and surfactants, a large library of diverse nanoparticles can be created, varying according to their size, charge, amorphous or crystalline structure. Combination SDNs may also be produced via ETFD by the inclusion of two or more hydrophobic compounds in the oil phase, as has been demonstrated by the formation of lopinavir and ritonavir combination SDNs [103] as well as SDNs containing two fluorescent dyes produced to demonstrate fluorescence (Förster) resonance energy transfer [104].

This approach has been successfully applied to two anti-retroviral drugs with low water solubility, achieving improved oral bioavailability in a rat model [102, 103]. The increase in bioavailability achieved by these formulations offers the potential to reduce the current dose of these drugs and therefore improve patient adherence. A lower dose would also greatly reduce the costs associated with

manufacturing. This SDN technology has demonstrated scalability through the successful manufacture of the two anti-retroviral formulations by industrial-scale spray-drying, as well as long term stability in capsule form [103]. In fact, the overall efficiency of high-throughput screening of potential SDN candidates via ETFD has led to the relatively rapid approval and commencement of bioequivalence trials in humans to confirm the potential for dose reduction achieved by SDN formulation of efavirenz and lopinavir (EudraCT number 2013-004913-41).

1.2.3 Nanomedicine opportunities for improved prednisolone therapy

Due to the limitations of adverse effects on an otherwise potent and efficacious drug, PRD is an ideal candidate for optimisation using nanomedicine. Several examples of nanoformulated PRD have already been reported in the literature, including the two injectable liposomal nanocarriers described above in section 1.2.1.3 which demonstrated prolonged activity and improved efficacy, and altered targeting respectively. PRD nanoparticles have also been developed for topical application, such as PRD nanocapsules for ocular application with prolonged drug release [105] and methyl-prednisolone loaded polymeric nanoparticles for intratympanic treatment of cisplatin-induced ototoxicity [106]. As well as improving efficacy or decreasing the rate of drug release, nanoscale drug delivery systems may offer the potential to target specific tissues. This is particularly interesting for drugs like PRD, which ideally would target inflamed tissues and avoid other tissues where side effects occur. For example, for

treatment of asthma with PRD, a nanoformulation could preferentially target the lung endothelium to achieve local anti-inflammatory effects through particle shape and surface modifications. Anselmo *et al.* have demonstrated this concept with a combination of rod-shaped particles, surface modification with antibodies, and red blood cell "hitchhiking" that improves distribution to the lung whilst reducing accumulation in the liver and spleen [62]. Targeting tissues with tuneable nanoparticle size also has potential to treat proteinuric kidney diseases, as demonstrated by Bruni *et al.* who developed polymeric dexamethasone particles able to permeate the kidney glomerulus and podocytes [107]. Polymeric PRD nanoparticles synthesised by conjugation of methyl PRD to cyclodextrin-PEG polymers have been developed for potential treatment of rheumatoid arthritis, designed to exploit the enhanced permeability and retention (EPR) effect and selectively target inflamed tissues [108]. Therapeutics which utilise the EPR effect are also useful for targeting tumours, which contain abnormal leaky vasculature. This was exemplified by Banciu *et al.* who demonstrated inhibition of tumour growth with glucocorticoid (prednisolone phosphate, methylprednisolone disodium phosphate, budesonide disodium phosphate and dexamethasone disodium phosphate) liposomes [109]. These liposomes have since been investigated further for their potential as theranostic agents. By incorporating a magnetic resonance imaging (MRI) probe in the bilayers of liposomes encapsulating prednisolone phosphate, Cittadino *et al.* were able to visualise the *in vivo* biodistribution of the formulation whilst retaining the efficacy of the drug [110]. More recently, the success of prednisolone phosphate liposomes in reducing inflammation in atherosclerotic rabbits led to a first-in-human trial which unfortunately found the inverse effect of increased

inflammation in patients treated with this formulation, as well as macrophage lipotoxicity as a result of liposome accumulation in atherosclerotic macrophages [94, 111, 112].

Despite all these promising advances in PRD nanomedicine development, none have yet been successful in demonstrating clinical improvement in comparison to conventional, non-nanoformulated PRD. Furthermore, the focus is mainly on liposomal formulations and other nanocarriers which require intravenous or topical administration. The development of an orally administered PRD nanomedicine that does not rely on a carrier system would make an important contribution to this area of research and have the potential to positively impact upon the drawbacks of current clinical use of PRD. To this end, the investigation of SDN formulation of PRD was instigated and forms the basis of this thesis.

1.3 Thesis Aims

This thesis explored the hypothesis that it is possible to produce an SDN formulation of PRD using the ETFD method, and that this formulation can improve the bioavailability and biodistribution of prednisolone towards developing a novel oral nanomedicine for enhanced anti-inflammatory efficacy and reduced side effects. The following chapters describe the formulation, optimisation and characterisation of PRD SDNs (Chapter 2); *in vitro* assessment of PRD SDN cytotoxicity, intestinal permeation and efficacy against immune cells (Chapter 3); and *in vivo* assessment of PRD SDN pharmacokinetics and biodistribution (Chapter 4).

CHAPTER 2

DEVELOPMENT, OPTIMISATION AND CHARACTERISATION OF PRD SDNS

CONTENTS

2.1 Introduction

Emulsion-templated freeze-drying (ETFD), as discussed in Chapter 1, is an effective, non-attrition method of producing solid drug nanoparticles (SDNs) first reported by Zhang *et al.* [101]. This approach is well-suited to high-throughput screening, allowing rapid production of a library of candidates which can be characterised by dynamic light scattering (DLS) according to particle hydrodynamic diameter (expressed as the average size intensity of the sample: z-average, or "D_z"*)*, surface charge (expressed as zeta potential: ζ) and polydispersity index (PdI). By altering one or more variables of the process, multiple screens can be performed to find the optimum combination and identify lead candidates. These variables may relate to the concentration or ratio of drug or excipients, the oil to water (O/W) ratio, the solvent used as the oil phase or the sonication conditions during the emulsification step.

Producing SDNs via ETFD involves the use of two or more water-soluble excipients: a polymer to provide steric stabilisation of both emulsion droplets and dispersed nanoparticles and possibly to provide a nucleation point for the formation of nanoparticles, and an amphiphilic surfactant to provide surface charge or steric stabilisation of both emulsion droplets and dispersed nanoparticles. The excipients used here were chosen from the US Food and Drug Administration (FDA) Inactive Ingredient Database (IID) [113], a record of excipients that have previously been used in FDA-approved drug dosage forms, deemed to be safe but may affect drug toxicity in new combinations. The lowest possible concentration of excipients was targeted to enable stabilised particles with minimal inactive content.

As described in section 1.2.2, two or more hydrophobic compounds may be included in a SDN formulation. In this study, the inclusion of an additional inactive hydrophobic substance was investigated as a variable of the ETFD process to determine its effect on particle size.

To form an oil-in-water emulsion with an aqueous solution of excipients, prednisolone must be dissolved in a volatile, water-immiscible solvent. Both dichloromethane (DCM) and chloroform were used in initial screens. It is generally assumed that freeze drying removes the majority of such solvents so that their presence in the final product is likely to be less than the ICH (International Conference for Harmonisation) limit, and therefore less likely to pose any biocompatibility concerns [114]. The ICH limits for solvents used in this work are 600 ppm for DCM (dichloromethane) and 60 ppm for chloroform. Quantitative determination of residual solvents would be essential if the SDNs were to be manufactured as pharmaceutical products for clinical use, and as such was not conducted as it is beyond the scope of this thesis. Sonication of the aqueous excipients with a solution of PRD in DCM or chloroform produces an oil-in-water emulsion. The duration and intensity of sonication may affect the size and drug content of the oil droplets and therefore variations of these were explored.

For each screen, a set of selection criteria was applied to narrow down the SDN library to the "best" candidates based on particle size and size distribution determined by DLS. DLS was used as the primary method of particle sizing due to its suitability for rapid screening of large numbers of sample dispersions. SEM of particles was attempted to provide a secondary method of sizing (see section

2.3.10). For most screens, unless stated otherwise, the criteria were as follows: good sample dispersibility (determined by visual appraisal of suspension formation following addition of water), D_z of 3000 nm or less, a standard deviation below 15% of mean D_z (of three DLS scans of the same sample), and a PdI (width of the particle size distribution) of 0.75 or less. The size limit was applied as the aim was to produce nanoscale particles (<1000 nm) with some flexibility (<3000 nm) to allow for larger particles which may be reduced in size by later method optimisation. Limiting the standard deviation rejects particles which were not size-stable within the time taken for three repeat DLS measurements. Limiting particles by PdI of <0.75 rules out those with a broad size distribution whilst allowing some polydispersity, which was considered important as there is not one single particle size associated with drug nanoparticle efficacy. SDNs which did not readily disperse in water were discarded. SDNs which did not meet the criteria, or did not produce dispersions either at all or of insufficient quality for reliable results, did not meet the selection criteria.

Following screening and identification of potential candidates, this selection was further refined by repeating under identical conditions to assess reproducibility. Reproducibility was determined by analysis of particle size intensity and number mean for each single repeated DLS measurement of a given formulation, ensuring the DLS traces consisted of the same peaks corresponding to particle size populations. Lead SDN candidates were chosen based on optimal size, reproducibility and PdI and taken forward for more in-depth characterisation by powder X-ray diffraction (pXRD) and scanning electron microscopy (SEM). Drug stability was assessed by electrospray mass spectrometry (ES-MS) and ^{1}H

proton nuclear magentic resonance (^{1}H-NMR) before and after sonication and lyophilisation to ensure the drug was not degraded or altered during these processes. SDN dispersion stability was assessed in several bio-relevant media by monitoring particle hydrodynamic diameter using DLS over six hours following dispersion. SDNs are required to be dispersed in phosphate buffered saline (PBS) or cell culture media (Dulbecco's Modified Eagles Media, DMEM) for various *in vitro* and *in vivo* studies. Dispersion stability in simulated gastric and intestinal fluids was also studied, for the implications of oral dosing and how the SDNs may be affected by the GI system prior to absorption into and subsequent distribution to target tissues by the systemic circulation. Dispersion stability was measured by DLS over a period of six hours, chosen to correlate with the maximum duration of planned *in vitro* and *in vivo* experiments and also average transit time through the stomach and small intestine [115]. The presence of proteins in fed-state simulated gastric fluid was anticipated to interfere with DLS measurements due to comparable sizes to nanoparticles, therefore an amended protocol for preparing FeSSGF with 50% less milk was employed (see section 2.2.15).

The aims of this Chapter were to produce a library of PRD SDNs using ETFD, optimise the process for PRD, select the best candidates, characterise these and assess their stability in bio-relevant media.

2.2 Materials and Methods

2.2.1 Materials

D-α-Tocopherol polyethylene glycol 1000 succinate (TPGS), benzethonium chloride (hyamine), sodium deoxycholate (NDC), Pluronic® F-68 (F68), polyvinylpyrrolidone K 30 (PVP), (hydroxypropyl)methyl cellulose (HPMC), hydroxypropyl cellulose (HPC), polyethylene glycol 1000 (PEG 1K), polyethylene glycol 600 (PEG 600), Pluronic® F-127 (F127), polyvinyl alcohol 80% hydrolysed (PVA), sodium dodecyl sulphate (SDS), sodium myristate (NaM), dioctyl sulfosuccinate sodium salt (AOT), sodium alginate (NaA), Brij® 58, cetyl trimethylammonium bromide (CTAB), hydrolysed gelatin (HGel), prednisolone (PRD), beeswax (BW), Dulbecco's Modified Eagles Serum (DMEM), phosphate buffered saline (PBS) tablets and all general laboratory reagents were purchased from Sigma (Poole, UK). Kollicoat® Protect, Cremophor® EL (crem.EL) and Solutol® HS 15 (solutol) were purchased from BASF (Tunbridge Wells, UK). Tween™ 20 (T20), Tween™ 80 (T80), sodium caprylate (NaC), dichloromethane (DCM), chloroform, dimethyl sulfoxide (DMSO) and ethanol were purchased from Fisher Scientific (Loughborough, UK). Ultrapure de-ionised water (dH_2O) was obtained from a Millipore Milli-Q® Integral Water Purification System (Watford, UK).

2.2.2 Generic emulsion-template freeze-drying (ETFD) method

All screens were performed according to a generic ETFD method described as follows. Aqueous stock solutions of stabilisers were prepared to a concentration of 22.5 mg mL^{-1} in dH_2O and stirred overnight to dissolve completely. This

specific concentration was chosen to enable correct stabiliser concentration and oil:water (O/W) ratio in the emulsion. A solution of PRD was prepared in a volatile, water-immiscible solvent (termed oil phase) to the required concentration. Stock solutions were combined in a 4 mL sample vial with additional dH_2O as required to achieve the desired phase ratio of oil:water. This mixture was ultrasonicated using a Covaris S2x acoustic homogenisation system for 15-60s with a duty cycle of 20, an intensity of 10 and 500 cycles per burst in frequency sweeping mode. The resulting emulsion was immediately cryogenically frozen and lyophilised using a Virtis benchtop K freeze-dryer for 48 hours. The resulting dry, porous monoliths were stored in a humidity-controlled dessicator.

2.2.3 Screen 1: 30 wt% PRD in DCM

Aqueous stock solutions of the following stabilisers were prepared as described in 2.2.2: TPGS, T20, T80, hyamine, NDC, AOT, solutol, NaM, NaC, SDS, crem.EL, brij 58, NaA, CTAB, F68, PVP, HPMC, PEG 1K, F127, kollicoat, PVA, HPC, HGel and PEG 600. A solution of PRD was prepared in DCM to achieve a stock concentration of 30 mg mL^{-1}. 30 mg mL^{-1} was found to be the maximum achievable solubility of PRD in DCM. Stock solutions were combined according to the ratio 100:267:44 µL (PRD solution: polymer:surfactant respectively) resulting in a solid mass ratio of 30:60:10 % (PRD:polymer:surfactant). Additional dH_2O (89 µL) was included in each vial so that the phase ratio of the final mixture was 1:4 DCM:dH_2O. This mixture was ultrasonicated, lyophilised and stored as described in 2.2.2. D_z of the redispersed monoliths were determined by DLS as described in 2.2.12.

2.2.4 Screen 2: 30 wt% PRD in chloroform

Aqueous stock solutions of the following stabilisers were prepared as described in 2.2.2: TPGS, T20, T80, hyamine, NDC, AOT, solutol, F68, PVP, HPMC, PEG 1K, F127, kollicoat and PVA. As this screen was intended purely to observe effect of solvent on particle size, it was deemed unnecessary to include all 24 stabilisers. A solution of PRD was prepared in chloroform to achieve a stock concentration of 30 mg mL^{-1}. Stock solutions were combined according to the ratio 100:267:44 µL (PRD solution:polymer solution:surfactant solution respectively) resulting in a solid mass ratio of 30:60:10 % (PRD:polymer:surfactant). Additional dH_2O (89 µL) was included in each vial so that the phase ratio of the final mixture was 1:4 chloroform:dH_2O. This mixture was ultrasonicated, lyophilised and stored as described in 2.2.2. D_z of the redispersed monoliths were determined by DLS as described in 2.2.12.

2.2.5 Screen 3: 10 wt% PRD in DCM

Aqueous stock solutions of the following stabilisers were prepared as described in 2.2.2: TPGS, T20, T80, hyamine, NDC, AOT, solutol, F68, PVP, HPMC, PEG 1K, F127, kollicoat and PVA. A solution of PRD was prepared in DCM to achieve a stock concentration of 10 mg mL^{-1}. Stock solutions were combined according to the ratio 100:267:44 µL (PRD solution:polymer solution:surfactant solution respectively) resulting in a solid mass ratio of 10:80:10 % (PRD:polymer:surfactant). Additional dH_2O (89 µL) was included in each vial so that the phase ratio of the final mixture was 1:4 DCM:dH_2O. This mixture was ultrasonicated, lyophilised and stored as described in 2.2.2. D_z of the redispersed monoliths were determined by DLS as described in 2.2.12.

2.2.6 Screen 4: 30 wt% PRD, O/W 1:4, varying surfactant content

Aqueous stock solutions of the following stabilisers were prepared to a concentration of 50 mg mL^{-1} in dH_2O and allowed to dissolve completely overnight on a roller mixer: TPGS, T20, T80, hyamine, NDC, AOT, solutol, F68, PVP, HPMC, PEG 1K, F127, kollicoat and PVA. A stock solution of PRD was prepared in DCM to achieve a concentration of 30 mg mL^{-1}. Stock solutions were combined as shown in Table 2.1 to achieve three different drug/stabiliser ratios. Additional dH_2O (260 µL) was included in each vial so that the phase ratio of the final mixtures was 1:4 DCM:dH_2O. The mixtures were ultrasonicated, lyophilised and stored as described in 2.2.2. D_z of the redispersed monoliths were determined by DLS as described in 2.2.12.

Table 2.1 Screen 4: constituent volumes of PRD, polymer and surfactant combined to produce mixtures containing 5, 10 or 15 wt% surfactant.

% surfactant	30 mg mL^{-1} PRD solution (µL)	50 mg mL^{-1} polymer solution (µL)	50 mg mL^{-1} surfactant solution (µL)	Solid mass ratio (wt%) PRD:P:S
5	100	130	10	30:65:5
10	100	120	20	30:60:10
15	100	110	30	30:55:15

2.2.7 Screen 5: 30 wt% PRD, O/W 2:3, varying surfactant content

Aqueous stock solutions of the following stabilisers were prepared to a concentration of 50 mg mL^{-1} in dH_2O and allowed to dissolve completely overnight on a roller mixer: TPGS, T20, T80, hyamine, NDC, AOT, solutol, F68, PVP, HPMC, PEG 1K, F127, kollicoat and PVA. A stock solution of PRD was prepared in DCM to achieve a concentration of 30 mg mL^{-1}. Stock solutions were combined as shown in Table 2.2 to achieve three different drug/stabiliser ratios. Additional dH_2O (160 µL) was included in each vial so that the phase ratio of the

final mixtures was 2:3 DCM:dH_2O. The mixtures were ultrasonicated, lyophilised and stored as described in 2.2.2. D_z of the redispersed monoliths were determined by DLS as described in 2.2.12.

Table 2.2 Screen 5: constituent volumes of PRD, polymer and surfactant combined to produce mixtures containing 5, 10 or 15 wt% surfactant.

% surfactant	30 mg mL^{-1} PRD solution (µL)	50 mg mL^{-1} polymer solution (µL)	50 mg mL^{-1} surfactant solution (µL)	Solid mass ratio (wt%) PRD:P:S
5	100	130	10	30:65:5
10	100	120	20	30:60:10
15	100	110	30	30:55:15

2.2.8 Screen 6: SDNs formulated with beeswax as additional hydrophobic component

Aqueous stock solutions of the following stabilisers were prepared as described in 2.2.2: TPGS, T20, T80, hyamine, NDC, AOT, solutol, F68, PVP, HPMC, PEG 1K, F127, kollicoat and PVA. A solution of PRD and beeswax (BW) was prepared in DCM to achieve a stock concentration of 25 mg mL^{-1} each, with overall hydrophobic concentration of 50 mg mL^{-1}. Stock solutions were combined according to the ratio 100:178:44 µL (DCM solution: polymer:surfactant respectively) resulting in a solid mass ratio of 25:25:40:10 % (PRD:BW:polymer:surfactant). Additional dH_2O (178 µL) was included so that the phase ratio of the final mixture was 1:4 DCM:dH_2O. This mixture was ultrasonicated using a Covaris S2x acoustic homogenisation system for 60 seconds with a duty cycle of 20, an intensity of 10 and 500 cycles per burst in frequency sweeping mode. The resulting emulsion was lyophilised and stored as described in 2.2.2.

Five formulations which met the selection criteria of screen 6 were chosen and repeated in triplicate to assess reproducibility. D_z and ζ were determined by DLS as described in 2.2.12. The equivalent PRD-only formulations of these five were produced for comparison as detailed in Table 2.3. BW-only formulations equivalent to the two lead PRD/BW combination formulations were produced as detailed in Table 2.3 and D_z and zeta potential (ζ) were determined by DLS as described in 2.2.12.

Table 2.3 Composition of 25 wt% PRD- or BW-only SDNs

	Hydrophobic	Polymer	Surfactant	Water
wt%	25	65	10	-
Volume (µL)	100	288	44	68

2.2.9 Screen 7: Variation of oil/water ratio and emulsion sonication duration

Aqueous stock solutions of the following stabilisers were prepared to a concentration of 22.5 mg mL^{-1} in dH_2O and allowed to dissolve completely overnight on a roller mixer: TPGS, T20, T80, hyamine, solutol and kollicoat. A stock solution of PRD was prepared in DCM to achieve a concentration of 30 mg mL^{-1}. Stock solutions were combined in a 4 mL sample vial according to the ratio 100:178:44 µL (DCM solution: polymer:surfactant respectively) resulting in a solid mass ratio of 25:25:40:10 % (PRD:BW:polymer:surfactant). Additional dH_2O (178 or 78 µL) was included so that the phase ratio of the final mixture was 1:4 or 1:3 DCM:dH_2O. The mixtures were ultrasonicated for 15 or 60 seconds, then lyophilised and stored as described in 2.2.2. D_z of the redispersed monoliths were determined by DLS as described in 2.2.12.

2.2.10 Screen 8: Varying relative ratio of drug and beeswax

Aqueous stock solutions of the following stabilisers were prepared to a concentration of 22.5 mg mL^{-1} in dH_2O and allowed to dissolve completely overnight on a roller mixer: TPGS, T20, T80, hyamine, solutol and kollicoat. Three stock solutions of PRD and BW were prepared in DCM to achieve concentrations as described in Table 2.4. Stock solutions were combined in a 4 mL sample vial to achieve one of three solid mass ratios as described in Table 2.4. Additional dH_2O (178 µL) was included so that the phase ratio of the final mixture was 1:4 DCM:dH_2O. The mixtures were ultrasonicated for 60 seconds, lyophilised and stored as described in 2.2.2. D_z of the redispersed monoliths were determined by DLS as described in 2.2.12.

Table 2.4 Corresponding hydrophobic concentrations, hydrophobic ratios and solid mass ratios (total hydrophobic:polymer:surfactant) of SDNs produced in 2.2.10.

Hydrophobic concentrations PRD:BW (mg mL^{-1})	Hydrophobic ratio (wt%) PRD:BW	Solid mass ratio (wt%) H:P:S
25:25	50:50	50:40:10
30:20	60:40	50:40:10
35:15	70:30	50:40:10
25:25	50:50	40:60:10
30:20	60:40	40:60:10
35:15	70:30	40:60:10
25:25	50:50	30:70:10
30:20	60:40	30:70:10
35:15	70:30	30:70:10

2.2.11 Production of half-scale SDNs

To reduce the amount of radiolabelled PRD required for producing radiolabelled PRD/BW SDNs, a method was devised to produce half-mass SDNs as follows. Aqueous stock solutions of the following stabilisers were prepared as described in 2.2.2: TPGS, solutol and kollicoat. A solution of PRD and BW was prepared in DCM to achieve a stock concentration of 25 mg mL^{-1} each, with overall

hydrophobic concentration of 50 mg mL^{-1}. Stock solutions were combined according to the ratio 50:89:22 μL (DCM solution: polymer:surfactant respectively) resulting in a solid mass ratio of 25:25:40:10 % (PRD:BW:polymer:surfactant). Additional dH_2O (89 μL) was included so that the phase ratio of the final mixture was 1:4 DCM:dH_2O. Sonication and freeze-drying were performed as described in 2.2.8 to produce half-mass freeze-dried monoliths. D_z of the redispersed monoliths were determined by DLS as described in 2.2.12.

2.2.12 Determination of particle hydrodynamic diameter and surface charge using dynamic light scattering

Addition of dH_2O to the freeze-dried monoliths produced a dispersion of nanoparticles, the D_z, PdI and ζ of which were determined by DLS using a Zetasizer Nano ZS (Malvern, UK) set to 25°C and automatic attenuator and measurement position. Samples were diluted to 0.83 mg mL^{-1} (unless stated otherwise) in dH_2O, relative to PRD concentration, and vortexed to ensure thorough dispersion. 1 mL of the dispersion was transferred to a 1 cm path length cuvette or capillary zeta cell (for ζ measurements) and measured three times. The Zetasizer software takes into account the fit of the data to the algorithms used to calculate hydrodynamic diameter. In cases of particle aggregation or dissolution during DLS measurement, the software cannot calculate particle size from unstable particles and these samples automatically fail. Particle size data was checked for populations of small particles of 1-10 nm diameter which would indicate micellisation of excipients rather than drug nanoparticles. Similarly, number mean data were checked to confirm that size intensity of nanodispersions

was not skewed by small populations of large particles over a micron in diameter.

2.2.13 Characterisation of PRD SDN structure

Two lead candidate PRD/BW SDN formulations with good reproducibility, PdI below 0.5 and standard deviation below 15% of mean D_z were chosen to progress to detailed characterisation and pharmacological assessment (Chapters 3 and 4). These will be referred to as: SDN1 (25 wt% PRD/25 wt% BW/40 wt% kollicoat/10% TPGS) and SDN2 (25 wt% PRD/25 wt% BW/40 wt% kollicoat/10% solutol).

Crystal morphology of SDNs 1 and 2 was determined as follows to provide an initial qualitative observation of particle crystallinity. pXRD measurements were collected in transmission mode on solid monolith or powder samples held on a thin Mylar film in aluminium well plates on a Panalytical X'Pert PRO MPD instrument with X'Pert Operator Interface (version 1.0b) software. The instrument utilised a high throughput screening XYZ stage, X-ray focusing mirror, and PIXcel detector, using Ni-filtered Cu K α radiation. Data were measured over the range 4–50° in 0.013° steps over 60 minutes. Monolith samples of the three lead PRD/BW SDN candidates, powder/wax samples of PRD, kollicoat, TPGS, solutol and BW were measured.

Scanning electron microscopy (SEM) images were recorded using a Hitachi S-4800 FE-SEM at 3 kV. Glass coverslips were stuck onto the aluminium stubs with carbon tabs. The sample (dispersed to 0.5 mg mL −1) was added to surface

of the coverslip and blotted dry. The samples were gold coated for 1 min at 15 μA using a sputtercoater (EMITECH K550X) prior to imaging.

2.2.14 PRD stability following lyophilisation

MS and ^{1}H-NMR were used to qualify both non-formulated, powder PRD and a sonicated, lyophilised solution of non-formulated PRD in DMSO to determine if the drug was affected by these processes.

MS was performed on a Micromass LCT Premier time-of-flight mass spectrometer (Waters) using electrospray ionisation (positive ion) mode. PRD samples were dissolved in methanol for analysis.

For NMR analysis, PRD samples were dissolved in deuterated DMSO and placed into 5 mm Bruker NMR tubes. ^{1}H-NMR spectroscopy was performed on an Avance 400 MHz spectrometer (Bruker).

2.2.15 Six hour stability of SDN dispersions in bio-relevant fluids

Stability of the lead SDN dispersions was assessed in several bio-relevant media by monitoring particle hydrodynamic diameter over six hours following dispersion.

PBS was prepared according to manufacturer's instructions, by dissolving one PBS tablet in 200 mL to yield 0.01 M phosphate buffer, 0.0027 M potassium chloride and 0.137 M sodium chloride, pH 7.4, at 25 °C. DMEM was used as provided. Simulated gastric and intestinal (fed or fasted state) were prepared as detailed in Tables 2.5 and 2.6, according to recipes from Marques *et al.* [116]. FeSSGF was amended to contain 50% less milk to decrease protein interference

in DLS particle size measurements. FeSSGF containing no nanoparticles was analysed by DLS to confirm its components did not produce a peak that would overlap with those of the nanoparticle size distributions.

Table 2.5 Preparation of 500 mL fasted-state (FaSSGF) and fed-state (amended middle stage, FeSSGF) simulated gastric fluids, according to Marques *et al.* (2011).

Component	FaSSGF	FeSSGF
Sodium taurocholate (μM)	80	-
Lecithin (μM)	20	-
Pepsin (mg/mL)	0.1	-
Sodium chloride (mM)	34.2	237.02
Acetic acid (mM)	-	17.12
Sodium acetate (mM)	-	29.75
Orthophosphoric acid (mM)	-	-
Sodium dihydrogen phosphate	-	-
Milk:buffer	-	0.5:1
pH	1.6	5

Table 2.6 Preparation of 500 mL fasted-state (FaSSIF) and fed-state (FeSSIF) simulated intestine fluids, according to Marques *et al.* (2011).

Component	FaSSIF	FeSSIF
Sodium taurocholate (μM)	3	10
Lecithin (μM)	0.2	2
Maleic acid (mM)	19.12	55.02
Sodium hydroxide (mM)	34.8	81.65
Sodium chloride (mM)	68.62	125.5
Glyceryl monocholate (mM)	-	5
Sodium oleate (mM)	-	0.8
pH	6.5	5.8

PBS and simulated gastric and intestinal fluids were prepared fresh on the day of use. SDN monoliths were dispersed to 1 mg mL^{-1} in each fluid and the hydrodynamic diameter of the particles was measured by DLS (as described in 2.2.12) immediately, then every thirty minutes for six hours.

2.3 Results

2.3.1 Screen 1: Formulation of SDNs with 30 wt% PRD in DCM

Of the 140 samples in Screen 1, 73 met the criteria (Table 2.7). The largest had a D_z of 2938 nm and the smallest D_z was 1210 nm. Most samples containing HPMC met the criteria but were among the largest particles, with an average D_z of 2165 nm. Of the failed samples, most fitted the criteria in terms of size, PdI and %SD but failed due to poor quality data as determined by the Zetasizer software. As none of the samples in this screen were 1000 nm or smaller, and therefore not technically nanoparticles, the following screens aimed to optimise the ETFD method for producing nanoscale PRD particles.

Table 2.7 D_z values for Screen 1 determined by DLS (25°C). Samples dispersed in dH_2O to 0.83 mg mL^{-1}. SDN composition: 30 wt% PRD, 60 wt% polymer, 10 wt% surfactant. Initial mixture 1:4 DCM:dH_2O. Pass criteria: <3000 nm, SD <15, PdI <0.75. Green cells: sample met pass criteria. Uncoloured cells: sample failed to meet pass criteria. Blank cells: sample did not disperse in dH_2O.

	F68	PVP	HPMC	PEG 1K	F127	Kollicoat	PVA	HPC	HGel	PEG 600
TPGS	1638	1943	2046	1502	1628	1598	1969		1488	1756
T20	1467	1849	1964	1489	1842	1970	1545		1473	1787
T80	1475	1935	1951	1626	1933	1634	1745		1464	1731
Hyamine	2543	2720	2045	2229	1580	2007	1594		2517	2190
NDC	1836	1533	2197	1381	1357	1499	1502	2461	1474	1935
AOT	2326	2401	2352	1996	2171	2108	1954		1670	2011
Solutol	1435	2026	2287	1538	1815	1592	1551		1574	2017
NaM	2024	2206	2938	2098	1939	1786			1431	1846
NaC	1890	1944	2162	2345	2443	1621	1878		2037	1625
SDS	1834	2090	2234	1877	1584	1793	2092		1408	1614
Crem. EL	1561	1210	1952	1433	1625	1712	1623		1441	1498
Brij 58	1927	1643	2383	1666	1757	1826	1708		1290	1729
NaA	1731	1861	1786	2093	1584	1524	2089	1619		
CTAB	1382	1613	2008	1419	1562	1464	1440	1454		

2.3.2 Screen 2: Formulation of SDNs with 30 wt% PRD in chloroform

In screen 2 an alternative volatile solvent, chloroform, was used to investigate if choice of solvent affected particle size. Of the 49 samples in Screen 2, 18 met the criteria (Table 2.8). The largest had a D_z of 2442 nm and the smallest D_z was 1415 nm. In this screen, most samples containing kollicoat or PVA passed the criteria whereas none of those containing HPMC passed. Most failed samples were due to poor quality data. Again, no particles were 1000 nm or smaller so the next screen aimed to reduce the size range by decreasing drug loading.

Table 2.8 D_z values for Screen 2 determined by DLS (25°C). Samples dispersed in dH_2O to 0.83 mg mL^{-1}. SDN composition: 30 wt% PRD, 60 wt% polymer, 10 wt% surfactant. Initial mixture 1:4 chloroform:dH_2O. Pass criteria: <3000 nm, SD <15, PdI <0.75. Green cells: sample met pass criteria. Uncoloured cells: sample failed to meet pass criteria. Blank cells: sample did not disperse in dH_2O.

	F68	PVP	HPMC	PEG 1K	F127	Kollicoat	PVA
TPGS	1415	1961		1980	2340	1843	1573
T20	1624	2194	3405	1884	1634	1555	1740
T80	1672	2418	3731	2370	2153	1571	1593
Hyamine	4091	2348	3936		6173	1675	1578
NDC	2913	1822	3668	1572	3384	1682	1487
AOT	2510	3731	5025	1829	2795	2442	2085
Solutol	2152	2339	3428	2067	2032	1617	1886

2.3.3 Screen 3: 10 wt% PRD in DCM

The use of chloroform in screen 2 showed no benefit in terms of size reduction, and in fact more samples were larger than 3000 nm, therefore DCM was used in screen 3. Of the 49 samples in Screen 3, 16 met the criteria (Table 2.9). The largest had a D_z of 2207 nm and the smallest D_z was 1031 nm. In this screen,

most samples containing PEG 1K or solutol passed the criteria whereas none of those containing HPMC or PVA passed. Again, no particles were 1000 nm or smaller so the next two screens aimed to reduce the size range by altering the surfactant content and O/W ratio of a select number of formulations.

Table 2.9 D_z values for Screen 3 determined by DLS (25°C). Samples dispersed in dH_2O to 0.83 mg mL^{-1}. SDN composition: 10 wt% PRD, 80 wt% polymer, 10 wt% surfactant. Initial mixture 1:4 DCM:dH_2O. Pass criteria: <3000 nm, SD <15, PdI <0.75. Green cells: sample met pass criteria. Uncoloured cells: sample failed to meet pass criteria. Blank cells: sample did not disperse in dH_2O.

	F68	PVP	HPMC	PEG 1K	F127	Kollicoat	PVA
TPGS		1951	3445	1066	2207	1036	2294
T20	2700	1982	1421	1339	1841	2565	1852
T80	1888	1831	1635	1031	1873	2086	1835
Hyamine	4047	3023	2750	2251	3092	2276	2353
NDC	6226	1437	2301	1150	2117	1331	3036
AOT	3545	1970	643	1245	2193	2537	2938
Solutol	1960	1990	2867	2049	1540	1642	2303

2.3.4 Screen 4: 30 wt% PRD, O/W 1:4, varying surfactant content

In Screen 4, five formulations from Screen 1 were chosen to investigate the effect of varying surfactant concentration on particle size. This small selection was intended to limit variables other than surfactant and therefore contained only formulations containing kollicoat as the polymer stabiliser. In this way, the effect of changing surfactant and surfactant content could be easily observed. Of the 15 samples in Screen 4, 6 met the criteria (Table 2.10). The largest had a D_z of 2180 nm and the smallest D_z was 1391 nm. In this screen, samples containing 5 wt% surfactant were more likely to pass the criteria, but there was no observable trend of surfactant type or content on particle size.

Table 2.10 D_z values for Screen 4 determined by DLS (25°C). Samples dispersed in dH_2O to 0.83 mg mL^{-1}. SDN composition: 30 wt% PRD + [65 wt% polymer + 5 wt% surfactant], [60 wt% polymer + 10 wt% surfactant] or [55 wt% polymer + 15 wt% surfactant]. Initial mixture 1:4 DCM:dH_2O. Pass criteria: <3000 nm, SD <15, PdI <0.75. Excipient combination A: kollicoat + TPGS, B: kollicoat + T20, C: kollicoat + T80, D: kollicoat + hyamine, E: kollicoat + solutol. Green cells: sample met pass criteria. Uncoloured cells: sample failed to meet pass criteria.

wt% surfactant	A	B	C	D	E
5	1623	1747	1990	1391	2180
10	1791	1768	1745	1719	2400
15	1892	1962	2037	1330	2330

2.3.5 Screen 5: 30 wt% PRD, O/W 2:3, varying surfactant content

Screen 5 also focused on just five polymer-surfactant combinations as in Screen 4, but included an additional variable by changing the oil:water ratio from 1:4 to 2:3 to investigate effect on particle size. Of the 15 samples in Screen 5, 7 met the criteria (Table 2.11). The largest had a D_z of 1958 nm and the smallest D_z was 1251 nm. As in screen 4, samples containing 5 wt% surfactant were more likely to pass the criteria but there was no observable trend of surfactant choice or content, or O/W ratio on particle size.

Table 2.11 D_z values for Screen 5 determined by DLS (25°C). Samples dispersed in dH_2O to 0.83 mg mL^{-1}. SDN composition: 30 wt% PRD + [65 wt% polymer + 5 wt% surfactant], [60 wt% polymer + 10 wt% surfactant] or [55 wt% polymer + 15 wt% surfactant]. Initial mixture 2:3 DCM:dH_2O. Pass criteria: <3000 nm, SD <15, PdI <0.75. Excipient combination A: kollicoat + TPGS, B: kollicoat + T20, C: kollicoat + T80, D: kollicoat + hyamine, E: kollicoat + solutol. Green cells: sample met pass criteria. Uncoloured cells: sample failed to meet pass criteria.

wt% surfactant	A	B	C	D	E
5	1776	1709	1859	1251	1945
10	1675	1914	2023	1281	1958
15	1703	1912	1701	1405	3335

2.3.6 Screen 6: SDNs formulated with beeswax as additional hydrophobic component

As neither altering surfactant content nor changing the O/W ratio succeeded in producing nanoscale particles, a different variable was investigated in the form of co-formulating an additional hydrophobic component with PRD (Screen 6), with the intention of this hydrophobic substance restricting the growth of the PRD SDN below 1000 nm. For this purpose, beeswax was chosen as an inactive hydrophobic substance from the FDA IID and by merit of its common use in food products, indicating potential biocompatibility. Of the 49 samples formulated with beeswax in Screen 6, 22 met the criteria (Table 2.12). The largest had a D_z of 2203 nm and the smallest D_z was 670 nm. All samples containing T80 passed the criteria, whereas those containing hyamine, NDC or AOT all failed. Samples containing kollicoat made the smallest particles with an average of 1165 nm. Most failed samples were due to poor quality data or had a %SD higher than 15.

Table 2.12 D_z values for Screen 6 determined by DLS (25°C). Samples dispersed in dH_2O to 0.83 mg mL^{-1}. SDN composition: 25 wt% PRD, 25 wt% BW, 40 wt% polymer + 10 wt% surfactant. Initial mixture 1:4 DCM:dH_2O. Pass criteria: <3000 nm, SD <15, PdI <0.75. Green cells: sample met pass criteria. Uncoloured cells: sample failed to meet pass criteria. Blank cells: sample did not disperse in dH_2O.

	F68	PVP	HPMC	PEG 1K	F127	Kollicoat	PVA
TPGS		1082	2203	1392	1249	670	1103
T20	2072	1706	2153	2075	1479	1165	1540
T80	1417	1072	2050	1257	1257	755	1360
Hyamine		384	3052			724	1908
NDC			2154				
AOT	5832	812	4413	715	3354	2979	2078
Solutol	1747	2106	1870	1805	1298	699	1385

At this stage, 5 candidates were chosen from the smallest particles, whether they had passed the criteria or not: kollicoat/TPGS, kollicoat/T20, kollicoat/T80, kollicoat/hyamine, kollicoat/solutol and kollicoat/AOT (cells bordered in red in Table 2.12). These were repeated to determine their reproducibility (Fig. 2.1). From this point, the pass criteria were changed to encompass only particles with D_z <1000 nm (SD <15% and PdI <0.75 were unchanged). In terms of size, kollicoat/hyamine and kollicoat/T80 SDNs were the most reproducible when dispersed to 3 mg mL^{-1} in dH_2O. When dispersed to 1 mg mL^{-1} in dH_2O, kollicoat/TPGS and kollicoat/solutol SDNs appeared to be more reproducible.

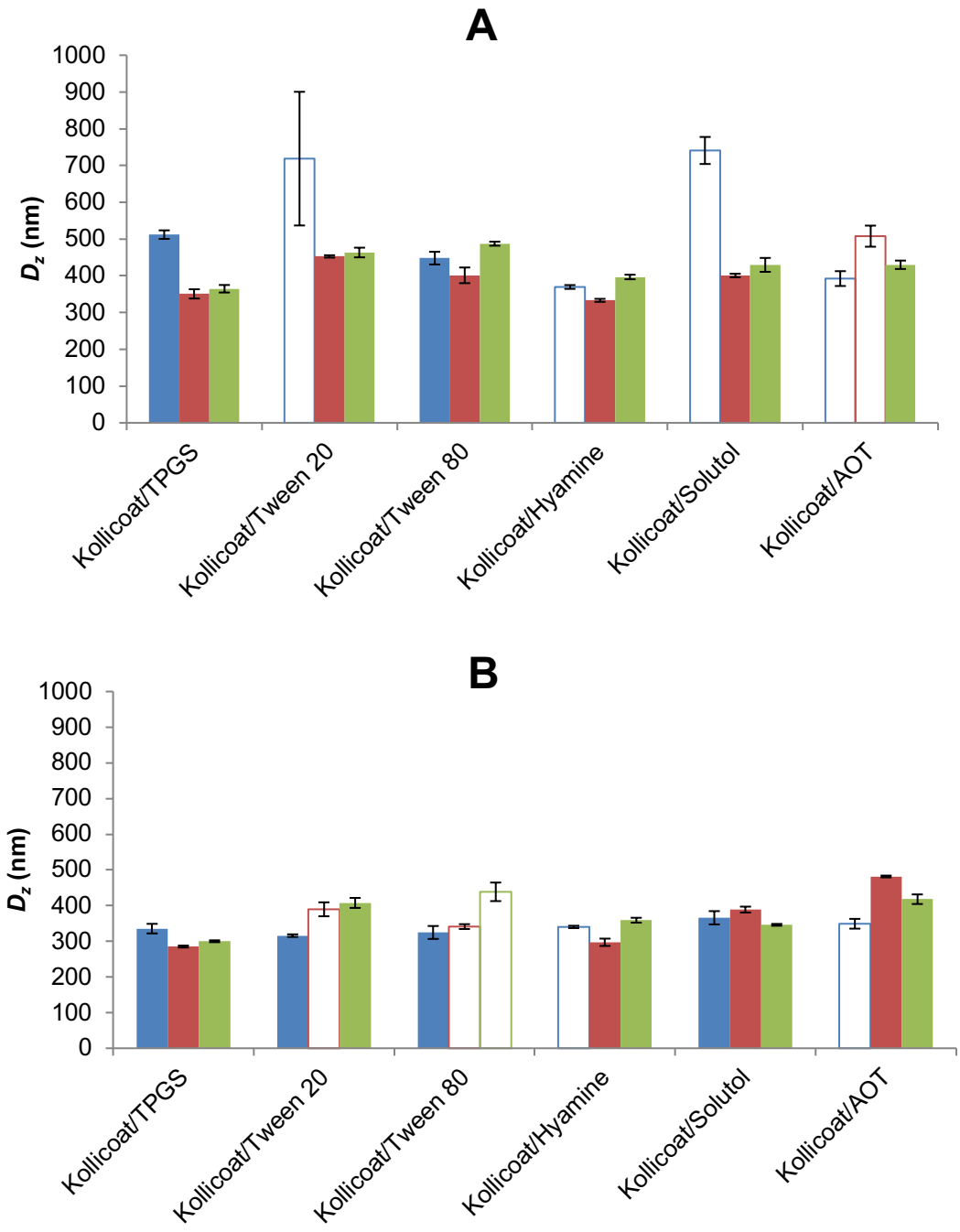

Figure 2.1 D_z values of candidates that passed screen 6 repeated in triplicate, determined by DLS (25°C). Error bars show standard deviation between three consecutive D_z measurements of the same sample. Samples dispersed in dH_2O to 3 mg mL^{-1} (A) or 1 mg mL^{-1} (B). SDN composition: 25 wt% PRD, 25 wt% BW, 40 wt% polymer + 10 wt% surfactant. Initial mixture 1:4 DCM:dH_2O. Pass criteria: <1000 nm, SD <15, PdI <0.75. Coloured bars: sample met pass criteria. Uncoloured bars: sample failed to meet pass criteria.

The repeats of the five formulations were also assessed for ζ by DLS (Fig. 2.2). Despite the non-ionic nature of kollicoat and the surfactants TPGS, T20, T80 and solutol, SDNs formulated with kollicoat and these surfactants have a ζ around -20 mV. AOT is an anionic surfactant, but the ζ of the kollicoat/AOT SDN is about -10 mV – lower than that of the SDNs formulated with non-ionic surfactants. Hyamine is cationic, and this is reflected in the ζ of the kollicoat/hyamine SDN which is ~40 mV.

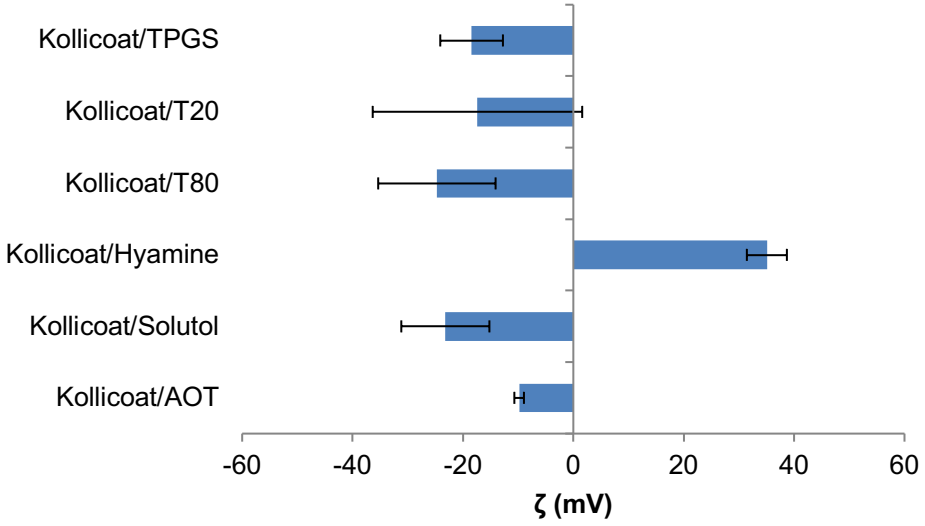

Figure 2.2 ζ values of candidates that passed screen 6 repeated in triplicate, determined by DLS (25°C). Error bars show standard deviation between ζ measurements of three separate samples. Samples dispersed in dH_2O to 1 mg mL^{-1}. SDN composition: 25 wt% PRD, 25 wt% BW, 40 wt% polymer + 10 wt% surfactant. Initial mixture 1:4 DCM:dH_2O.

To compare the size difference between PRD/BW combination SDNs and the equivalent (with regard to wt% PRD) PRD-only SDNs, samples of the five candidate formulations were produced in triplicate and analysed (Fig. 2.3). All of the PRD-only SDNs were much larger than their PRD/BW equivalents, with sizes ranging from around 2000-3000 nm compared to 300-400 nm.

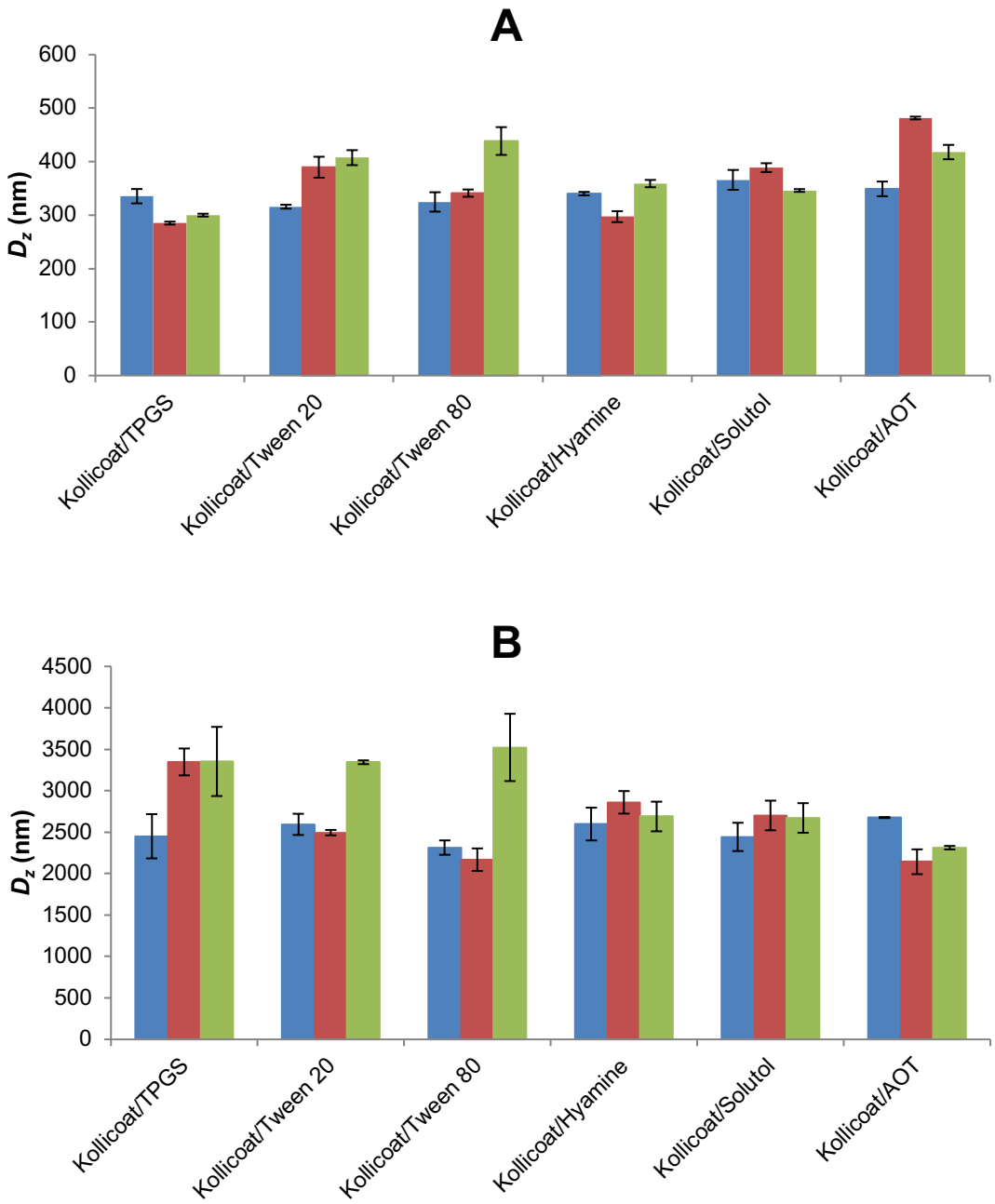

Figure 2.3 D_z values of PRD/BW SDNs (A) and equivalent PRD-only SDNs (B) repeated in triplicate, determined by DLS (25°C). Error bars show standard deviation between three consecutive D_z measurements of the same sample. Samples dispersed in dH_2O to 0.83 mg mL^{-1}. PRD/BW SDN composition: 25 wt% PRD, 25 wt% BW, 40 wt% polymer + 10 wt% surfactant. PRD-only SDN composition: 25 wt% PRD, 65 wt% polymer + 10 wt% surfactant. Initial mixture 1:4 DCM:dH_2O.

Equivalent BW-only formulations were also produced to compare with PRD/BW combination SDNs. Samples of two lead formulations were produced in triplicate and analysed (Fig. 2.4). The average D_z of these formulations were very similar to that of the equivalent PRD/BW combination SDNs.

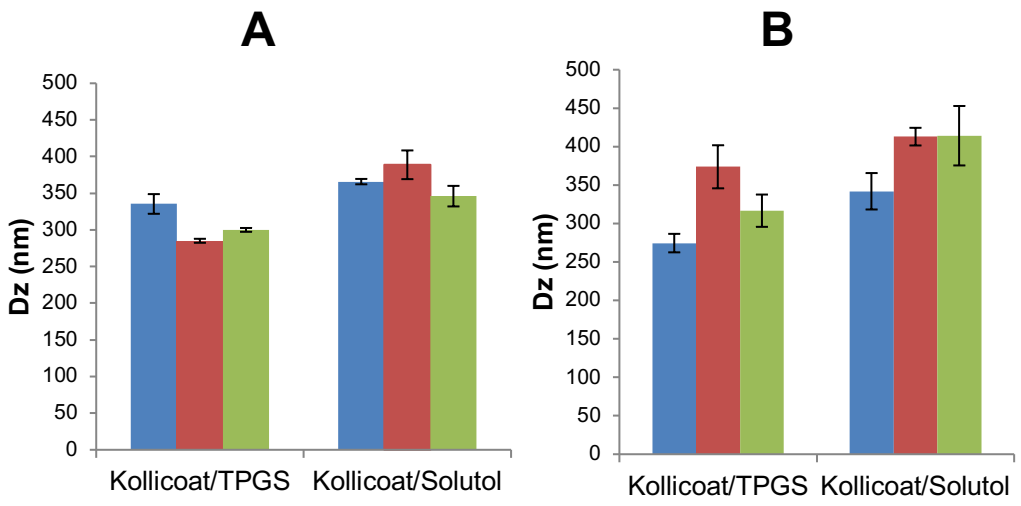

Figure 2.4 D_z values of PRD/BW SDNs (A) and equivalent BW-only SDNs (B) repeated in triplicate, determined by DLS (25°C). Error bars show standard deviation between three consecutive D_z measurements of the same sample. Samples dispersed in dH_2O to 0.83 mg mL^{-1}. PRD/BW SDN composition: 25 wt% PRD, 25 wt% BW, 40 wt% polymer + 10 wt% surfactant. BW-only SDN composition: 25 wt% BW, 65 wt% polymer + 10 wt% surfactant. Initial mixture 1:4 DCM:dH_2O.

2.3.7 Screen 7: Variation of oil/water ratio and emulsion sonication duration

There was no uniform trend of effect of O/W ratio or sonication time across the five lead SDNs (Fig. 2.5). An O/W ratio of 1:3 and 60 seconds sonication reduced the size of the kollicoat/TPGS SDN from around 300 nm to 200 nm. The kollicoat/T20 SDN remained a similar size under all four conditions. The size of the kollicoat/T80 SDN reduced with increasing sonication time and altering O/W

ratio from 1:3 to 1:4. A slight reduction in size was seen with kollicoat/solutol SDNs with O/W ratio of 1:4.

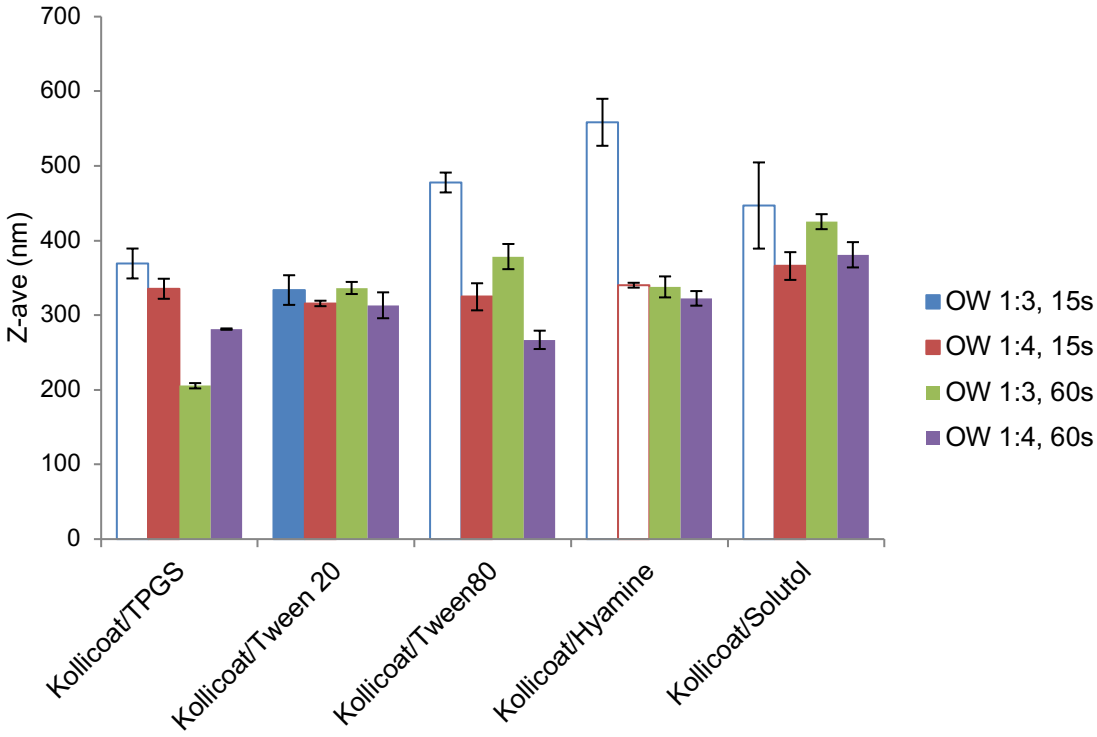

Figure 2.5 D_z values of PRD SDNs sonicated at emulsion-forming stage for 15 or 60 seconds, determined by DLS (25°C). Error bars show standard deviation between three consecutive D_z measurements of the same sample. Samples dispersed in dH_2O to 0.83 mg mL^{-1}. SDN composition: 25 wt% PRD, 25 wt% BW, 40 wt% polymer + 10 wt% surfactant. Initial mixture 1:4 DCM:dH_2O or 1:3 DCM:dH_2O. Pass criteria: <1000 nm, SD <15, PdI <0.75. Coloured bars: sample met pass criteria. Uncoloured bars: sample failed to meet pass criteria.

2.3.8 Screen 8: Varying relative ratio of drug and beeswax

With the exception of kollicoat/solutol (Fig. 2.6), formulations with 50% total hydrophobic content produced larger SDNs compared to those formulated with 40 or 30%. Generally, SDNs with a ratio of 60:40 PRD to BW were larger than those with a 50:50 or 70:30 ratio.

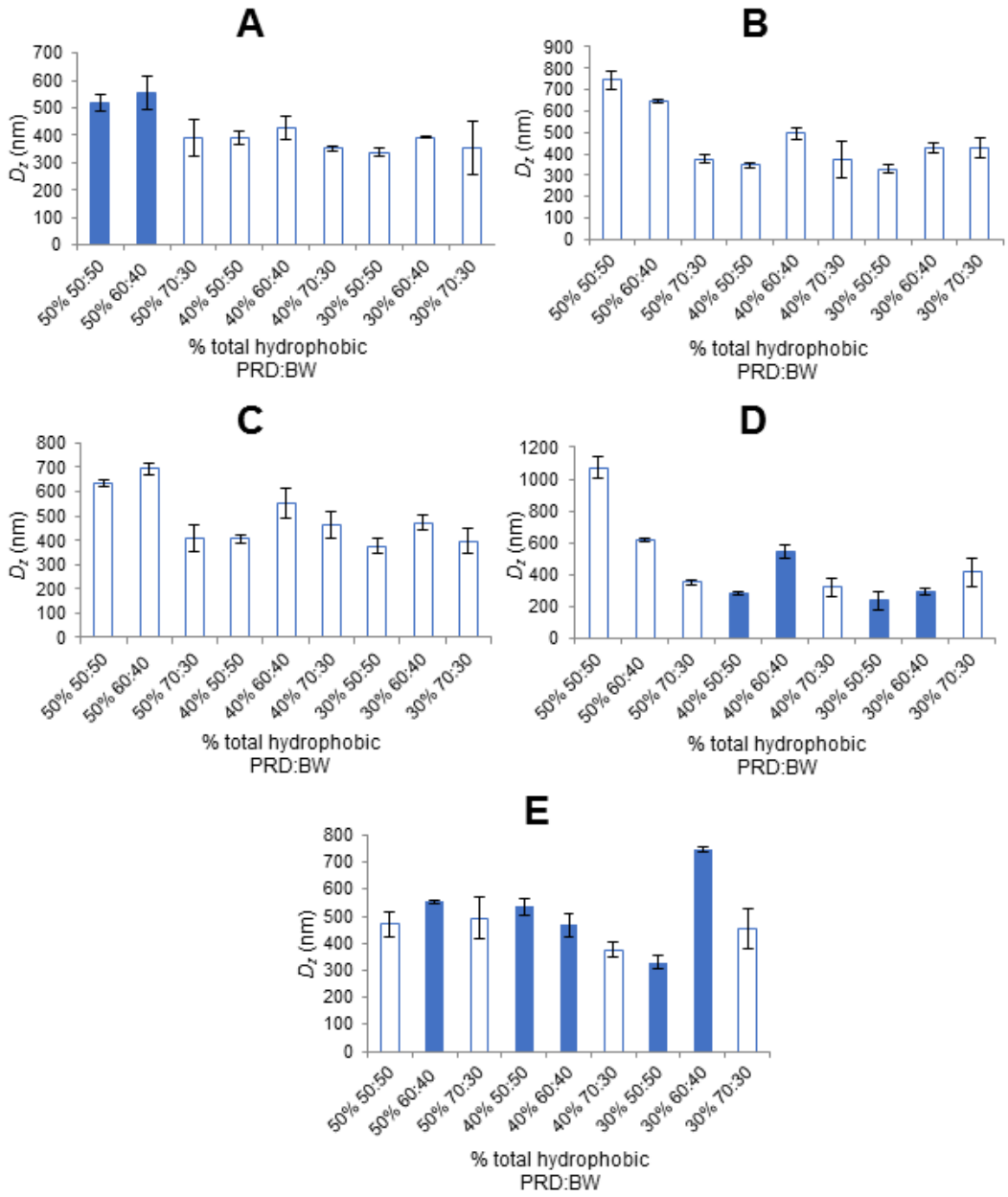

Figure 2.6 A: kollicoat/TPGS, B: kollicoat/T20, C: kollicoat/T80, D: kollicoat/hyamine, E: kollicoat/solutol. D_z values of SDNs A-E with varying hydrophobic content and ratio, determined by DLS (25°C). Error bars show standard deviation between three consecutive D_z measurements of the same sample. Samples dispersed in dH_2O to 0.83 mg mL^{-1}. SDN composition [see Table 2.4]. Initial mixture 1:4 DCM:dH_2O. Pass criteria: <1000 nm, SD <15, PdI <0.75. Coloured bars: sample met pass criteria. Uncoloured bars: sample failed to meet pass criteria.

2.3.9 Production of half-scale SDNs

As neither varying the sonication time, O/W ratio or hydrophobic ratio appeared to confer any benefit to formulation in terms of D_z or reproducibility, the original method of producing PRD/BW SDNs as described in 2.2.8 was used from this point onwards. However, to reduce the amount of radiolabelled PRD necessary for producing radiolabelled PRD/BW SDNs, a method was devised to produce half-scale SDNs. Two of the five lead candidate PRD/BW SDN formulations were chosen to proceed with from this point. Kollicoat/TPGS (SDN1) was chosen for its reproducibility and by virtue of the inhibitory effect of TPGS on the efflux transporter ABCB1/P-glycoprotein (P-gp) [117], which has the potential to reduce P-gp efflux activity at barrier sites including the intestinal and lung epithelia and the blood-brain barrier [118, 119]. Kollicoat/solutol (SDN2) was chosen for its reproducibility and the difference in structure of solutol compared to TPGS.

The D_z of SDN1 remained the same (within error, shown as standard deviation) when produced by the original method or the half volume method, with either 30 or 60 second sonication (Fig. 2.7). SDN2 was slightly smaller when made at half volume with 60 seconds sonication.

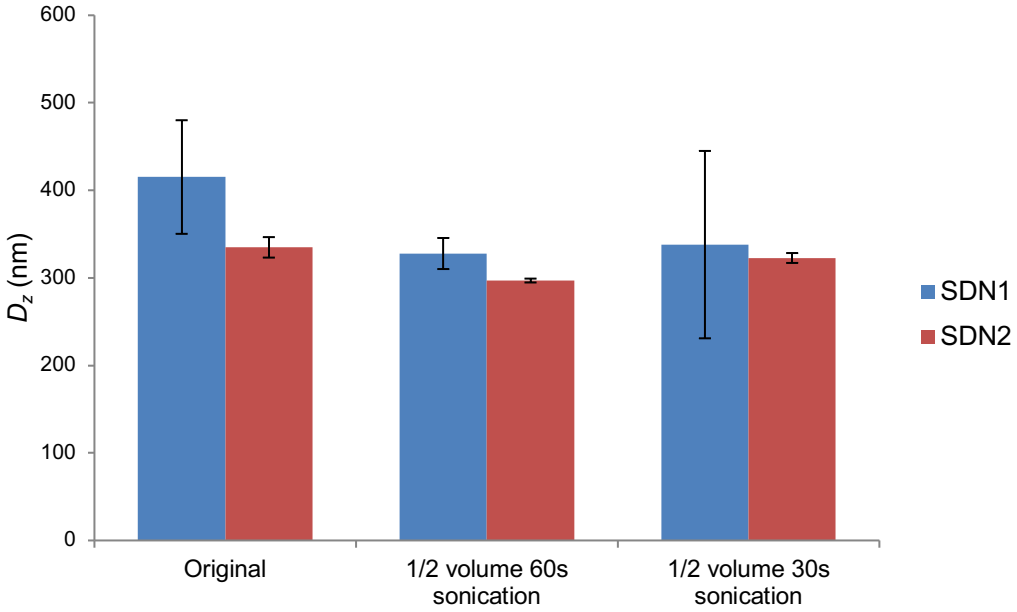

Figure 2.7 D_z values of SDNs 1 and 2 made by original method or ½ volume method with 60 or 30 second sonication time, determined by DLS (25°C). Error bars show standard deviation between three consecutive D_z measurements of the same sample. Samples dispersed in dH_2O to 0.83 mg mL^{-1}. SDN composition: 25 wt% PRD, 25 wt% BW, 40 wt% polymer + 10 wt% surfactant. Initial mixture 1:4 DCM:dH_2O.

2.3.10 Characterisation of PRD SDN structure

Both SDN formulations were found to be crystalline from pXRD analysis, as was unformulated PRD (Fig. 2.8). The loss of distinction between the characteristic PRD peaks may indicate that the SDN formulations have some amorphous character. TPGS, solutol, kollicoat and beeswax were all amorphous.

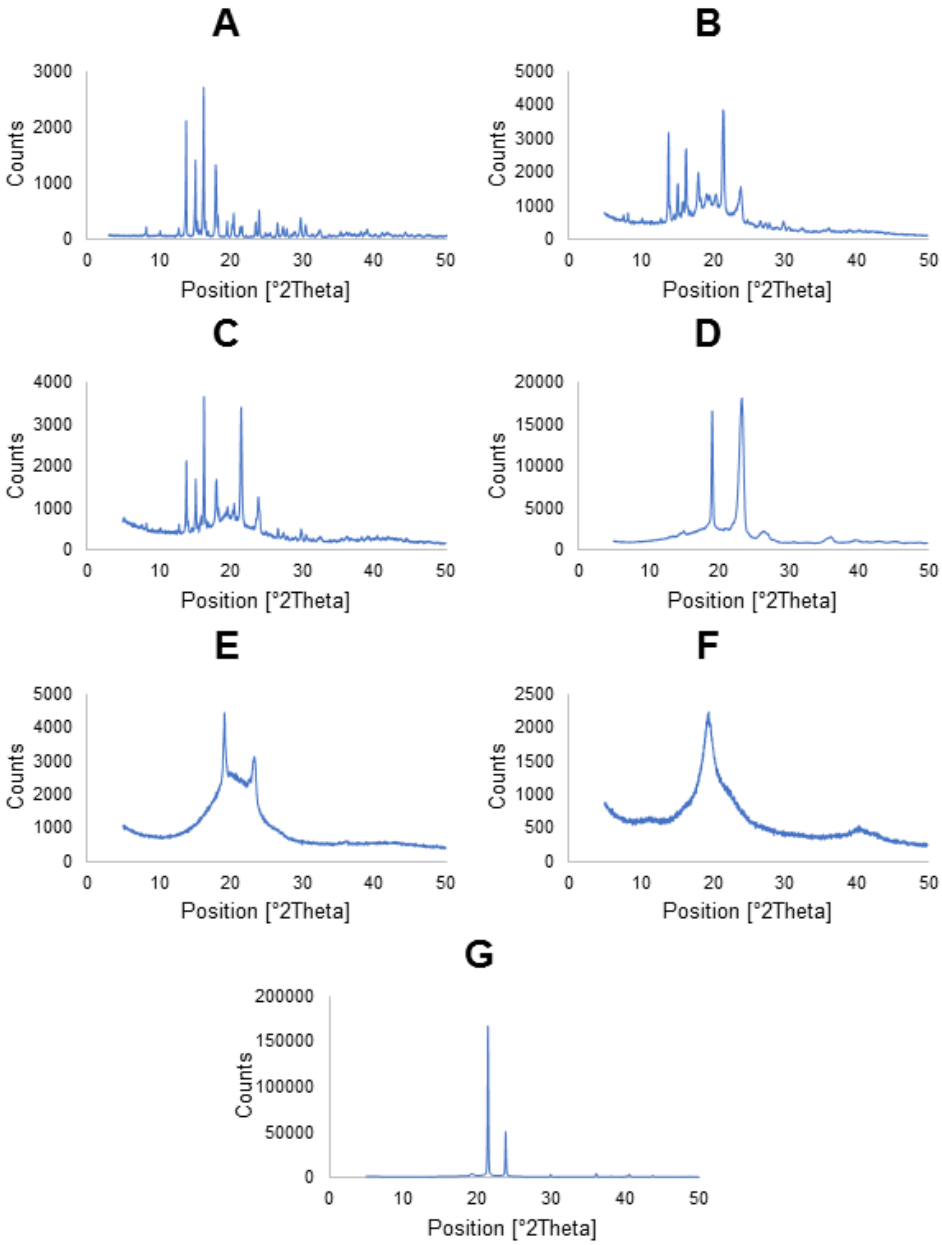

Figure 2.8 Powder X-ray diffraction patterns of A: PRD, B: SDN1, C: SDN2, D: TPGS, E: solutol, F: kollicoat and G: BW.

SEM images of SDN1 and SDN2 showed large crystals of around 10 – 100 µm (Fig. 2.9). However the technique requires drying of SDN dispersions which is not how SDNs are designed to be used, so the extensive crystallisation observed is unlikely to occur under normal conditions.

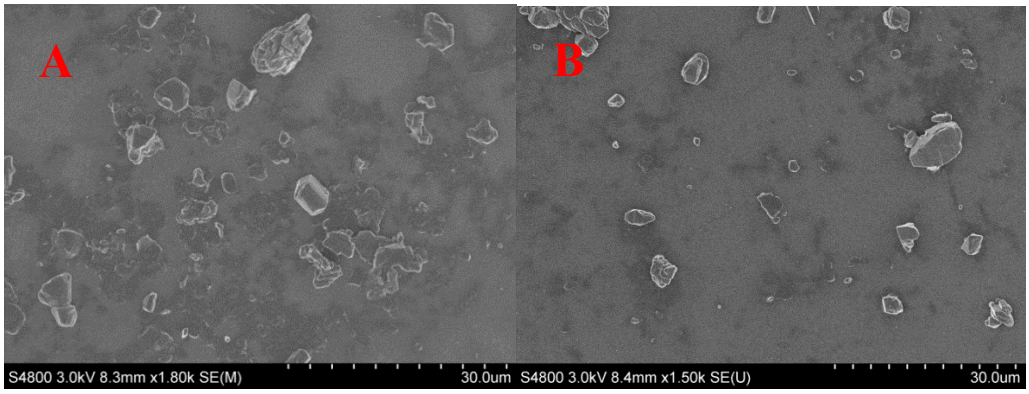

Figure 2.9 SEM images of SDN1 (A) and SDN2 (B) showing large crystals of various sizes, in the range of 10 to 100 µm in length.

2.3.11 Drug stability following lyophilisation

Mass spectra of standard PRD powder and PRD following 60 seconds sonication and 48 hours lyophilisation show that the drug structures are identical (Fig. 2.10).

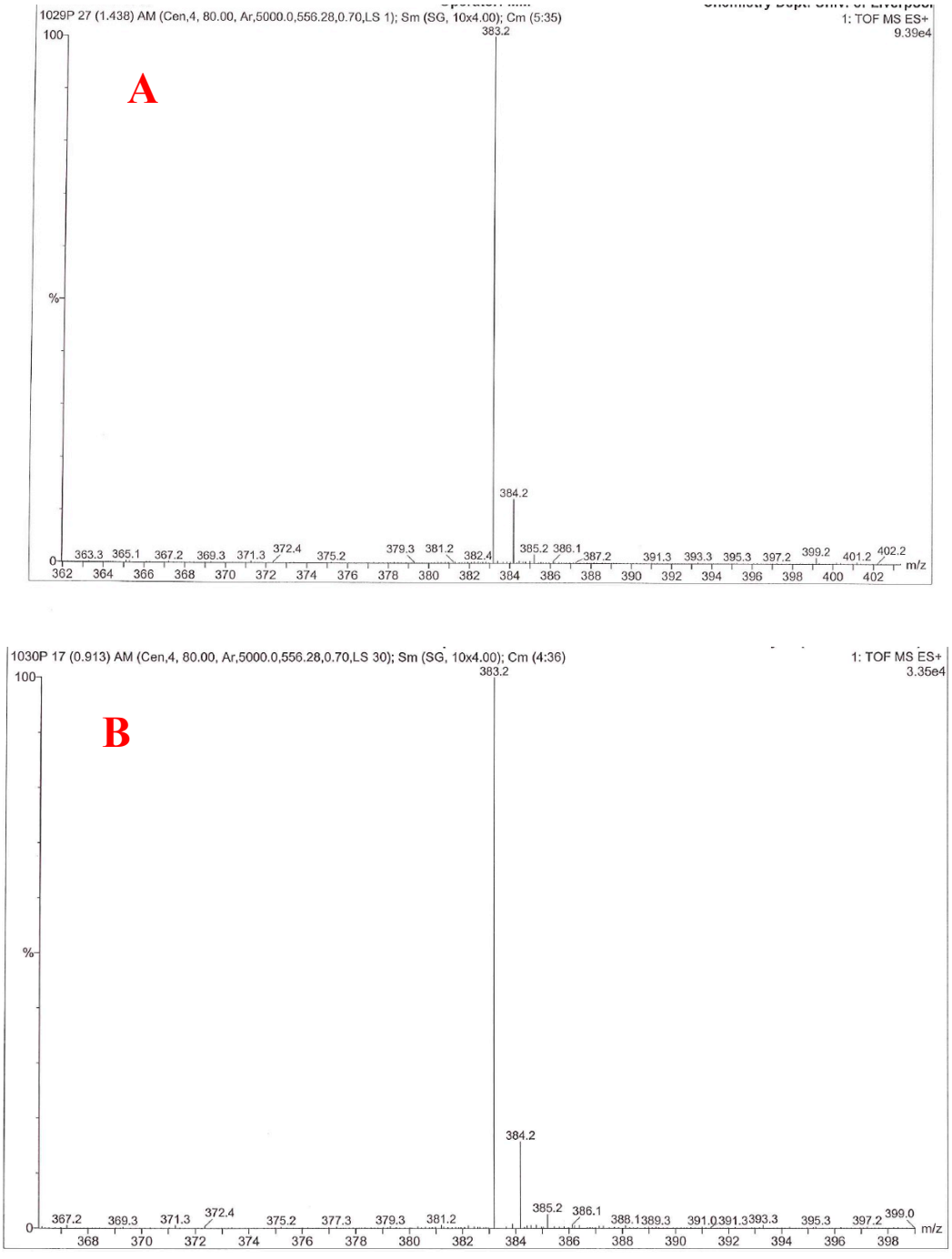

Figure 2.10 Mass spectra of powdered PRD as supplied (A) and sonicated, lyophilised PRD (B).

Analysis by ^{1}H-NMR shows no change in PRD structure when sonicated for 60 seconds and lyophilised for 48 hours (Fig. 2.11).

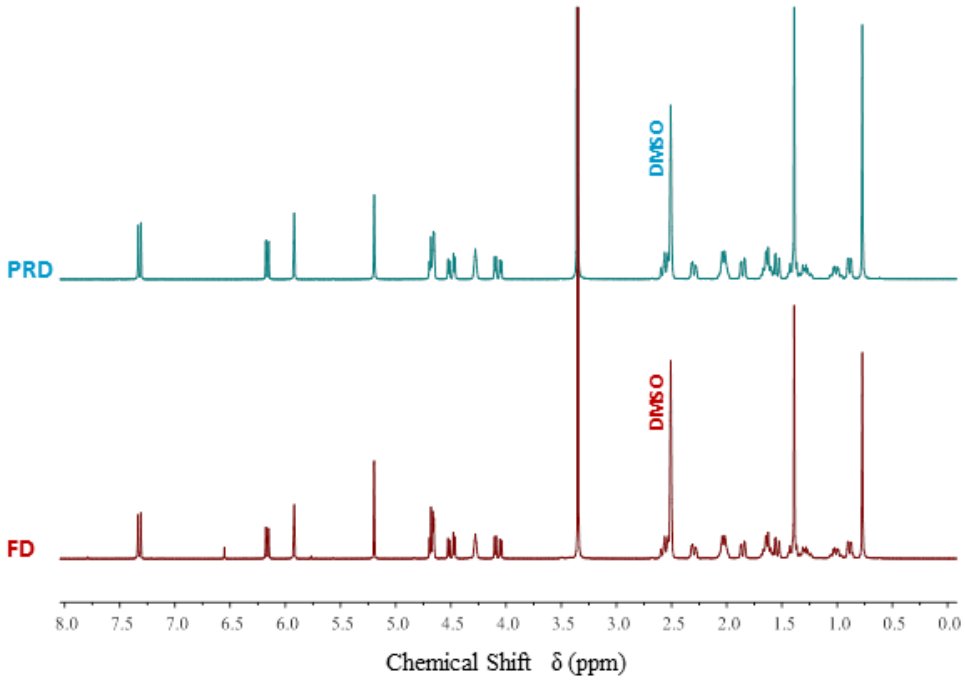

Figure 2.11 ^{1}H-NMR spectra of PRD and 60 seconds sonicated, 48 hours lyophilised PRD (FD). Determined using a Bruker Avance 400 MHz NMR Spectrometer (15 minute scan). Samples were dissolved in DMSO.

2.3.12 Six hour stability of SDN dispersions in bio-relevant fluids

Both SDN1 and SDN2 showed size stability over 6 hours in all seven media, with the exception of SDN2 which, in FaSSGF, appeared to increase over the 6 hours by 200-300 nm (Fig. 2.12). However, these measurements exhibited the largest standard deviation error of the whole set of stability experiments and would benefit from repeating. The measurement error of samples in FaSSIF and FeSSIF was also relatively large, so more repeats for each media are required.

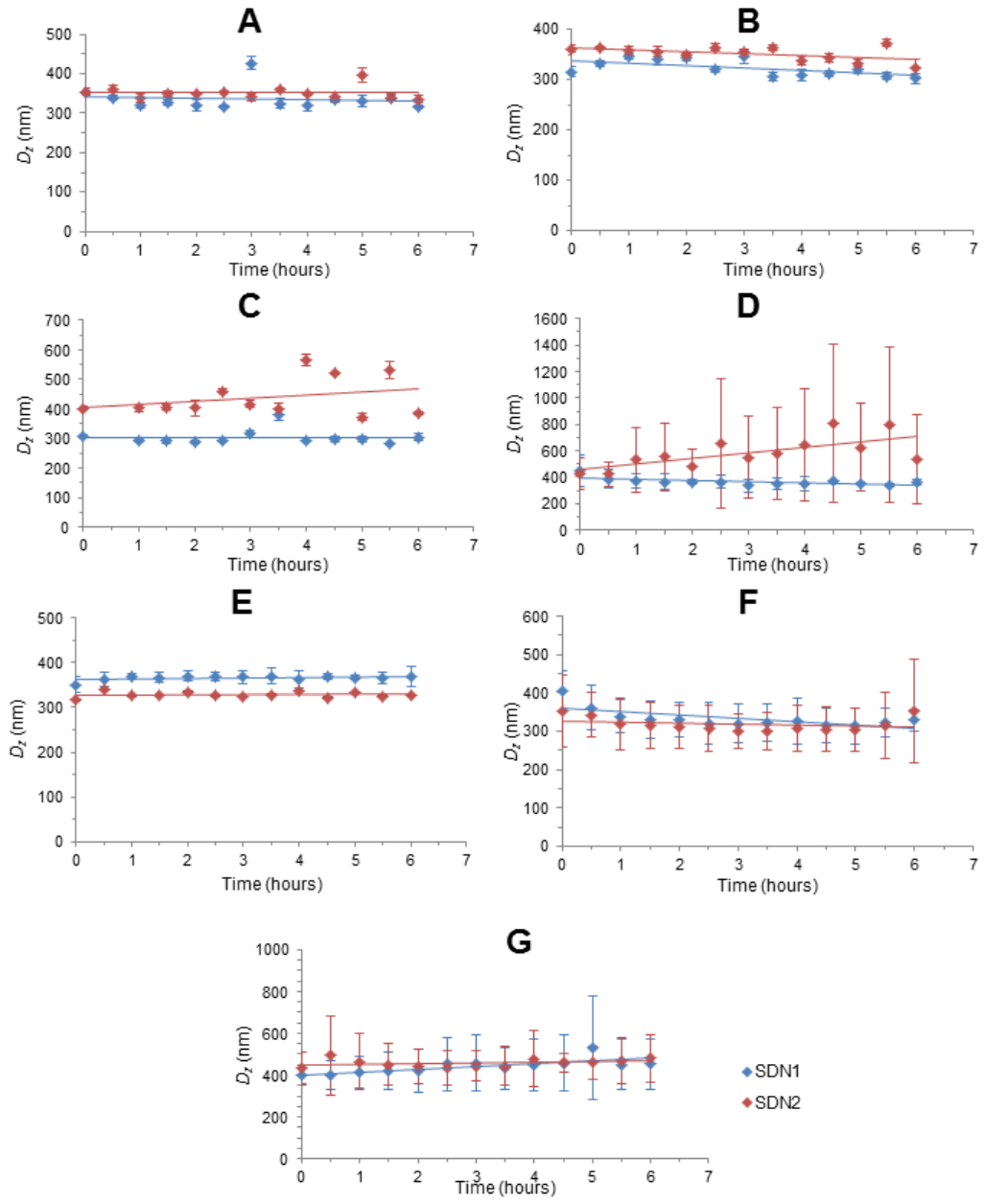

Figure 2.12 D_z values for SDNs 1 and 2 in bio-relevant fluids (A: dH_2O, B: PBS, C: DMEM, D: FaSSGF (fasted-state simulated gastric fluid), E: FeSSGF (fed-state simulated gastric fluid), F: FaSSIF (fasted-state simulated intestinal fluid), G: FeSSIF (fasted-state simulated intestinal fluid)) over 6 hours determined by DLS (25°C). Samples dispersed in dH_2O to 0.83 mg mL^{-1}. SDN composition: 25 wt% PRD, 25 wt% BW, 40 wt% polymer + 10 wt% surfactant. Initial mixture 1:4 DCM:dH_2O. Pass criteria: <1000 nm, SD <15, PdI <0.75.

2.4 Discussion

The initial screens (1 – 5) for potential PRD SDN candidates all yielded large particles with D_z of several microns. Investigation of multiple approaches including changing solvent, increasing and decreasing drug loading, varying O/W ratio and varying excipient ratios, found that each had a small impact on D_z, but not enough to produce sub-micron particles (sections 2.3.1- 2.3.5). As these variables were not having the expected impact on particles size, the drug itself was likely the dominant factor.

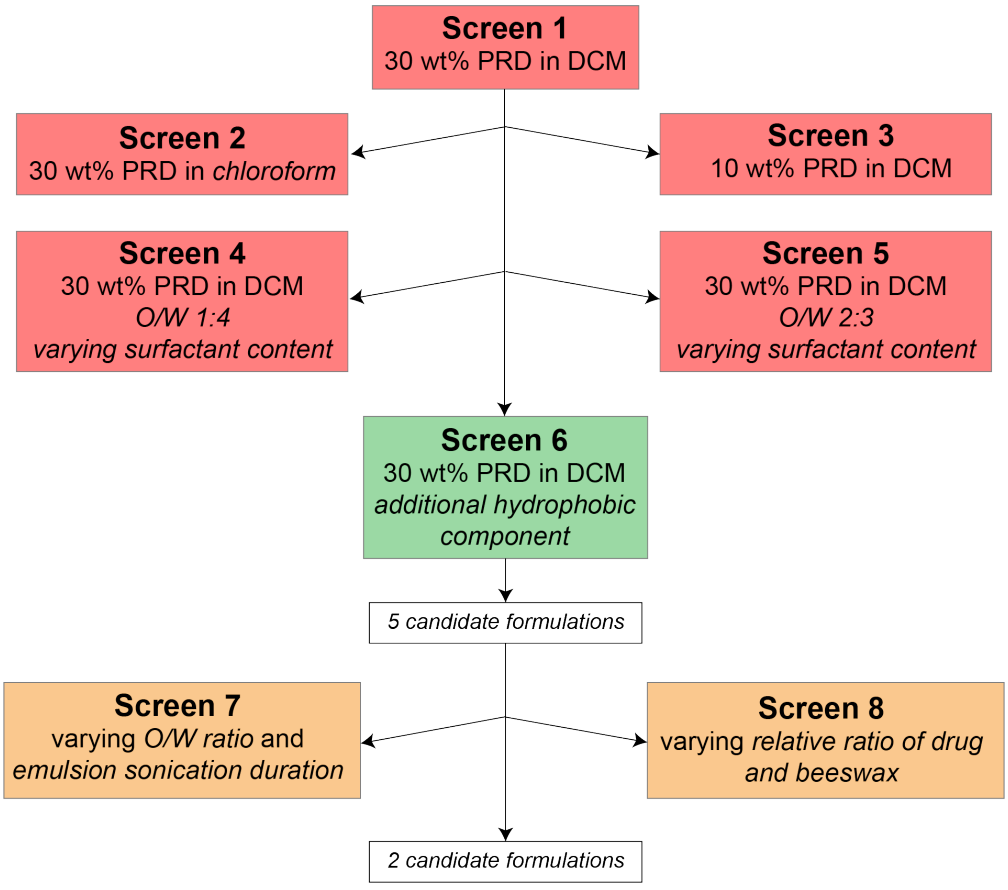

Figure 2.13 Flowchart to illustrate rationale for Screens. Red: variables to reduce particle size were not sufficiently effective. Green: Introduction of an additional hydrophobic component produced sub-micron particles. Orange: variables which did not improve the characteristics or reproducibility of the 5 candidate formulations.

To overcome this, it was hypothesised that altering the hydrophobic phase during the emulsion-forming stage, i.e. the solution of PRD in DCM, might produce a more considerable effect on particle size. To do this, beeswax was selected as an inactive excipient to act as an additional hydrophobic compound included in the DCM solution and this procedure succeeded in producing sub-micron particles (section 2.3.6). Nano-scale particles have previously been produced through the same ETFD method without the need for additional hydrophobic constituents, for example oil red SDNs were produced at 90 nm [101], an efavirenz formulation has an average D_z of 300 nm [102], and a lopinavir formulation has an average D_z of 393 nm [103]. The tendency of PRD to form microparticles despite attempted optimisation of the process may suggest that in this case, the size of particles formed by ETFD is determined chiefly by PRD, and any effects of excipients, sonication and O/W ratio are less substantial and certainly less apparent. This is in agreement with a previous example of SDN production by ETFD, in which the authors found no observable trend associated with excipient concentration and effect on D_z [102].

The observation that co-formulation of PRD with an additional hydrophobic component, BW, enabled formation of sub-micron particles in Screen 6 may be best interpreted in context of Figure 2.8. Having an amorphous state is a desirable property of nanoparticles formulated for improved solubility, as the material will have a higher dissolution rate [120]. Several methods of formulation have been reported which produce amorphous particles containing PRD. Two examples of PRD microparticles stabilised with the amorphous polymers Eudragit E, L and S were shown to be amorphous [121, 122].

Furthermore, production of spray- and freeze-dried amorphous nano-liposomal formulations of PRD has been demonstrated [123].

pXRD analysis of PRD and PRD/BW SDNs indicated that these are crystalline structures. This supports the possible explanation that PRD has a strong tendency to form crystalline particles when produced via ETFD, even when formulated with amorphous excipients. The co-formulation of BW, by merit of its presence in the oil phase together with PRD in the initial mixture of DCM and dH_2O, may permit an interaction between these two hydrophobic components during emulsification, lyophilisation or dispersion which results in BW limiting the growth of PRD crystals during particle formation. Without beeswax, large particles of crystalline PRD are formed (Fig. 2.14, A). Additionally, it seems that for this to occur optimally, the amount of BW in relation to PRD must be equal, as varying the hydrophobic ratio to anything other than 50:50 (Fig. 2.6) generally produced particles which failed due to poor quality DLS data. Interestingly, the D_z of BW-only SDNs are very similar to that of the equivalent lead formulations, indicating that BW may limit particle growth, perhaps by affecting nucleation during the formation of BW SDNs whether or not they also contain PRD.

There are several possibilities for the arrangement of PRD and BW in a dispersed combination particle and although this is unknown, each example lends itself to a different concept of how the particles may be formed during production. Firstly, PRD and BW may be completely mixed within a dispersed particle (Fig. 2.14, B) which could occur if PRD and BW do not behave differently during freezing, solvent removal or redispersion. Secondly, each particle may consist of a PRD core surrounded by a layer of BW (Fig. 2.14, C), which supports the theory that

beeswax prevents excessive PRD particle growth as seen in PRD-only particles. Thirdly, the inverse may occur with particles forming from a core of BW surrounded by a layer of PRD (Fig. 2.14, D).

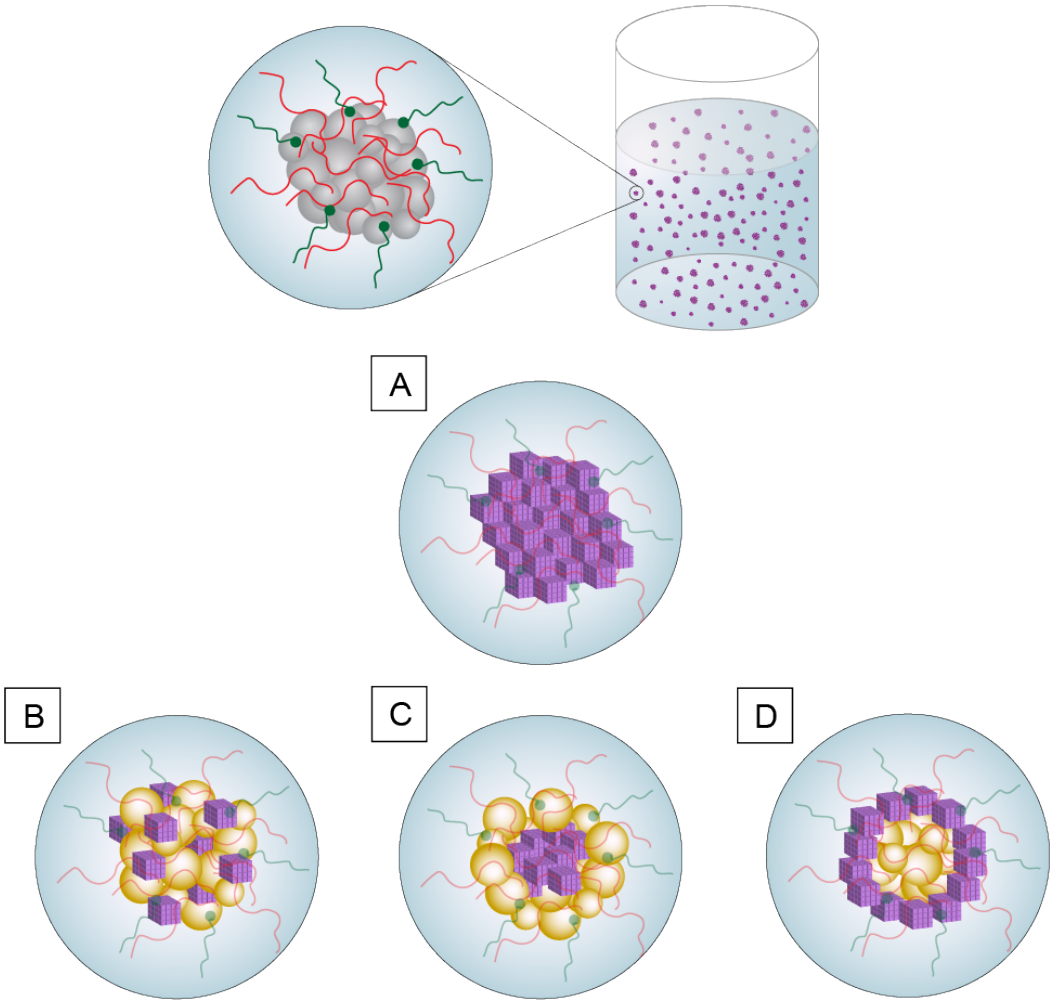

Figure 2.14 Possible structures of PRD and PRD/BW SDNs when dispersed in aqueous media. A: PRD-only SDN, each particle consisting of crystalline PRD (purple), B: PRD/BW combination particle, consisting of a mix of crystalline PRD (purple) and amorphous BW (yellow), C: PRD/BW combination particle, consisting of crystalline PRD (purple) surrounded by BW (yellow), D: PRD/BW combination particle, consisting of BW (yellow) surrounded by crystalline PRD (purple). Red: polymer, green: surfactant.

After progressing with this hydrophobic combination approach, it was again observed that varying factors of the process such as sonication time and O/W ratio were not generally correlatable to outcome of particle size (Fig. 2.5). This supports the hypothesis that the size of PRD SDNs is predominantly influenced by the hydrophobic components.

The drug and particle dispersion stability tests carried out and described in this chapter all produced encouraging results. Firstly, the chemical structure of PRD is stable to the physical stresses of ultrasonication and lyophilisation involved in ETFD SDN production (Figures 2.10 and 2.11). This is of course essential to maintaining the therapeutic action of the drug, which could be altered if the chemical structure is changed in any way. The stability of PRD in SDN formulations is also of importance when it comes to quantifying PRD, as any degradation of drug would lead to a discrepancy between the intended drug loading and measurable drug.

Secondly, PRD SDNs appear to be stable as particle dispersions in a variety of media (Fig. 2.12) for at least six hours. This implies that when dispersed in these media, the SDNs will still be in particle form, allowing any benefits of this formulation to be realised at least in *in vitro* assays using these media. To some extent, the stability of PRD SDNs in simulated gastric and intestinal fluids infers the potential for dispersions of these particles to avoid particle breakdown and dissolution or aggregation in the GI tract *in vivo*, therefore increasing the likelihood of these formulations being absorbed into the systemic circulation as intact nanoparticles. Destabilisation of nanoparticles in GI fluids may be a result of protonation of anionic surfactants at low pH, an effect which has been

observed when phosphatidylcholine- and taurocholate-stabilised cyclosporine-A lipid nanoparticles were incubated in simulated gastric fluid [124]. The surfactants used in the two SDN formulations studied in this Chapter, TPGS and solutol (Fig. 2.15), are both non-ionic; which could explain why both SDN1 and SDN2 were stable in simulated gastric fluid during the six hour incubation.

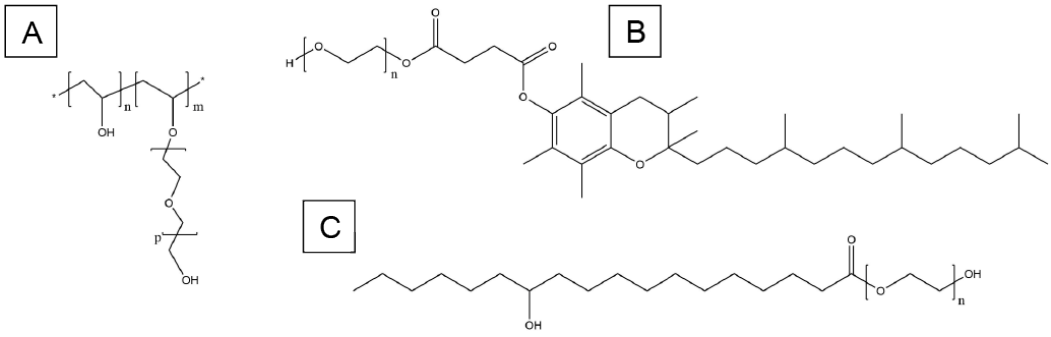

Figure 2.15 Chemical structures of PRD SDN excipients. A: kollicoat, B: TPGS, C: solutol.

Unarguably, simulated body fluids are no real substitute to stability testing in real gastric or intestinal fluid, but there are complications associated with obtaining these, as well as the difficulty of DLS analysis for more complex biological media due to the presence of biomolecules of a similar size to the drug nanoparticles under observation. For this reason, the use of established simulated fluids was deemed acceptable for this work.

With the selection of two PRD/BW SDN formulations for further assessment, the aims of this Chapter have been achieved. These formulations resulted from extensive optimisation of the ETFD process for PRD and have been characterised by DLS, pXRD and stability assessment in several bio-relevant media. The following Chapter will document the continuing assessment of these lead candidates in several *in vitro* investigations.

Acknowledgements

pXRD and SEM were performed by M. Giardiello.

MS and NMR were performed by Chemistry Department Analytical services.

CHAPTER 3

IN VITRO ASSESSMENT OF PRD SDN CYTOTOXICITY, TRANSCELLULAR PERMEATION AND EFFICACY

CONTENTS

3.1 Introduction

In the previous chapter, PRD SDN formulations were successfully developed, and two of these formulations were selected for further assessment. Several *in vitro* tests were selected to investigate the interactions of the SDNs with cells regarding cytotoxicity, transcellular permeation and efficacy.

Firstly, the two SDN candidates were compared with unformulated PRD to determine cytotoxic effects on cell lines *in vitro*. Two cell lines were studied, chosen for their relevance to the proposed future clinical use of the SDNs for oral administration to treat inflammatory diseases. An important site to consider when developing an orally administered formulation is the intestinal epithelium. Here, the drug or nanoparticle will interact with the cells lining the intestinal lumen in order to pass through the barrier and enter the systemic circulation. Nanoparticles have the potential to exert toxic effects on the cells of the GI system, either in a similar manner to the unformulated drug or via an independent mode as a result of the physicochemical properties of the nanoparticle [125]. Depending on the way in which the SDNs cross the intestinal epithelium, if indeed they remain intact rather than dissolving in the intestinal lumen, multiple detrimental effects may occur both extracellularly and intracellularly. These include disruption of tight junctions between cells in monolayers, damage to cell membranes, damage to mitochondria resulting in generation of reactive oxygen species (ROS) and consequent damage to other cellular structures or cell death [126]. Therefore one of the cell lines chosen was Caco-2, derived from human epithelial colorectal adenocarcinoma cells, as a model of the human intestinal epithelium.

The second cell line used was human lung adenocarcinoma cells, A549, as a model of the human alveolar epithelium. This was intended to be a model of a typical target site where PRD would exert its therapeutic effect when used to treat an inflammatory condition, in this case an inflammatory lung disease such as asthma. In contrast to the movement of PRD SDNs across the intestinal epithelium which may occur transcellularly or paracellularly, cellular uptake of PRD is essential for its therapeutic effect and therefore assessment of intracellular damage caused by PRD SDNs was deemed to be important.

For both cell lines, cytotoxicity following incubation with PRD SDNs was determined by MTT and CellTiter-Glo assays and compared with unformulated PRD, unformulated excipients and combinations of these (Results 3.3.1). Both MTT and CellTiter-Glo assays are measures of cellular metabolic activity used to determine mitochondrial function. The basis of the MTT assay is the reduction of the yellow-coloured tetrazolium salt, 3-(4,5-Dimethylthiazol-2-yl)-2,5—diphenyltetrazolium bromide (MTT), by NAD(P)H-oxidoreductases to form purple-coloured formazan crystals which are then spectrophotometrically detected, and assumed to be proportional to the number of viable cells [127]. The CellTiter-Glo assay utilises the ATP-dependent reaction of luciferin and luciferase which produces a chemiluminescent signal proportional to the amount of ATP present, which is in turn proportional to the viability of cells [128].

This chapter also covers the *in vitro* assessment of PRD SDN ability to permeate the intestinal epithelium and reach the systemic circulation (Results 3.3.2). To determine the intestinal transcellular permeation of PRD SDNs, a model of the intestinal epithelium was utilised, consisting of Caco-2 monolayers grown to

confluence on transwell plates (vertically coupled wells separated by a polycarbonate membrane, Fig. 3.1).

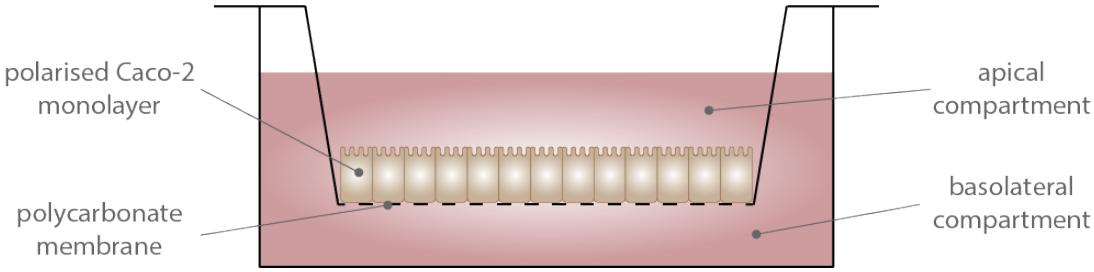

Figure 3.1 A single well of a transwell plate, used as a model of the gut epithelium to study drug transcellular permeation. Caco-2 cells are grown to confluence on the polycarbonate membrane where they form a polarised monolayer. Drug may be added to the apical compartment and transcellular permeation across the monolayer can be measured from the basolateral compartment.

This model is widely used as the Caco-2 cells are able to differentiate and polarise on the membrane, and express transporters involved with uptake or efflux of drugs. However, the limitations of this model include under-expression of some metabolising enzymes such as CYP3A4 and the static nature of the donor and acceptor compartments i.e. no transit of intestinal contents or blood flow as there would be *in vivo* [129]. An important intestinal transporter involved in PRD absorption is P-gp but as this is similarly expressed in both Caco-2 cells and primary human intestinal epithelial cells, the use of the more established Caco-2 model was deemed appropriate for this study [130].

Finally, the *in vitro* efficacy of PRD SDNs against pro-inflammatory immune responses was determined in two models. A549 cells were again used as a model PRD target, and stimulated with TNF-α to produce IL-8 following incubation with PRD SDNs (Results 3.3.4). In response to stimulation by IL-1, lipopolysaccharide (LPS) and tumour necrosis factor (TNF)-α, alveolar epithelial

cells (*in vivo*) and A549 cells secrete IL-8, which acts as a potent neutrophil chemoattractant [131]. Secondly, peripheral blood mononuclear cells (PBMCs) were obtained from healthy volunteer blood samples and used to compare the inhibitory effects of PRD and PRD SDNs against production of IL-4 (Results 3.3.5). *In vivo*, T helper cell type 2 (Th2) lymphocytes, mast cells and basophils produce IL-4, a cytokine responsible for inducing Th2 differentiation [132], activation of M2 macrophages [133] and control of B cell immunoglobulin class expression [134].

The aims of this Chapter were to investigate the cellular interactions of PRD SDNs using *in vitro* models, including assessment of cytotoxicity, transcellular permeation and efficacy. These tests were selected to provide a preliminary indication of the suitability of PRD SDNs for oral administration, by predicting safety, intestinal absorption and therapeutic effect.

3.2 Materials and Methods

3.2.1 Materials

Dulbecco's Modified Eagles Medium (DMEM), Hanks buffered saline solution (HBSS), Trypsin-EDTA, bovine serum albumin (BSA), 4-(2-Hydroxyethyl)piperazine-1-ethanesulfonic acid (HEPES), 3-(4,5-Dimethylthiazol-2-yl)-2,5—diphenyltetrazolium bromide (MTT reagent), D-α-Tocopherol polyethylene glycol 1000 succinate (TPGS), prednisolone (PRD), beeswax (BW), phorbol 12-myristate 13-acetate (PMA), ionomycin, SDS, glacial acetic acid, sulphuric acid (H_2SO_4), Histopaque®-1077 and all general laboratory reagents were purchased from Sigma (Poole, UK). Caco-2 human epithelial colorectal adenocarcinoma cells were purchased from the American Tissue Culture Collection (ATCC) (Manassas, US). A549 cells were purchased from European Cell Culture Authenticated Collection (ECCAC) (Salisbury, UK). Kollicoat® Protect and Solutol HS 15 were purchased from BASF (Ludwigshaven, Germany). Fetal bovine serum (FBS) and Roswell Park Memorial Institute 1640 cell culture medium (RPMI) were purchased from Gibco (Paisley, UK). The CellTiter-Glo® Luminescent Cell Viability Assay kit was from Promega (Wisconsin USA). Tween 20 and dimethylformamide (DMF) were purchased from Fisher Scientific (Loughborough, UK). Tritiated PRD (^{3}H-PRD) was purchased from Moravek (Brea, USA). Gold Star liquid scintillation cocktail was purchased from Meridian Biotechnologies (Surrey, UK). TNF-α was purchased from Peprotech (London, UK). HetaSep™ was purchased from STEMCELL technologies (Cambridge, UK).

3.2.2 Adherent cell culture

3.2.2.1 Caco-2 cell culture

Media for Caco-2 cell culture was prepared by adding 15% sterile filtered FBS to DMEM. Caco-2 cells were initially raised from frozen cell stocks containing 5 million cells per vial in FBS supplemented with 10% DMSO. The vial was rapidly thawed and its contents added to 10 mL pre-warmed media in a Nunc™ T25 flask (Fisher Scientific, Loughborough, UK). Following a 24 hour incubation at 37°C, 5% CO_2, flask media was replaced to remove residual DMSO. Cells were maintained by replacing media every 2-3 days until growth reached 80-90% confluence at which point cells were passaged as follows. Media was aspirated and cells were washed three times with HBSS to remove all media. 5 mL of trypsin-EDTA was added to cells and incubated for 10 minutes. After this time any cells still adhered to the flask surface were dislodged by either gentle tapping of the flask or with a cell scraper. 10 mL of media was added to inactivate the trypsin then the cell suspension was centrifuged for 5 minutes at 2000 RPM. The supernatant was discarded and the cell pellet resuspended with 1 mL of media. This suspension was diluted as required to allow cell counting to determine appropriate counts for reseeding flasks or experimental use. Cells were reseeded when necessary to expand or maintain stocks in 20 mL media in Nunc T75 flasks or in 35 mL media in Nunc T125 flasks as appropriate. Cell counts were performed using a NucleoCounter® (Chemometec, Denmark) automated system.

3.2.2.2 A549 cell culture

Media for A549 cell culture was prepared by adding 10% sterile filtered FBS to DMEM. A549 cells were initially raised from frozen cell stocks containing 5 million cells per vial in FBS supplemented with 10% DMSO. The vial was rapidly thawed and its contents added to 10 mL pre-warmed media in a Nunc™ T25 flask (Fisher Scientific, Loughborough, UK). Following a 24 hour incubation at 37°C, 5% CO_2, flask media was replaced to remove residual DMSO. Cells were maintained by replacing media every 2-3 days until growth reached 80-90% confluence at which point cells were passaged as in section 3.2.2.1. Cell counts were performed using a haemocytometer.

3.2.3 Cytotoxicity of PRD SDNs in Caco-2 and A549 cells

96-well plates were seeded at a density of 1 x 10^5 cells (Caco-2 or A549) per well and allowed to adhere for 24 hours at 37°C, 5% CO_2. Media was aspirated and replaced with media containing various concentrations of PRD, SDN, excipients or a combination of the above as described in Table 3.1.

Table 3.1 Concentration ranges of PRD, SDN, excipients or combinations added to cells for cytotoxicity assays.

<table>
<tr><td rowspan="3">Concentrations (µg mL^{-1} PRD or BW):
36, 18, 9, 4.5, 2.25, 1.13, 0.563, 0.281, 0.141, 0.07</td><td rowspan="3">Aqueous PRD

SDN1
SDN2</td><td rowspan="3">SDN1 (PRD only)
SDN2 (PRD only)
SDN1 (BW only)
SDN2 (BW only)</td><td rowspan="3">[aqueous PRD + Kollicoat + TPGS]</td></tr>
<tr><td rowspan="2">Concentrations (µg mL^{-1} polymer):
100, 50, 25, 12.5, 6.25, 3.125, 1.563, 0.781, 0.391, 0.195</td><td rowspan="2">Kollicoat</td></tr>
<tr><td rowspan="2">[Kollicoat + TPGS]</td></tr>
<tr><td>Concentrations (µg mL^{-1} surfactant):
25, 12.5, 6.25, 3.125, 1.563, 0.781, 0.391, 0.195, 0.0975, 0.048</td><td>TPGS

Solutol</td><td>[Kollicoat + Solutol]</td><td>[aqueous PRD + Kollicoat + Solutol]</td></tr>
</table>

Control wells consisted of cells and untreated media (negative) and no cells and untreated media (positive). Plates were incubated at 37°C, 5% CO_2 for 24 or 120 hours prior to analysis.

The excipients were studied alone and in combination with each other and aqueous PRD to determine if any cytotoxic effects could be attributed to PRD, excipients or SDNs. As BW could not be solubilised to study on its own, BW-only SDNs (i.e. containing no PRD) were produced as described in Chapter 2, section 2.2.8. PRD-only SDNs (i.e. containing no BW) were also produced for comparison.

3.2.3.1 MTT assay

Following the incubation period, 20 µL MTT reagent (5 mg mL^{-1}) was added to each well then incubated for a further 2 hours. Cells were then lysed with MTT lysis buffer (50% DMF, 10% SDS, adjusted to pH 3.2 using glacial acetic acid) and incubated for a further 24 hours, before absorbance of wells was measured using a Tecan GENios plate reader (Tecan Group, Manndorf, Switzerland) set to 560 nm.

3.2.3.2 CellTiter-Glo assay

Following the incubation period, plates were equilibrated to room temperature for 30 minutes. Wells were then aspirated to leave 20 µL to which was added 20 µL CellTiter-Glo reagent. Plates were placed on an orbital shaker for 10 minutes to allow the luminescent signal to stabilise then luminescence was measured using a Tecan GENios plate reader.

3.2.4 Transcellular permeation of PRD across Caco-2 monolayer

Half scale radiolabelled SDNs were prepared as described in section 2.2.11 with the addition of tritiated PRD (^{3}H-PRD) to the original PRD/BW solution in DCM. Immediately before addition to cells, one vial of freeze dried product per formulation was reconstituted with transport buffer (HBSS, 25mM HEPES, 0.1% BSA) then diluted further in transport buffer to make dispersions of 5 or 10 μM PRD.

24-well transwell plates (polycarbonate membrane, 3.0 μM pore size – Corning, NY, USA) were seeded with 3.5 x 10^4 cells per apical compartment. Cells were incubated for 24 hours at 37°C, 5% CO_2 to allow adherence to the transwell membrane. Media was replaced every 2-3 days. Trans-epithelial electrical resistance (TEER) values were monitored over 14-21 days until they were between 600 and 1800Ω, indicating a tight monolayer had been formed. When TEER values had reached this range, plates were treated with each radiolabelled SDN or aqueous radiolabelled PRD solution diluted to a concentration of 10 or 5 μM with transport buffer either in the apical compartment or the basolateral compartment. Adjacent compartments and control wells consisted of transport buffer. Samples of 100 μL were taken from adjacent compartments at 1, 2, 3 and 4 hours and replaced with 100 μL transport buffer. 4ml scintillation fluid was added to samples then measured for radioactivity on a Packard 3100 TR liquid scintillation analyser.

3.2.4.1 Transcellular permeation of mannitol across Caco-2 monolayer

Following the 4 hour incubation and sampling of wells, 250 μL of carbon-14 (^{14}C) radiolabelled mannitol was added to three 4-hour treated apical

compartments of each plate and incubated for 1 hour. After this period 100 µL samples were taken from each basolateral well to which 4ml scintillation fluid was added. Samples were measured for radioactivity on a Packard 3100 TR liquid scintillation analyser.

3.2.5 Quantification of SDN drug loading

Extraction and HPLC methods were optimised to determine drug loading of PRD SDNs. To solubilise PRD, an extraction method was developed to dissolve the SDNs. The HPLC method was optimised to produce a chromatogram with a clear PRD peak distinct from matrix noise.

3.2.5.1 Extraction of prednisolone from SDNs

SDNs redispersed to 1 mg mL^{-1} were diluted to 2 µg mL^{-1} in dH_2O, then 500 µL of this was diluted in 2 mL ethanol and mixed on an orbital shaker for one hour. Following this, the sample was dried for 4.5 hours at 40°C in a vacuum centrifuge. The resulting dry residue was reconstituted in 500 µL 40% acetonitrile (ACN) and transferred to an Eppendorf. A further 500 µL 40% ACN was added to the dried vial, vortexed and transferred to the same Eppendorf. The dried vial was then centrifuged for five minutes at 1000 RPM to facilitate collection of residual liquid. 200 µL samples of extracted PRD were added to 1.8 mL HPLC vials then immediately analysed by HPLC.

3.2.5.2 HPLC method

A calibration curve was produced with a top concentration of 8000 ng mL^{-1} PRD in 40% ACN and seven further points ranging down to 62.5 ng mL^{-1}, produced by successive 1 in 2 dilutions with 40% ACN. Quality control samples were also

included in each run consisting of high: 7000 ng mL^{-1}, medium: 700 ng mL^{-1} and low: 70 ng mL^{-1} concentrations of PRD in 40% ACN. A chemical mix was included in each run consisting of 200 µL of a 1µg mL^{-1} of PRD in 40% ACN. An equivalent "extracted" chemical mix was also included in each run, produced by applying the extraction method (3.2.6.1) to 1 µg non-formulated PRD in 500 µL 40% ACN. Mobile phases consisted of: (A) dH_2O and (B) 100% ACN. The initial starting conditions of each run were 40% B, changing to 90% after 5.2 minutes and holding at this percentage for 2.1 minutes. The final 2.2 minutes of the run returned the flow to 40% B, ready for the injection of the next sample. PRD was eluted at around 3 minutes into the run. The flow throughout the run was 1 mg mL^{-1}.

3.2.6 Efficacy of SDN inhibition of IL-8 production in A549 cells

3.2.6.1 Cell incubation

1 x 10^5 A549 cells in 1 ml DMEM were added to each well of 24 well plates. Cells were incubated at 37°C, 5% CO_2 until adherent. Once confluent, PRD or SDN was added to each well to achieve final concentrations of 0.01, 0.1, 1, 10 and 100 ng mL^{-1}. One hour later, TNF-α was added at 10 ng mL^{-1} then cells were incubated for 24 hours. Following this, supernatants were collected and frozen at -20°C prior to analysis by ELISA. Control wells were included consisting of no cells or cells with TNF-α only (no drug).

3.2.6.2 IL-8 ELISA

To measure IL-8 produced by A549s, an R&D Human CXCL8/IL8 DuoSet® ELISA Development kit was used.

Mouse anti-human IL-8 capture antibody was diluted to 4 μg mL^{-1} in PBS, added to Nunc MaxiSorp 96-well plates and incubated overnight at room temperature. Plates were washed with a 0.05% Tween 20/PBS wash buffer three times then blocked with 1% BSA in PBS for 1 hour at room temperature. Seven standards were prepared from a 2-fold serial dilution of 2000 pg mL^{-1} of recombinant human IL-8 diluted with a reagent diluent consisting of 0.1% BSA and 0.05% Tween 20 in PBS. Cell supernatant samples were thawed and diluted 1 in 50 (TNF-α, 0.01, 0.1 and 1 ng mL^{-1} drug concentration) or 1 in 20 (0, 10 and 100 ng mL^{-1} drug concentration) with reagent diluent. Plates were washed as before then incubated for 2 hours at room temperature with standards and samples added in duplicate. Plates were washed as before then incubated for 2 hours with 20 ng mL^{-1} of biotinylated goat anti-human IL-8 detection antibody diluted in reagent diluent. Following a further wash, plates were incubated for 20 minutes with 0.005% streptavidin conjugated to horseradish peroxidase diluted with reagent diluent. After a final wash, substrate solution was added to each well and colour was allowed to develop for about 5 minutes. 2N sulphuric acid (H_2SO_4) was added to stop the reaction then well absorbance was read at 450 nm on a BioTek ELx800 plate reader.

3.2.7 Efficacy of SDN inhibition of IL-4 production in PBMCs

3.2.7.1 PBMC isolation from whole blood

Approval for the sampling and storage of human blood samples under the protocol "Analysis of normal blood leukocyte function using cells from healthy volunteers" was gained from the University of Liverpool Committee in Research Ethics (Ref: RETH000773).

Immediately after collection, whole blood was mixed with HetaSep™ to the ratio 5:1. The mixture was incubated at room temperature for thirty minutes until it had separated to approximately half plasma and half red blood cells (RBCs). The plasma layer was removed and added to four-fold volume of PBS, then centrifuged for ten minutes at 200 g. The pellet was resuspended in 1 mL RPMI, layered onto 2 mL Histopaque®-1077 then centrifuged for twenty minutes at 2000 RPM. The resulting supernatant (PBMC layer) was removed and washed with an equal volume of PBS, centrifuged for five minutes at 3000 RPM then the pellet was resuspended in RPMI.

3.2.7.2 Cell incubation

PBMCs were counted using a haemocytometer slide and adjusted to 1 million cells per mL in RPMI. 500 µL of this suspension was added to the wells of 24 well plates to achieve 5 x 10^5 cells per well. PRD or SDN was added to each well to achieve final concentrations of 0.1, 10 and 100 ng mL^{-1}. Four hours later, phorbol 12-myristate 13-acetate (PMA) and ionomycin were added at 1 µg mL^{-1} then cells were incubated for 24 hours. Following this, entire well contents were centrifuged for five minutes at 3000 RPM to remove cells, then the supernatants were collected and frozen at -20°C prior to analysis by ELISA. Control wells were included consisting of no cells or cells with PMA and ionomycin only (no drug).

3.2.7.3 IL-4 ELISA

To measure IL-4 produced by PBMCs, an Affymetrix Human IL-4 ELISA Ready-SET-Go!® kit was used.

Anti-human IL-4 capture antibody was diluted in coating buffer, added to Nunc MaxiSorp 96-well plates and incubated overnight at 2-8 °C. Plates were soaked for one minute with wash buffer three times then blocked with ELISA diluent for 1 hour at room temperature. Seven standards were prepared from a 2-fold serial dilution of 200 pg mL^{-1} of recombinant human IL-4 diluted with ELISA diluent. Plates were washed as before then incubated for 2 hours at room temperature with standards and undiluted samples added in duplicate. Plates were washed as before then incubated for 1 hour with anti-human IL-4 Biotin detection antibody diluted in ELISA diluent. Following five washes, plates were incubated for 30 minutes with Avidin-HRP. After five washes, 3,3',5,5'-Tetramethylbenzidine (TMB) solution was added to each well and colour was allowed to develop for 15 minutes. 2N H_2SO_4 was added to stop the reaction then plates were measure for absorbance at 450 nm on a CLARIOstar plate reader (BMG Labtech).

3.2.8 Data analysis

Cytotoxicity data were analysed using Graphpad Prism 5 software, using a non-linear regression sigmoidal dose response curve analysis, after data had been expressed as percentage of control and log transformed. Cytotoxic concentrations causing 50% cell death (CC_{50} values) were derived from these curves. All data were presented as mean ± standard deviation of experiments conducted in quadruplicate (concentration-response curves, Appendices I and II).

Apparent permeability (P_{app}) of PRD delivered as an aqueous solution or in SDN formulations to Caco-2 monolayers was determined by the following equation:

$$P_{app} = \frac{\left(\frac{dQ}{dt}\right) \times v}{A \times C_0}$$

Where *dQ/dt* is the rate of drug transport (μM min^{-1}); *v* is the volume of the receiver compartment (mL); *A* is the surface area of the membrane (cm^2); and C_0 is the initial concentration of drug added to the donor compartment (μM).

Cytokine expression data were expressed as percentage of control. Statistical analysis was performed using SPSS 22 and GraphPad Prism 5 for Windows. Data was assessed for normality using the Shapiro-Wilk test, then analysed by T test to determine significance between aqueous PRD (control) and SDN1 or SDN2.

3.3 Results

3.3.1 Cytotoxicity of PRD SDNs in Caco-2 and A549 cells

Cytotoxicity of PRD SDNs, aqueous PRD, excipients, PRD-only and BW-only SDNs was assessed in Caco-2 and A549 cells by measuring cell viability following 24 and 120 hour incubations with the materials using MTT and CellTiter-Glo assays. Cell viability was calculated as percentage of non-treated control wells average cell viability, log transformed and plotted as sigmoidal dose-response curves. For dose-response curves, see Appendices I (MTT) and II (CellTiter-Glo). Cytotoxic concentrations causing 50% cell death (CC_{50} values) were derived from these curves, but in some cases this was not possible due to insufficient cytotoxicity observed across the concentration range used.

3.3.1.1 MTT assay

Following 24 hours incubation with Caco-2 cells, for all materials and combinations, 50% cytotoxicity was not observed within the range of concentrations studied, thus all CC_{50} values were extrapolated and not considered reliable (Table 3.2). From these data, all of the materials and combinations tested were considered not cytotoxic at relevant concentrations.

Following 120 hours incubation with Caco-2 cells, a decrease in viability was observed in cells treated with higher concentrations of SDN1 and SDN2, CC_{50} values of 0.83 and 1.2 μg mL^{-1} respectively, compared to aqueous PRD, CC_{50} N/D (Table 3.2). For the other materials and combinations, 50% cytotoxicity was not observed within the range of concentrations studied. From these data, SDN1 and SDN2 may be cytotoxic at higher concentrations if cells are exposed for 120

hours. The other materials and combinations tested were considered not cytotoxic at relevant concentrations.

Table 3.2 Average CC_{50} values for treatments incubated with Caco-2 or A549 cells for 24 or 120 hours, determined by MTT assay. N/D: not determined within concentration range. N = 8.

Treatment	Caco-2 CC_{50} (µg mL^{-1})		A549 CC_{50} (µg mL^{-1})	
	24 hours	120 hours	24 hours	120 hours
Aqueous PRD	N/D	N/D	N/D	3.5
PRD/BW SDN1	N/D	0.83	N/D	N/D
PRD/BW SDN2	N/D	1.2	3.5	N/D
Aqueous PRD + kollicoat + TPGS	N/D	N/D	N/D	N/D
Aqueous PRD + kollicoat + solutol	N/D	N/D	N/D	N/D
Kollicoat + TPGS	N/D	43.4	N/D	N/D
Kollicoat + solutol	N/D	50.7	N/D	N/D
Kollicoat	N/D	N/D	N/D	N/D
TPGS	N/D	N/D	N/D	N/D
Solutol	N/D	11.7	N/D	N/D
PRD SDN1	N/D	N/D	N/D	N/D
PRD SDN2	N/D	N/D	N/D	N/D
BW SDN1	3.3	N/D	N/D	N/D
BW SDN2	N/D	0.72	1.5	N/D

Following 24 hours incubation with A549 cells, an increase in cytotoxicity was observed in cells treated with higher concentrations of SDN1 (Table 3.2). SDN1 caused just less than 50% cytotoxicity at the highest concentration, so the CC_{50} value is fairly reliable despite being extrapolated. The CC_{50} value for SDN1 is much higher than the concentrations used in *in vitro* assays*, in vivo* experiments and for therapeutic doses of PRD. For the other materials and combinations, 50% cytotoxicity was not observed within the range of concentrations studied. From these data, all materials and combinations tested were considered not cytotoxic at relevant concentrations.

Following 120 hours incubation with A549 cells, an increase in cytotoxicity was observed in cells treated with higher concentrations of [Aqueous PRD + kollicoat + TPGS] and [kollicoat + TPGS] (Table 3.2). [Aqueous PRD + kollicoat + TPGS] caused just more than 50% cytotoxicity at the highest concentration, so the CC_{50} value is reliable. However, the CC_{50} value for [Aqueous PRD + kollicoat + TPGS] is much higher than the concentrations used in *in vitro* assays*, in vivo* experiments and for therapeutic doses of PRD. For the other materials and combinations, 50% cytotoxicity was not observed within the range of concentrations studied. From these data, all materials and combinations tested were considered not cytotoxic at relevant concentrations.

3.3.1.2 CellTiter-Glo assay

Following 24 hours incubation with Caco-2 cells, no cytotoxicity was observed in cells treated with any of the materials or combinations (Table 3.3). For all materials and combinations, 50% cytotoxicity was not observed within the range of concentrations studied. From these data, all of the materials and combinations tested were considered not cytotoxic at relevant concentrations.

Following 120 hours incubation with Caco-2 cells, an increase in cytotoxicity was observed in cells treated with higher concentrations of [kollicoat + TPGS], and TPGS (Table 3.3). [kollicoat + TPGS], and TPGS caused greater than 50% cytotoxicity at the highest concentration, so these CC_{50} values are reliable. For the other materials and combinations, 50% cytotoxicity was not observed within the range of concentrations studied. From these data, [kollicoat + TPGS] and TPGS may be cytotoxic at higher concentrations if cells are exposed for 120

hours. The other materials and combinations tested were considered not cytotoxic at relevant concentrations.

Table 3.3 Average CC_{50} values for treatments incubated with Caco-2 or A549 cells for 24 or 120 hours, determined by CellTiter-Glo assay. N/D: not determined within concentration range. N = 8.

Treatment	Caco-2 CC_{50} (µM or µg mL^{-1})		A549 CC_{50} (µM or µg mL^{-1})	
	24 hours	120 hours	24 hours	120 hours
Aqueous PRD	N/D	N/D	N/D	N/D
PRD/BW SDN1	N/D	N/D	N/D	N/D
PRD/BW SDN2	N/D	N/D	N/D	N/D
Aqueous PRD + kollicoat + TPGS	N/D	N/D	N/D	N/D
Aqueous PRD + kollicoat + solutol	N/D	N/D	N/D	N/D
Kollicoat + TPGS	N/D	49.0	N/D	N/D
Kollicoat + solutol	N/D	N/D	N/D	N/D
Kollicoat	N/D	N/D	N/D	N/D
TPGS	N/D	6.8	N/D	N/D
Solutol	N/D	N/D	N/D	N/D
PRD SDN1	N/D	N/D	N/D	N/D
PRD SDN2	N/D	N/D	N/D	N/D
BW SDN1	N/D	N/D	N/D	N/D
BW SDN2	N/D	N/D	N/D	N/D

Following 24 hours incubation with A549 cells, 50% cytotoxicity was not observed within the range of concentrations studied (Table 3.3). From these data, all of the materials and combinations tested were considered not cytotoxic at relevant concentrations.

Following 120 hours incubation with A549 cells, 50% cytotoxicity was not observed within the range of concentrations used, thus all CC_{50} values are extrapolated and not reliable. From these data, all of the materials and combinations tested were considered not cytotoxic at relevant concentrations (Table 3.3).

3.3.2 Transcellular permeation of PRD SDNs across Caco-2 monolayer

Transcellular permeation of PRD across a Caco-2 monolayer was studied as a model of intestinal absorption. Mannitol, a sugar which is usually unable to permeate intact monolayers, was added to wells following 4 hour incubation with drug to assess monolayer integrity.

SDN 1 showed enhanced permeation in the A → B direction and decreased permeation in the B → A direction compared to aqueous PRD (Fig. 3.2). SDN 2 showed a similar permeability profile but the large error in the A → B data reduced its reliability (Fig. 3.2). No significant differences were found at each time point for apical to basolateral permeation. Basolateral to apical permeation of PRD was significantly lower at all time points for Caco-2 cell monolayers treated with SDNs 1 and 2 compared to aqueous PRD (Table 3.4) ($P < 0.05$).

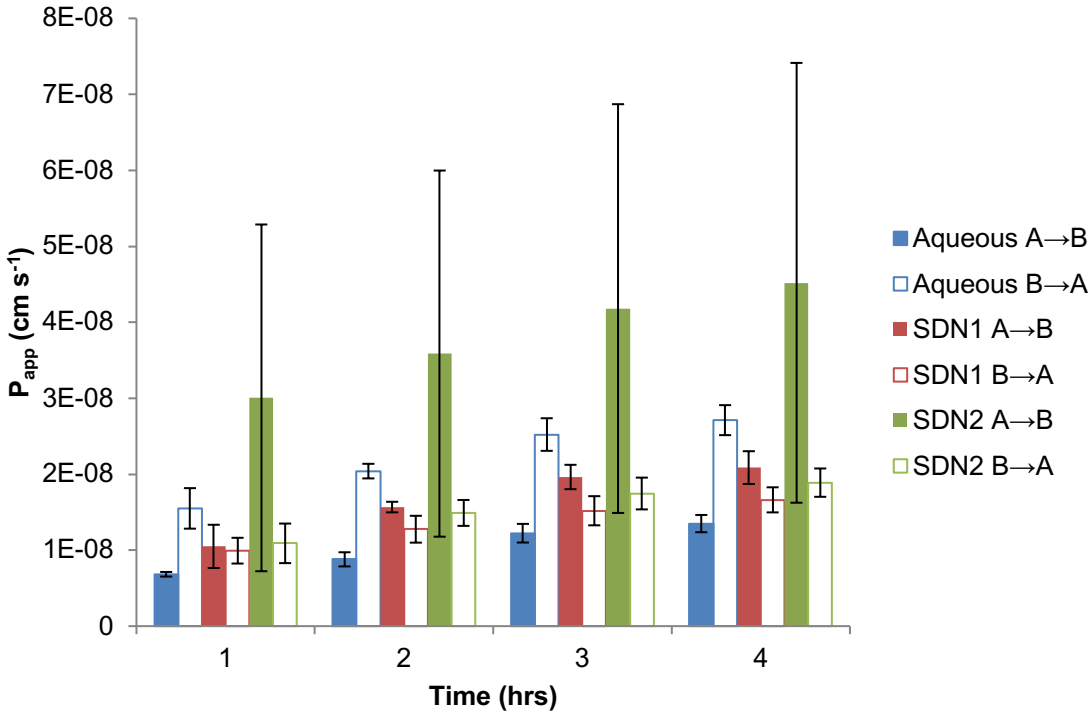

Figure 3.2 Cumulative apparent permeability (P_{app}) of 10 µM PRD across a Caco-2 monolayer in aqueous or SDN form. (A → B apical to basolateral movement, B → A basolateral to apical movement). N = 4.

Table 3.4 *P*-values calculated by T test analysis of basolateral to apical apparent permeability of 10 µM PRD across Caco-2 monolayers treated with SDNs 1 and 2 compared to control (aqueous PRD).

Time (hrs)	SDN1	SDN2
1	0.013	0.049
2	0.0003	0.0014
3	0.0004	0.0021
4	0.0002	0.0009

P_{app} of mannitol in wells treated with SDNs 1 and 2 was higher than that of aqueous PRD (Fig. 3.3). This indicated that the cell monolayer may have become compromised following incubation with SDNs 1 and 2, therefore allowing mannitol to pass through to the basolateral compartment.

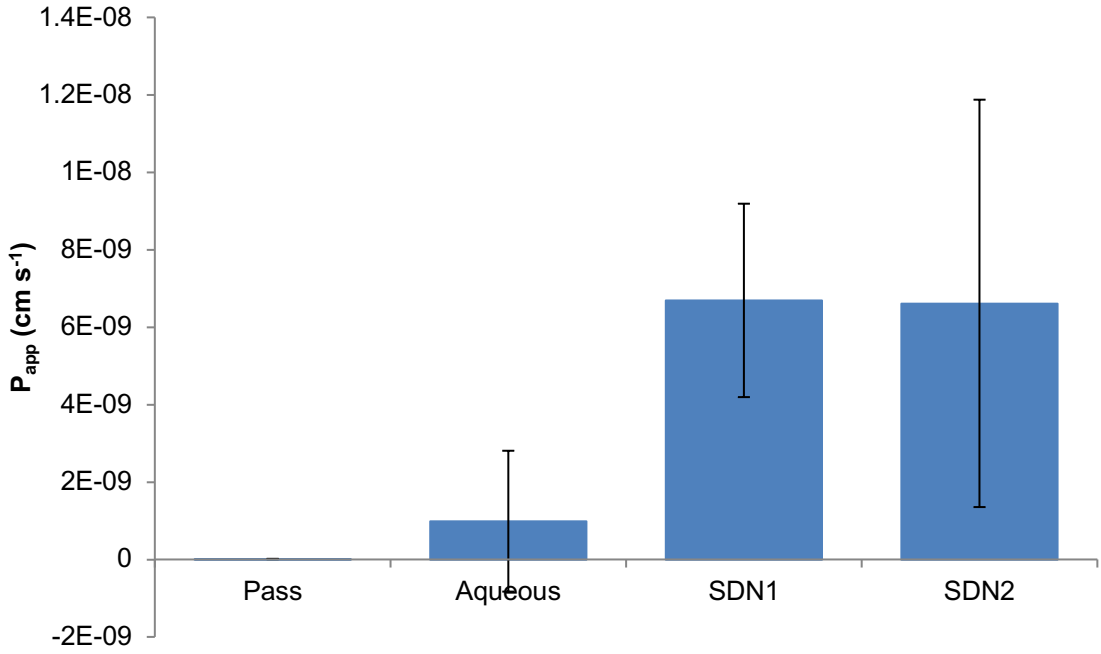

Figure 3.3 Cumulative apparent permeability (P_{app}) of mannitol across a Caco-2 monolayer at 4 hours in parallel with 10 µM aqueous PRD or PRD SDN. N = 4.

When PRD concentration was decreased to 5 µM, apical to basolateral permeation of PRD was greater for SDN1 compared to aqueous PRD at all time points but was not significant (Fig. 3.4). Apical to basolateral permeation of PRD was greater for SDN1 compared to aqueous PRD at 2, 3 and 4 hours but was only significantly higher at 2 hours (P = 0.041). Basolateral to apical permeation of PRD was significantly higher at all time points for Caco-2 monolayers treated with SDNs 1 and 2 compared to aqueous PRD (Table 3.5).

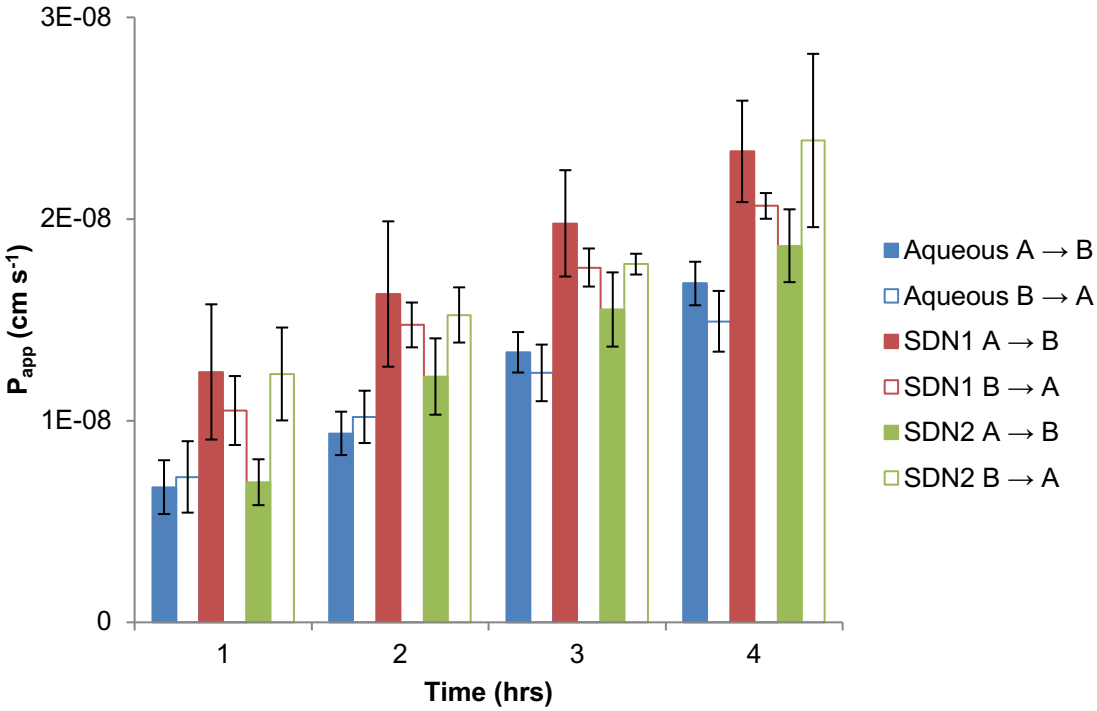

Figure 3.4 Cumulative apparent permeability (P_{app}) of 5 µM PRD across a Caco-2 monolayer in aqueous or SDN form. (A → B apical to basolateral movement, B → A basolateral to apical movement). N = 4.

Table 3.5 *P*-values calculated by T test analysis of basolateral to apical apparent permeability of 5 µM PRD across Caco-2 monolayers treated with SDNs 1 and 2 compared to control (aqueous PRD).

Time (hrs)	SDN1	SDN2
1	0.037	0.012
2	0.0018	0.02
3	0.0008	0.0285
4	0.0004	0.0036

Apparent permeability of mannitol in wells treated with SDNs 1 and 2 was comparable with that of wells treated with aqueous PRD (Fig. 3.5). However the P_{app} for these three conditions, as well as that of untreated wells, was above the maximum P_{app} limit. This indicated that the cell monolayer may be

compromised after four hours with or without added drug, therefore allowing mannitol to pass through to the basolateral compartment.

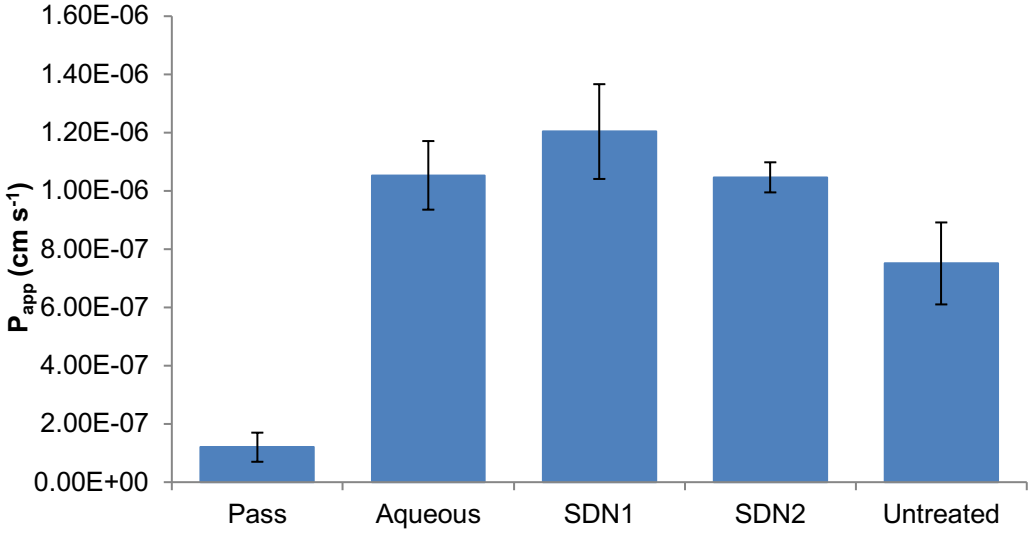

Figure 3.5 Cumulative apparent permeability (P_{app}) of mannitol across a Caco-2 monolayer at 4 hours in parallel with 5 µM aqueous PRD or PRD SDN. N = 4.

3.3.3 PRD HPLC calibration curve

Extraction and HPLC quantification methods were developed for PRD/BW SDNs. A calibration of known concentrations of unformulated PRD was performed and peak area at 253 nm was found to be linear in this concentration range (Fig. 3.6).

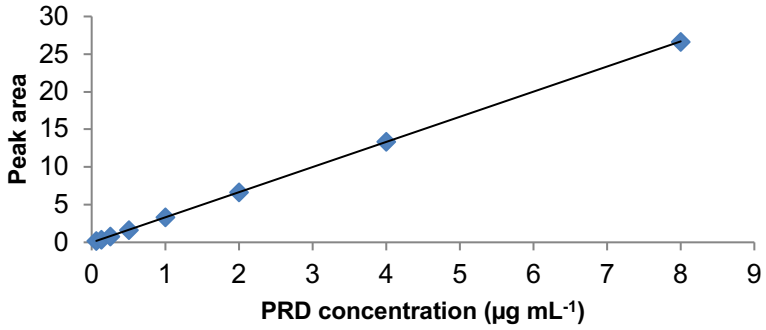

Figure 3.6 Calibration curve produced with an 8-point 1:1 serial dilution of aqueous PRD from 8 µg mL^{-1} to 0.0625 µg mL^{-1} in 40% ACN. R^2 = 0.999992.

3.3.4 Efficacy of SDN inhibition of IL-8 production in A549 cells

Inhibition of A549 IL-8 expression by PRD SDNs 1 and 2 was comparable to inhibition by aqueous PRD at all concentrations (Fig. 3.7).

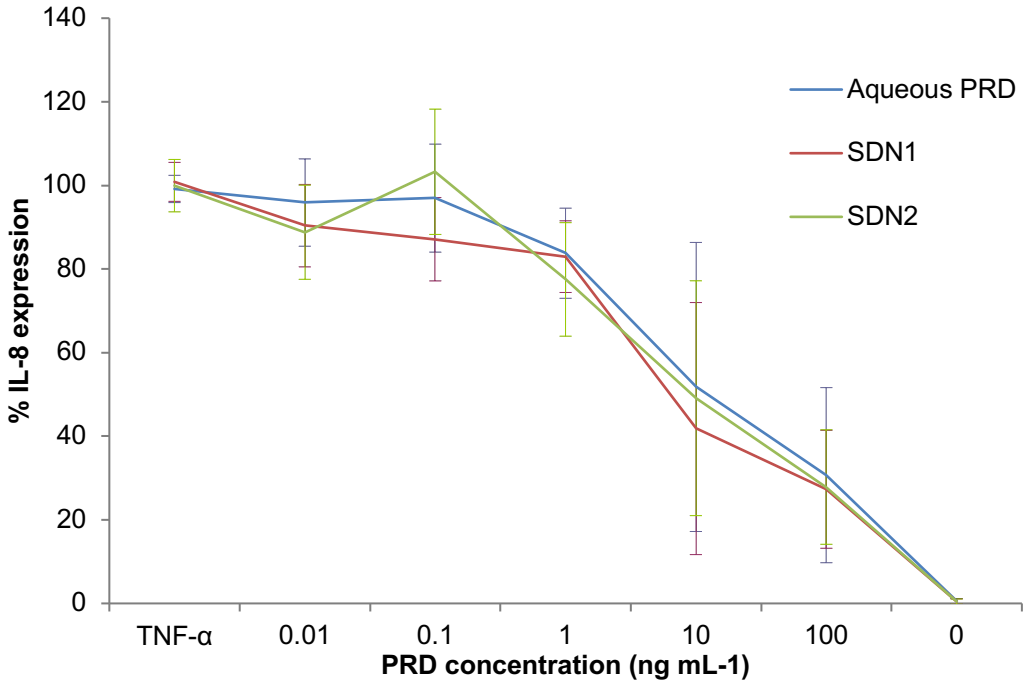

Figure 3.7 Average IL-8 expression observed following three repeat incubations of A549 cells with TNF-α and aqueous PRD or PRD SDNs, displayed as percentage of positive control (TNF-α, no drug). 0 = negative control, no TNF-α or drug. Error bars depict standard deviation on three repeats (N = 3).

3.3.5 Efficacy of SDN inhibition of IL-4 production in PBMCs

Inhibition of PBMC IL-4 expression by PRD SDNs 1 and 2 was comparable to inhibition by aqueous PRD at 100 ng mL^{-1} (Fig. 3.8). When treated with 0.1 ng mL^{-1} SDN1, IL-4 expression was significantly higher than cells treated with SDN2 or aqueous PRD ($P < 0.0001$). When treated with 10 ng mL^{-1} SDN2, IL-4 expression was significantly lower than cells treated with SDN1 or aqueous PRD ($P < 0.0001$).

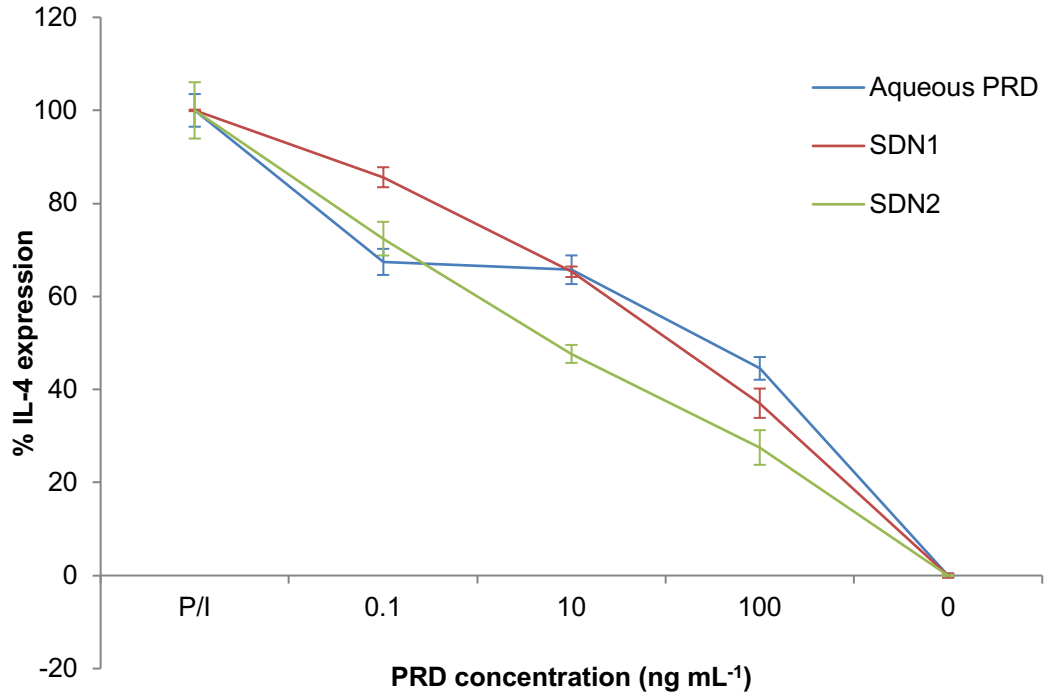

Figure 3.8 Average IL-4 expression observed following incubation of PBMCs with PMA/ionomycin and aqueous PRD or PRD SDNs, displayed as percentage of positive control (P/I: PMA and ionomycin, no drug). 0 = negative control, no PMA/ionomycin or drug. N = 1 (error bars show standard deviation between 4 repeats).

3.4 Discussion

Cytotoxicity of PRD SDNs was assessed in Caco-2 and A549 cell lines, determined by both MTT and CellTiter-Glo assays. A decrease in cell viability was observed following 120 hour incubations of SDN1 as well as SDN2 with Caco-2 cells determined by MTT assay, compared to aqueous PRD which did not decrease cell viability even at high concentrations (section 3.3.1.1, Table 3.2). However, when assessed by CellTiter-Glo assay, Caco-2 cells incubated with SDNs 1 and 2 as well as aqueous PRD for 120 hours showed comparable decreases in cell viability (section 3.3.1.2, Table 3.3). This could suggest the materials may be cytotoxic *in vivo* when orally administered at higher concentrations, but only if they persisted in proximity to the intestinal epithelium for 120 hours or more as could occur with successive dosing. A smaller decrease in viability was seen in A549 cells incubated with higher concentrations of SDNs 1 and 2 for 24 and 120 hours when assessed by MTT assay (section 3.3.1.1, Table 3.2). However, no decrease in viability was observed in the same 24 and 120 hour incubations when assessed by CellTiter-Glo assay (section 3.3.1.2, Table 3.3). As the CellTiter-Glo assay is arguably a more sensitive measure of cell viability as it can measure very small amounts of ATP, this result may be more illustrative of actual SDN cytotoxicity or any perturbation of cell homeostasis that would result in a change of ATP concentration [135].

Both MTT and CellTiter-Glo assays as used in these experiments can only provide a limited evaluation of cytotoxicity for several reasons. Firstly, as described in this chapter's Introduction, cell lines such as Caco-2 and A549 are used as isolated models of particular cell types and each will lack several features

of the *in vivo* systems they are emulating. These features include individual cell components such as transporters and enzymes, and interactive processes which *in vivo* would occur between different cell types within a tissue and in response to the extracellular environment. For example, transport across the intestinal epithelium also involves M cells and goblet cells, and the mucous layer secreted by the latter may provide a protective barrier against direct nanoparticle interactions with epithelial cells [136]. Secondly, both MTT and CellTiter-Glo assays measure mitochondrial activity as a marker of cell viability, through reduction of MTT reagent by mitochondrial enzymes and reaction of luciferase with ATP, the product of mitochondrial respiration, respectively. Mitochondrial activity is representative of the overall health of a cell, as any negative effects of a drug or nanoparticle on mitochondrial respiration will impact on normal cellular function. However, drugs and nanoparticles may have negative effects on cells via mechanisms not involving the mitochondria and therefore it would be prudent to evaluate these also. Other cytotoxicity assays which could be used include lactase dehydrogenase (LDH) assay, which is based on measuring extracellular LDH as a consequence of cell membrane damage [137], and neutral red assay, which measures uptake of neutral red into lysosomes and can indicate damage to lysosome or cell membranes [135].

At both 5 and 10 μM, SDN1 showed increased transcellular permeation across the Caco-2 monolayer into the basolateral compartment and equivalent or decreased permeation in the opposite direction into the apical compartment compared to aqueous PRD (section 3.3.2, Figs. 3.2 and 3.4). This implies that SDN1 may promote improved absorption of PRD from the intestinal lumen to the circulatory system *in vivo*. The large error between repeats of 10 μM SDN2

prevent a reliable conclusion to be taken from these results (section 3.3.2, Fig. 3.2).

To check the integrity of the Caco-2 monolayers, TEER values were obtained before addition of drug and these were within the acceptable range. However, mannitol movement was detected in all wells, including untreated wells, 4 hours after drug addition, indicating compromised monolayers (section 3.3.2, Figs. 3.3 and 3.5). As such, it cannot be assumed that movement of drug or SDN was not paracellular as there may have been substantial gaps between the Caco-2 cells.

The Caco-2 monolayer system as used here can provide a model for drug absorption; however it does not provide any information regarding the mode of transport across the monolayer. The two main possible mechanisms of transport are transcellular, where the drug or nanoparticle moves through the cell, or paracellular, where movement is via spaces between cells. PRD, due to its steroidal structure, is likely to move through cell membranes by passive transcellular movement (Fig. 3.9, A) but is also known to be a P-gp substrate and therefore undergoes efflux back into the intestinal lumen (Fig. 3.9. B) [138].The mode of transport of PRD SDNs has not been studied as part of this thesis, but may be investigated using inhibitors of various transport pathways or by tracking fluorescent-labelled nanoparticles [139, 140]. It is also possible to determine if the SDNs permeate the Caco-2 monolayer as intact particles, as demonstrated previously by McDonald *et al.* In this study, dual fluorescence (Förster) resonance energy transfer (FRET) dyes were incorporated within SDNs and the observation of acceptor fluorophore emission in receiver wells indicated proximity of the FRET fluorophores and therefore intact nanoparticles [104].

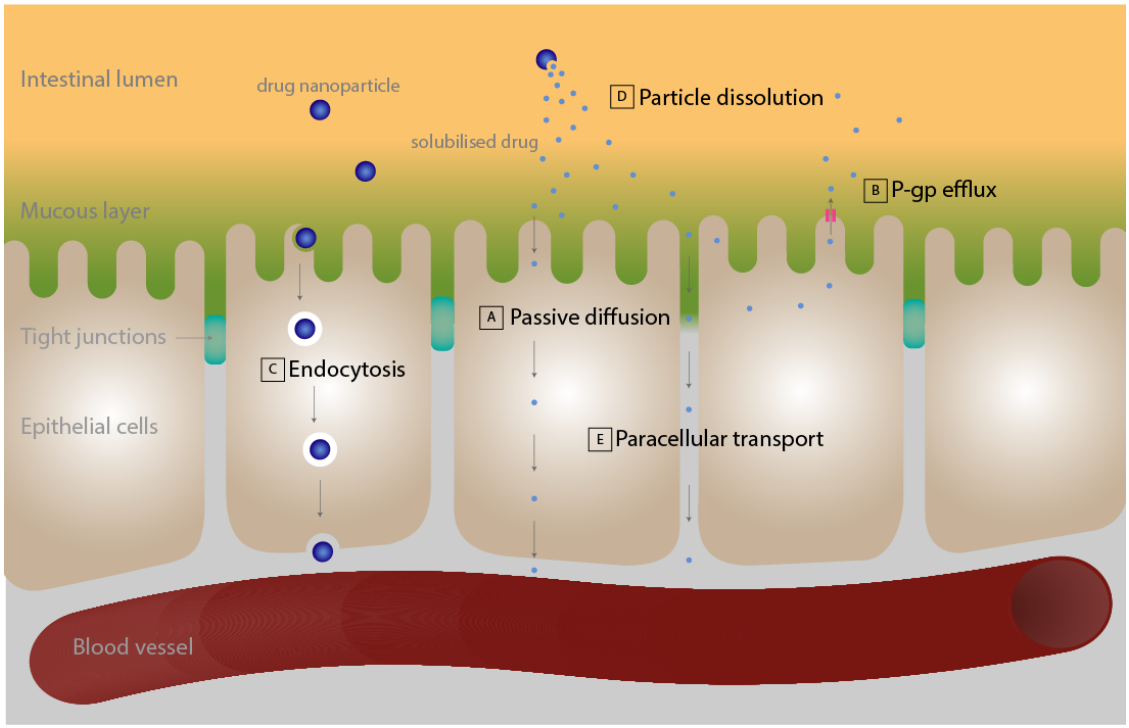

Figure 3.9 Possible mechanisms of intestinal absorption of free PRD or PRD SDNs following oral administration. A: free PRD may passively diffuse through cell membranes. B: PRD may be secreted back into the intestinal lumen via P-glycoprotein efflux. C: intact nanoparticles may pass through cells via endocytosis, an active process where material becomes wrapped in a section of the plasma membrane, internalises and detaches to form an endocytotic vesicle. D: nanoparticles may dissolve in the intestinal lumen or mucous layer then enter cells via passive diffusion, or E: pass between cells via paracellular transport.

Our study in simulated gastric and intestinal fluid indicated that PRD SDNs remain stable for at least six hours (Chapter 2, Fig. 2.19) therefore the SDNs may reach the intestine as intact particles. Once in the intestine the particles may be absorbed intact or eventually dissolve, releasing free PRD which is then absorbed. As the SDNs are around 300 nm in diameter, cellular uptake may occur via endocytosis, similar to that of biomacromolecules of a comparable size (Fig 3.9, C) [141]. Alternatively, dissolved SDNs may create a concentration

gradient allowing free PRD to passively diffuse through the epithelial layer and into the bloodstream (Fig. 3.9, D). Once dissolved, free PRD may also move paracellularly (Fig. 3.9, E).

PRD SDNs were found to be equally efficacious at inhibiting both IL-8 and IL-4 production from stimulated A549 cells and PBMCs respectively, compared to aqueous PRD (Figs. 3.7 and 3.8). Due to time constraints the IL-4 experiment was only carried out once, rather than in triplicate, so this is an obvious limitation which could be amended in future work. An additional control of unloaded nanoparticles could have been included to determine effects on IL-8 production. It is possible that the nanomaterial induces oxidative stress, in response to which IL-8 is produced, so this may interfere with the observed results [142]. Further investigation into the efficacy of PRD SDNs against inflammatory responses could be studied in additional cell types and model systems. For example, inhibition of mast cell cytokine production could be an indication of PRD SDN efficacy in treatment of immunoglobulin E (IgE)-mediated diseases. This could be studied using the RBL-2H3 (rat basophilic leukemia) cell line as a model, by stimulating the cells with IgE and DNP (2,4-dinitrophenol) and measuring the inhibition of IL-4 by aqueous PRD and PRD SDNs, as previously demonstrated with dexamethasone [143]. Using PBMCs can limit the observation of how other cell types present in the blood may be affected by SDNs. As mentioned above, basophils also produce IL-4 and these cells would be present in whole blood [144]. Therefore, addition of PRD or SDNs to whole blood could demonstrate the effect of these on IL-4 production from all circulating immune cells.

By incubating A459 cells and PBMCs with freshly dispersed SDNs, an assumption was made that this is the form in which SDN-formulated PRD would interact with lung epithelial and blood leukocytes *in vivo*. There can be reasonable confidence that the SDNs will be intact particles in the intestinal lumen following oral administration, owing to the stability tests in simulated gastric and intestinal fluids carried out as detailed in Chapter 2, so this assumption is partially supported with regards to the use of the Caco-2 model in this work. However, following absorption of SDNs into the circulation, their fate concerning particle stability and distribution is as yet unknown. It is likely that the particles will interact with proteins in the blood to form a protein corona, and this will have implications such as altered biodistribution, recognition, targeting and drug release [145]. In this conformation, it is possible that PRD in SDN form will not be able to interact with targets such as blood leukocytes and inflamed tissues [146]. There are difficulties associated with exploring the protein corona phenomenon *in vitro*, such as quantification, but potential methods have been developed [147]. Another possibility is that the particles dissolve, releasing free PRD and losing any benefits that nanoformulation may impart at target sites [148]. While worthy of consideration, investigating the formation of SDN-protein coronas is beyond the scope of this thesis.

The main limitation of the *in vitro* tests carried out in this chapter is that additional controls could have been included to account for nanoparticle-mediated interferences. Known as inhibition/enhancement controls (IEC), these considerations are important to ensure false positives are not generated from nanomaterial (non-drug) effects. Several mechanisms for these effects are possible, including optical interference with fluorescence/absorbance based

assays such as MTT and CellTiter-Glo; induction of cytokines as described above; and adsorption of proteins such as enzymes or cytokines, which would prevent accurate quantification of assay outcomes [149].

There are many more *in vitro* studies that could be performed to further assess the safety and efficacy of the two lead PRD SDNs, but the next chapter will address the next stage of pharmacological investigation *in vivo*. From the results in this chapter there is relative confidence that the SDNs can be absorbed from the GI tract and retain their anti-inflammatory efficacy as well as unformulated PRD, without inducing increased cytotoxicity. In the next chapter, the pharmacokinetics and biodistribution of PRD SDNs were compared to unformulated PRD in CD-1 mice.

Acknowledgements

Cell culture was in some cases performed by Rachel Corkhill.

CHAPTER 4

IN VIVO ASSESSMENT OF PRD SDN PHARMACOKINETICS AND BIODISTRIBUTION

CONTENTS

4.1 Introduction

In the previous chapter, PRD SDN formulations were tested *in vitro* to assess cytotoxicity, permeation across an intestinal cell monolayer and efficacy. These results indicated that the SDNs can be absorbed from the GI tract and retain comparable anti-inflammatory efficacy to unformulated PRD, without causing increased cytotoxicity. In order to further determine the potential for oral administration of PRD SDNs, the two lead formulations were progressed to an *in vivo* study of pharmacokinetics (PK) and biodistribution in CD-1 mice. *In vivo* studies such as this can provide more information about how different formulations can affect the PK and pharmacodynamics of a drug. In contrast to *in vitro* tests, many of which consist of single cell types in isolation, using animal models provides a complex system of functional and interactive processes and tissues. Previous studies of SDNs have found good correlation between *in vitro* models of intestinal absorption and *in vivo* oral bioavailability in rodents, and the success of this approach has led to first-in-human trials to confirm the potential for lower doses of SDN to achieve equivalent therapeutic exposure [102, 103].

In humans, the bioavailability of PRD following oral dosing is between 75-98% and maximum plasma concentration occurs 1-2 hours following administration [13]. The plasma half-life is between 3 and 4 hours [15]. As discussed in Chapter 3, oral dosing of a drug as a nanoparticle formulation could alter the route of absorption from the gut due to the difference in size and presence of excipients [150]. Altered absorption may have an effect on PK and/or biodistribution of the drug. The SDNs may dissolve in the gut releasing free drug or may be absorbed as intact particles which will affect the route and extent of absorption. If

absorbed as particles, interactions with plasma proteins may limit or enhance delivery of drug to tissues [146]. The presence of excipients in the SDN formulations may affect drug transporters and metabolic enzymes, resulting in altered absorption and metabolism of PRD [151]. Comparing the biodistribution of PRD SDNs to unformulated PRD allows observation of altered tissue accumulation of PRD which could affect efficacy and/or toxicity. Intravenous (IV)-administered liposomal formulations of PRD are thought to passively target sites of inflammation due to their nanoscale size, and this enhanced selective distribution allows for lower doses of drug which has the potential to reduce side effects in non-target tissues [152]. As PRD is used to treat inflammation in many sites, this study measured accumulation in the brain, heart, lungs, intestine, spleen, kidneys and liver of treated animals to give a broad picture of biodistribution. The dose of PRD chosen, 1 mg kg^{-1}, was based on one of its common uses as oral tablets to treat severe asthma, according to the BTS/SIGN guideline on the management of asthma.

In this chapter, the PK and biodistribution of PRD SDNs was determined following both IV and oral administration to CD-1 mice. By comparing these two routes of administration for PRD SDNs and unformulated PRD, the extent of PRD absorption and its effects on plasma concentration and tissue distribution were evaluated.

4.2 Materials and Methods

4.2.1 Materials and animals

Adult male CD-1 mice were purchased from Charles River (Kent, UK). ^{3}H-PRD was purchased from Moravek (Brea, USA). PRD, BW, TPGS, DMSO, 30% hydrogen peroxide (H_2O_2) and glacial acetic acid were purchased from Sigma (Poole, UK). PBS and FBS were purchased from Gibco (Paisley, UK). DCM was purchased from Fisher Scientific (Loughborough, UK). Heparin was purchased from Leo Pharma (Hurley, UK). Soluene-350 was purchased from Perkin Elmer (Seer Green, UK). Gold Star liquid scintillation cocktail was purchased from Meridian Biotechnologies (Surrey, UK).

This work was conducted within a Home Office approved project licence (number: 70/8563) and personal licence (number: I6DD3BB2F) according to an approved protocol.

4.2.2 Animal housing

72 male CD-1 mice in cages of 3 were acclimatised in the Biomedical Service Unit for 7 days prior to the experiment. Only male mice were used to limit variables and number of animals required. Mice were provided with food pellets and water, and cages were regulated at constant air flow and temperature. 3 days prior to the experiment, mice were weighed and labelled.

4.2.3 Administration of drug

4.2.3.1 Drug preparation

Radiolabelled preparations of aqueous PRD and SDNs 1 and 2 were produced as follows.

Aqueous PRD:

10 µl of a 100 mg mL^{-1} PRD solution in DMSO was added to 56 µCi of dried ^{3}H-PRD and mixed thoroughly. DMSO was necessary for PRD solubilisation but limited to 0.5% of the final administered solution. This was added to 9.99 ml of PBS and mixed thoroughly to give a 0.1 mg mL^{-1} solution of PRD with a specific activity of 0.031 nCi ng^{-1}. This solution was used for both IV and oral administration.

SDNs:

Half scale radiolabelled SDNs were prepared as described in section 2.2.11 with the addition of 69 µCi of ^{3}H-PRD to the original PRD/BW solution in DCM. Immediately before dosing, one vial of freeze dried product per formulation was reconstituted with 1.25 mL of PBS to make a 1 mg mL^{-1} dispersion. 800 µL of this dispersion was diluted further with 7.2 mL of PBS to make a 0.1 mg mL^{-1} dispersion with specific activity of 0.033 nCi ng^{-1} (SDN1) or 0.035 nCi ng^{-1} (SDN2). These dispersions were used for both IV and oral administration.

4.2.3.2 Dosing

Each drug formulation was administered to groups of three mice per time point and per route of administration as illustrated in Table 1. The dose for all animals and formulations was 1 mg kg^{-1} PRD.

Table 4.1 Allocation of animals to formulation (Aqueous PRD, SDN1 or SDN2) and route of drug administration (IV or oral).

Time (hours)	Aqueous PRD		SDN1		SDN2	
	IV	Oral	IV	Oral	IV	Oral
0.5	Cage 4 Mice 10-12	Cage 16 Mice 46-48	Cage 8 Mice 22-24	Cage 20 Mice 58-60	Cage 12 Mice 34-36	Cage 24 Mice 70-72
1	Cage 3 Mice 7-9	Cage 15 Mice 43-45	Cage 7 Mice 19-21	Cage 19 Mice 55-57	Cage 11 Mice 31-33	Cage 23 Mice 67-69
2	Cage 2 Mice 4-6	Cage 14 Mice 40-42	Cage 6 Mice 16-19	Cage 18 Mice 52-54	Cage 10 Mice 28-30	Cage 22 Mice 64-66
4	Cage 1 Mice 1-3	Cage 13 Mice 37-39	Cage 5 Mice 13-15	Cage 17 Mice 49-51	Cage 9 Mice 25-27	Cage 21 Mice 61-63

IV mice were transferred to a heat box at 37°C several minutes before dosing. Drug was then administered by injection into the tail vein. Oral drug was administered via gavage. Mice were then replaced into original cages for the duration of the experiment.

4.2.3.3 Sample collection

At 0.5, 1, 2 or 4 hours post-dose, animals were terminally anaesthetised with 5% isoflurane. Blood was immediately collected using heparinised syringes (5000 units mL^{-1}) via cardiac puncture and transferred to vials. Plasma was obtained by centrifugation of whole blood for 5 minutes at 10000 RPM and stored on ice for a maximum of 3 hours prior to analysis. Each animal was then sacrificed by cervical dislocation before dissection. The brain, heart, lungs, intestine, spleen, kidneys and liver were removed, washed in PBS, transferred to separate vials and frozen at -20 °C prior to analysis.

4.2.4 Processing of plasma and tissue samples for PRD quantification

A 100 µL aliquot of each plasma sample was transferred to a 5 mL scintillation vial to which 4 mL scintillation cocktail was added. The vials were then counted for radioactivity on a Packard 3100 TR liquid scintillation analyser.

Each collected organ was weighed then a sample of each (Table 4.2) was transferred into a 20 mL scintillation vial. 1 mL of soluene was added to each vial then incubated for 18 hours in a water bath at 50°C. Following this, 200 µL of 30% hydrogen peroxide (H_2O_2) was added to each vial then incubated for 1 hour at room temperature. 90 µL of glacial acetic acid was then added and incubated for 15 minutes at 50°C. Finally, 12 mL of scintillation cocktail was added to each vial, mixed by inversion then counted for radioactivity.

Table 4.2 Approximate mass of tissue taken for solubilisation and analysis. Exact values were recorded for calculation of tissue distribution.

Tissue type	Approximate mass (mg)
Brain	50
Heart	30
Lungs	100
Intestine	100
Spleen	30
Kidney	100
Liver	100

4.2.5 Quantification of SDN drug loading

SDN drug loading was quantified by HPLC as described in Chapter 3, section 3.2.5.

4.2.6 Data analysis

Statistical analysis was performed using SPSS 22 and GraphPad Prism 5 for Windows. As the sample size was small (n = 3) and could not be assessed for normality, data was log transformed prior to statistical analysis to minimise the chance of non-normality. Log transformed data was analysed by T test to determine significance between aqueous PRD (control) and SDN1 or SDN2. Plasma and tissue PK parameters were calculated using PKSolver plug-in for Microsoft Excel. Bioavailability (F) was calculated using the following equation:

$$\%F = 100\left(\frac{AUC_{oral}}{AUC_{IV}}\right)$$

4.3 Results

4.3.1 Drug loading of PRD SDNs

The intended drug loading of PRD for both IV and oral doses was 25 μg per 250 μL dose. Quantification by HPLC determined that actual PRD content of all three formulations was 33.3 μg per 250 μL dose (± 2%) (Table 4.3).

Table 4.3 PRD loading of SDN1 and SDN2 used to treat animals, as determined by HPLC.

	Average peak area	PRD (μg/mL)	% of CM	% exCM	PRD (μg/ 250 μL dose)
Chemical mix (CM)	1.09	0.99	100.00		
extracted chemical mix (exCM)	0.70	0.62	63.02	100.00	25.00
Aqueous PRD	0.92	0.83	83.72	132.85	33.21
SDN1	0.93	0.84	85.35	135.44	33.86
SDN2	0.90	0.82	82.42	130.79	32.70
Average drug loading					33.3

4.3.2 Pharmacokinetics of PRD and PRD SDNs

4.3.2.1 IV administration

The PK of radiolabelled aqueous PRD and SDNs 1 and 2 were studied *in vivo* following IV dosing to CD-1 mice. Plasma PRD concentrations of aqueous PRD, SDN1 and SDN2 treated mice were not significantly different at all time points (Fig. 4.1). Half-life ($t_{1/2}$), time to maximum concentration (T_{max}), maximum concentration (C_{max}) and area under curve (AUC_{0-t}) of SDNs 1 and 2 were not significantly different to aqueous PRD (Table 4.4).

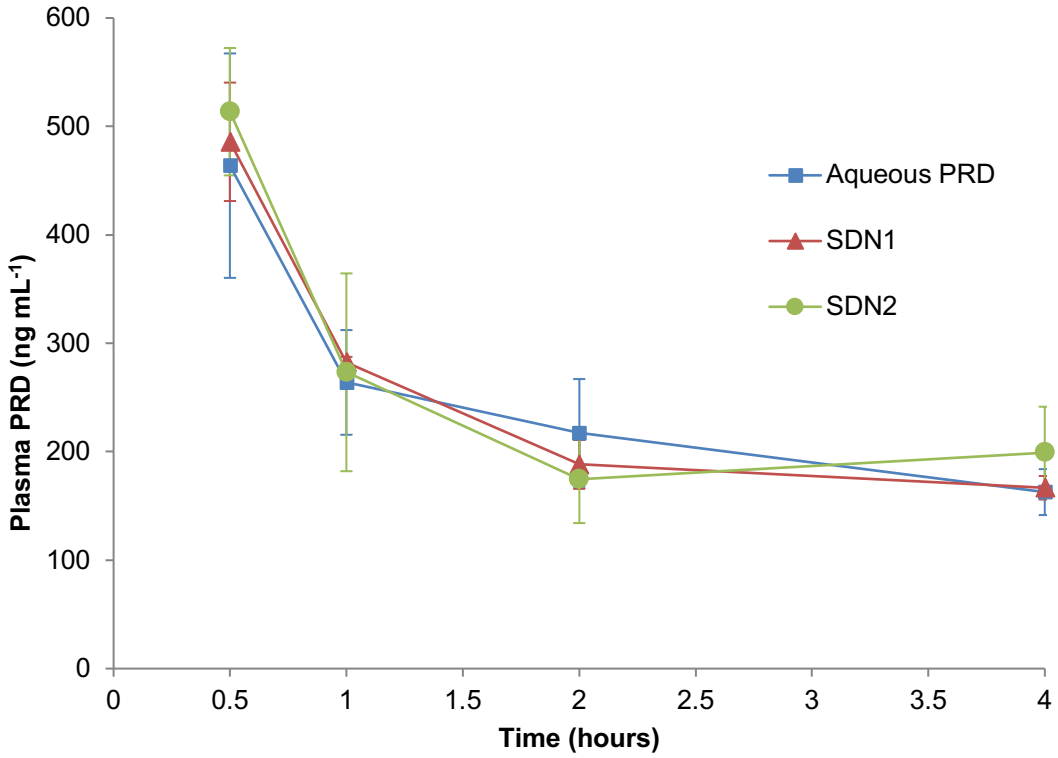

Figure 4.1 Pharmacokinetics of PRD and PRD SDNs at 0.5, 1, 2 and 4 hours following IV administration to CD1 mice. N = 3.

Table 4.4 Pharmacokinetic parameters with standard deviation for IV administration of PRD and PRD SDNs to CD1 mice. $T_{1/2}$: half-life, T_{max}: time to maximum concentration, C_{max}: maximum concentration, AUC_{0-t}: area under curve. *P*-values compared to aqueous PRD (control). N/C: not calculable or no variation.

	Aqueous PRD	**SDN1**	***P*-value**	**SDN2**	***P*-value**
$t_{1/2}$ (h)	3.41 ± 0.63	3.05 ± 0.36	0.47	3.57 ± 1.68	0.98
T_{max} (h)	0.5	0.5	N/C	0.5	N/C
C_{max} (ng mL^{-1})	463.82 ± 103.49	485.8 ± 54.61	0.71	513.57 ± 58.72	0.49
AUC_{0-t} (ng/mL*h)	1125.59 ± 89.65	1114.21 ± 90.93	0.88	1207.51 ± 139.27	0.44

4.3.2.2 Oral administration

The PK of radiolabelled unformulated (aqueous) PRD and PRD SDNs 1 and 2 were studied *in vivo* following oral dosing to CD-1 mice. Blood samples were

taken from separate groups following terminal anaesthesia at 0.5, 1, 2 and 4 hours post-dose. Plasma concentrations of PRD were determined by measuring radioactivity of samples. At 0.5 and 1 hour post-dose, plasma PRD concentrations of aqueous PRD, SDN1 and SDN2 treated mice were not significantly different between formulations (Fig. 4.2). At 2 hours, plasma PRD concentrations of SDN1 and SDN2 treated mice were significantly higher than those treated with aqueous PRD (P = 0.036 and P = 0.028 respectively). By 4 hours, the plasma PRD concentrations of all three groups were not significantly different. $T_{1/2}$ of SDN2 was found to be significantly higher than that of aqueous PRD (Table 4.5, P = 0.045). T_{max}, C_{max} and $AUC_{0\text{-}t}$ of SDNs 1 and 2 were not significantly different to aqueous PRD. There was no significant difference between bioavailability of SDNs 1 and 2 compared to unformulated PRD.

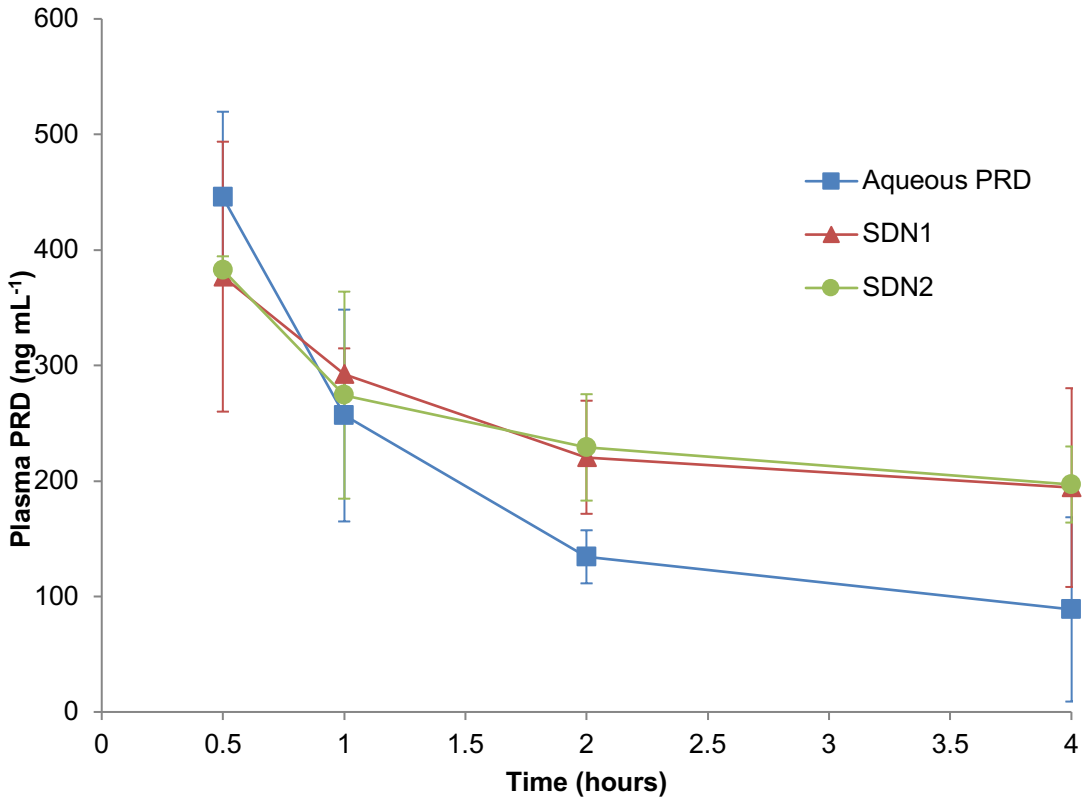

Figure 4.2 Pharmacokinetics of PRD and PRD SDNs at 0.5, 1, 2 and 4 hours following oral administration to CD1 mice. N = 3.

Table 4.5 Pharmacokinetic parameters with standard deviation for oral administration of PRD and PRD SDNs to CD1 mice. $T_{1/2}$: half-life, T_{max}: time to maximum concentration, C_{max}: maximum concentration, AUC_{0-t}: area under curve. P values compared to aqueous PRD (control), * significant *P*-value ($P < 0.05$). N/C: not calculable or no variation.

	Aqueous PRD	**SDN1**	***P*-value**	**SDN2**	***P*-value**
$t_{1/2}$ (h)	2.25 ± 0.68	4.19 ± 1.81	0.27	4.39 ± 0.74	0.045*
T_{max} (h)	0.5	0.67 ± 0.29	N/C	0.67 ± 0.29	N/C
C_{max} (ng mL^{-1})	445.3 ± 74.33	379.3 ± 113.48	0.42	383.47 ± 10.66	0.24
AUC_{0-t} (ng/mL*h)	798.31 ± 102.4	957.98 ± 131.46	0.24	937.44 ± 121.75	0.27
Bioavailability (%)	74.16 ± 14.59	85.75 ± 5.5	0.27	77.55 ± 1.3	0.64

4.3.3 Biodistribution of PRD and PRD SDNs

Tissue distribution of PRD was determined in CD-1 mice treated with radiolabelled aqueous PRD, SDN1 and SDN2 via IV or oral administration. Organs (brain, heart, lungs, intestine, spleen, kidney and liver) were collected from animals sacrificed 0.1, 1, 2 and 4 hours post-dose. Concentrations of PRD in tissue homogenates were determined by measuring radioactivity of samples.

Distribution of PRD to the brain differed with route of administration but not between formulations. IV PRD concentrations in the brain decreased between 0.5 and 1 hour then increased between 2 and 4 hours (Fig. 4.3, A), whereas oral PRD brain concentrations increased between 0.5 and 4 hours (Fig. 4.3, B). At each time point there was no significant difference in brain concentrations between the two PRD formulations and unformulated PRD.

At 0.5 hours, PRD concentrations in the heart were higher following IV administration of unformulated PRD and SDN1 (Fig. 4.3, C) compared to oral administration (Fig. 4.3, D) at 0.4 and 0.5 ng mg^{-1} versus 0.3 and 0.375 ng mg^{-1} respectively. At 0.5 hours, PRD concentration in the heart following

administration of IV SDN1 appeared higher than that of SDN2 but was not significant. However, half-life of SDN1 was found to be significantly shorter compared to aqueous PRD (P = 0.0018, Table 4.6). Other than this point, PRD concentrations and PK in the heart were comparable for all formulations at each time point.

PRD concentrations in the lungs were comparable at 0.5 hours following both IV and oral administration (Fig. 4.3, E and F). However between 0.5 and 4 hours, PRD concentrations for IV administered drug decreased more quickly to 0.15 ng mg^{-1} at 1 hour and 0.1 ng mg^{-1} at 4 hours, compared to orally administered drug with concentrations of 0.2-0.3 ng mg^{-1} at 1 hour and 0.15 ng mg^{-1} at 4 hours. At each time point there was no significant difference between lung concentrations or PK for each formulation.

Distribution of PRD to the intestine varied considerably within treatment groups with average values ranging from an observed maximum of 6 ng mg^{-1} at 1 hour down to 0.5-1 ng mg^{-1} at 4 hours. Tissue concentrations were similar between all formulations at each time point (Fig. 4.3, G and H).

In the spleen, concentrations of PRD were also similar between formulations and route of administration at each time point with no significant differences found (Fig. 4.3, I and J).

PRD concentration in the kidney appeared to be higher at 0.5 hours for unformulated and SDN1 compared to SDN2 following IV administration but was non-significant (Fig. 4.3, K). However at 2 hours, orally dosed SDN1 and SDN2 both reached a significantly higher PRD concentration compared to unformulated PRD (Fig. 4.3, L. P = 0.016 and 0.0006 respectively). This increase was also

significant for both SDN1 and SDN2 at 4 hours (P = 0.037 and 0.042 respectively). The AUC of IV dosed SDN1 was significantly smaller compared to unformulated PRD (Table 4.6, P = 0.04). The half-life of oral dosed SDN1 was significantly longer than that of unformulated PRD (Table 4.7, P = 0.035).

Liver concentrations of PRD were significantly lower following IV administration of SDN2 compared to unformulated PRD at 0.5 hours (Fig. 4.3, M. P = 0.019). At 1, 2 and 4 hours, PRD concentration was comparable between formulations and route of administration (Fig. 4.3, M and N). The PK of IV dosed SDN2 were significantly different compared to unformulated PRD (Table 4.6), having a longer half-life (P = 0.006), a lower C_{max} (P = 0.019) and larger AUC (P = 0.028).

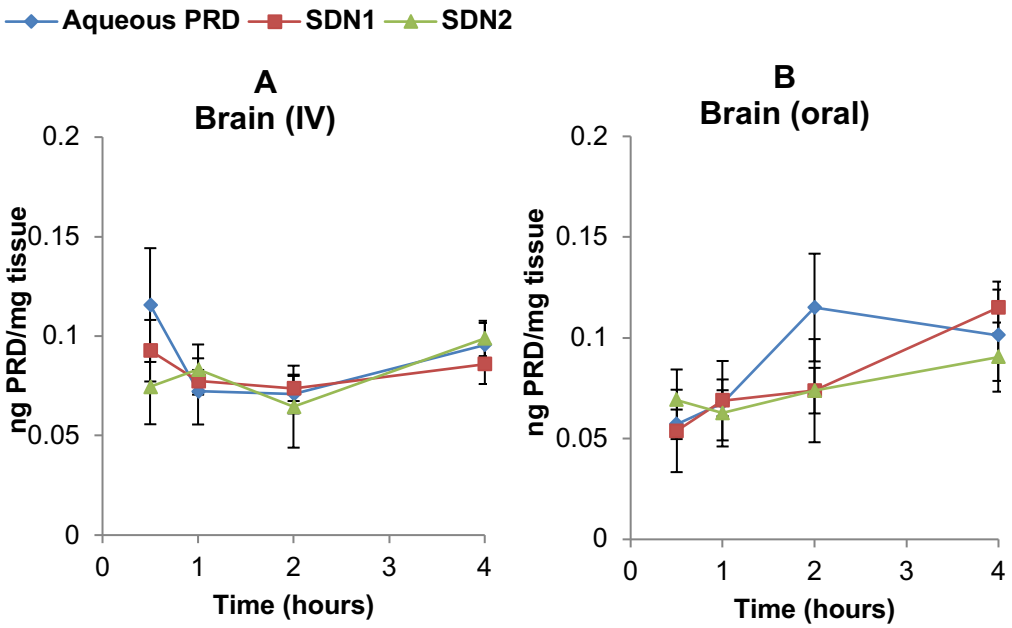

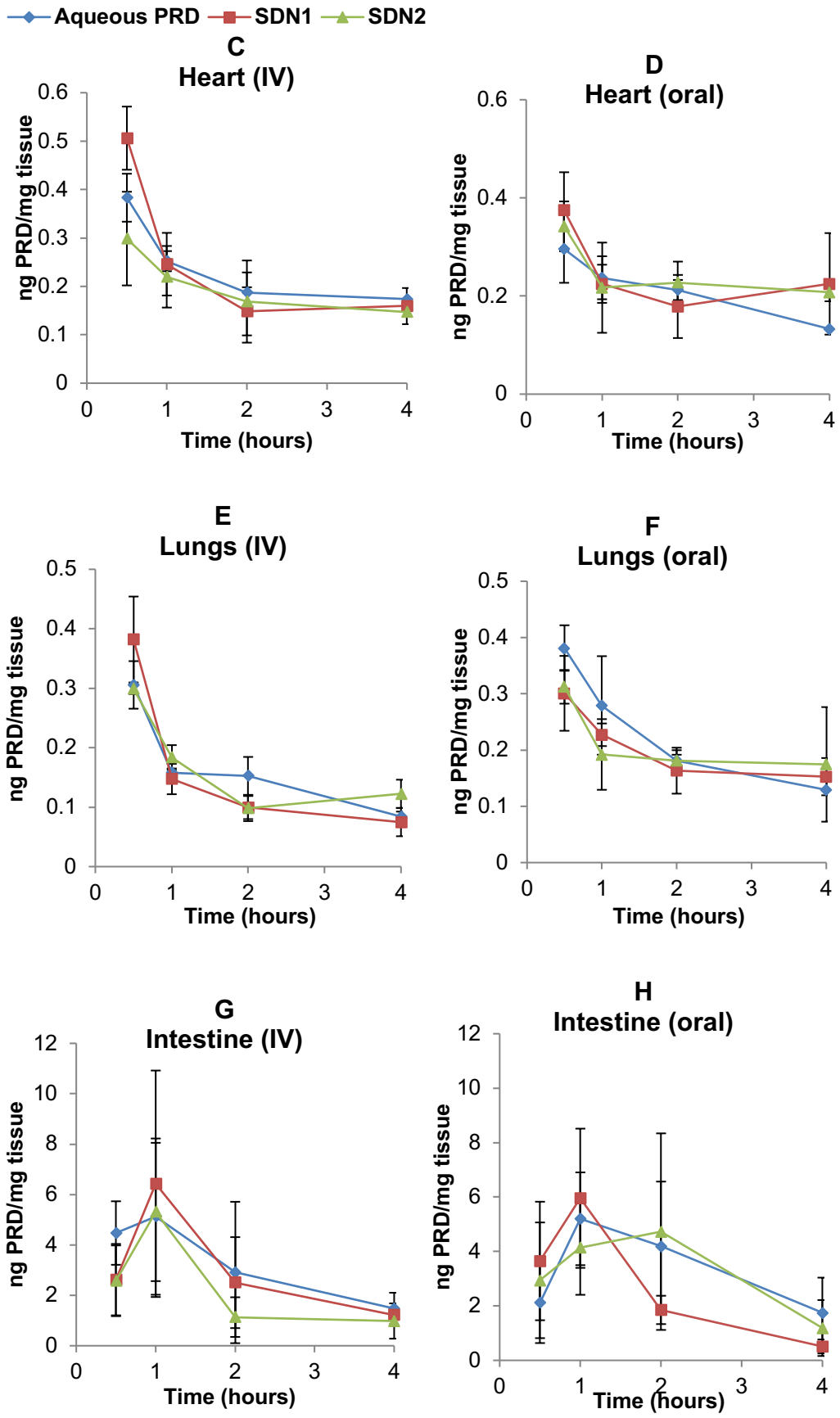
Aqueous PRD
SDN1
SDN2
C
Heart (IV)
ng PRD/mg tissue
Time (hours)
D
Heart (oral)
ng PRD/mg tissue
Time (hours)
E
Lungs (IV)
ng PRD/mg tissue
Time (hours)
F
Lungs (oral)
ng PRD/mg tissue
Time (hours)
G
Intestine (IV)
ng PRD/mg tissue
Time (hours)
H
Intestine (oral)
ng PRD/mg tissue
Time (hours)

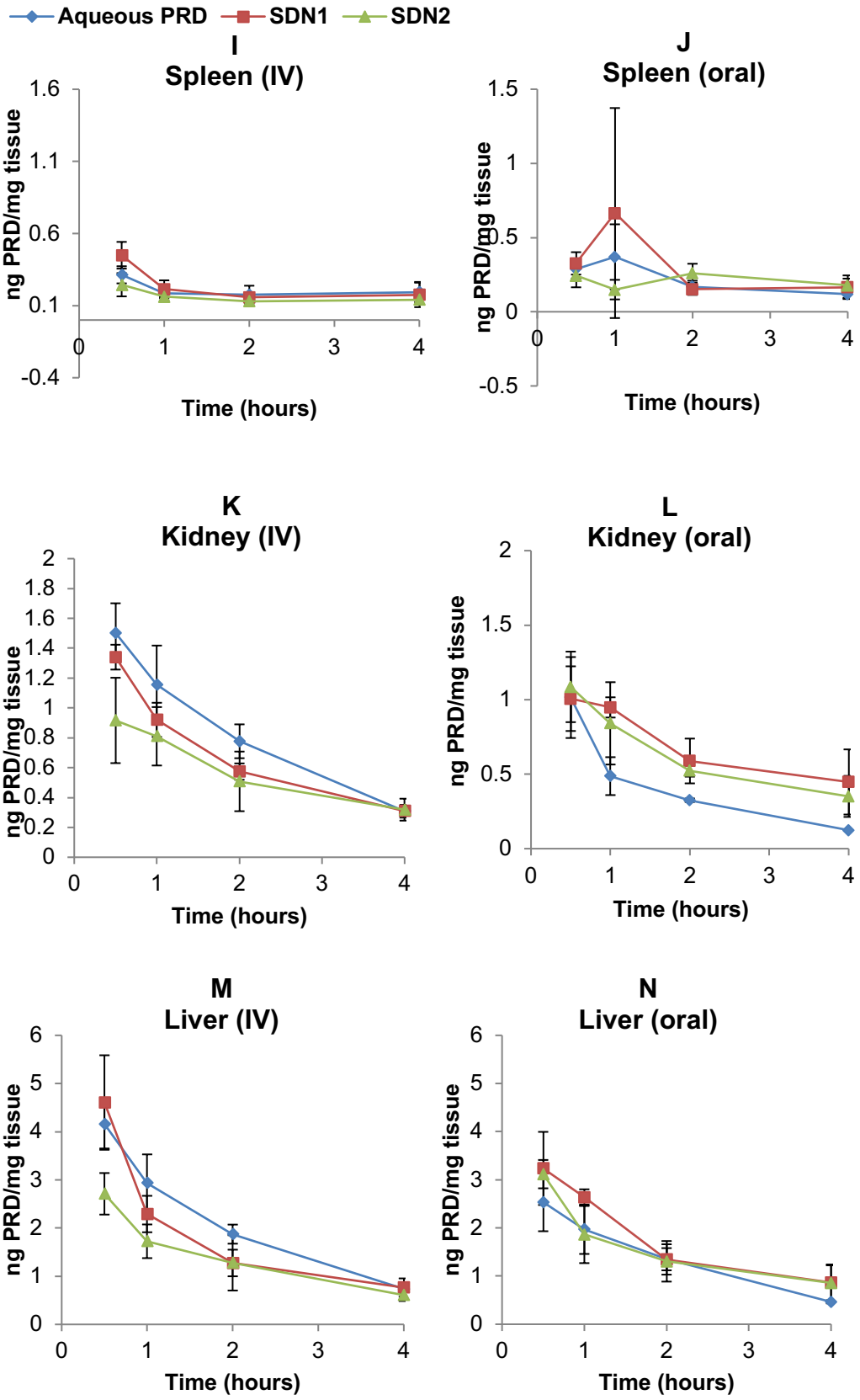

Figure 4.3 Tissue distribution of aqueous PRD, SDN1 and SDN2 0.5, 1, 2 and 4 hours following IV or oral administration to CD1 mice. N = 3.

Table 4.6 Tissue pharmacokinetic parameters with standard deviation for IV administration of PRD and PRD SDNs to CD1 mice. $T_{1/2}$: half-life, T_{max}: time to maximum concentration, C_{max}: maximum concentration, AUC_{0-t}: area under curve. P values compared to aqueous PRD (control), * significant *P*-value ($P < 0.05$). N/C: not calculable or no variation.

Tissue		**Aqueous PRD**	**SDN1**	***P*-value**	**SDN2**	***P*-value**
Brain	$t_{1/2}$ (h)	52.43 ± 37.68	43.29 ± 42.09	0.74	N/C	N/C
	T_{max} (h)	1.67 ± 2.02	1.67 ± 2.02	N/C	4	N/C
	C_{max} (μg mg^{-1})	0.12 ± 0.03	0.1 ± 0.01	0.35	0.1 0.01	0.39
	AUC_{0-t} (μg/mg*h)	0.36 ± 0.06	0.33 ± 0.01	0.44	0.31 ± 0.04	0.33
Heart	$t_{1/2}$ (h)	4.2 ± 0.61	2.02 ± 0.19	0.0018**	3.39 ± 0.84	0.28
	T_{max} (h)	0.5	0.5	N/C	1.0 ± 0.87	N/C
	C_{max} (μg mg^{-1})	0.38 ± 0.05	0.51 ± 0.07	0.059	0.32 ± 0.05	0.25
	AUC_{0-t} (μg/mg*h)	0.98 ± 0.11	1.05 ± 0.17	0.66	0.82 ± 0.03	0.056
Lung	$t_{1/2}$ (h)	2.76 ± 1.0	3.64 ± 2.91	0.82	3.16 ± 0.68	0.55
	T_{max} (h)	0.5	0.5	N/C	0.5	N/C
	C_{max} (μg mg^{-1})	0.31 ± 0.04	0.38 ± 0.07	0.2	0.3 ± 0.01	0.84
	AUC_{0-t} (μg/mg*h)	0.73 ± 0.06	0.79 ± 0.16	0.68	0.68 ± 0.06	0.31
Intestine	$t_{1/2}$ (h)	2.98	1.59 ± 0.9	N/C	1.82 ± 1.09	N/C
	T_{max} (h)	1.5 ± 0.87	0.83 ± 0.29	N/C	1.0	N/C
	C_{max} (μg mg^{-1})	9.72 ± 7.62	7.08 ± 3.61	0.7	5.31 ± 2.74	0.38
	AUC_{0-t} (μg/mg*h)	21.37 ± 14.25	12.08 ± 4.43	0.32	8.6 ± 1.41	0.1
Spleen	$t_{1/2}$ (h)	9.95 ± 7.09	7.51 ± 2.37	0.78	5.17 ± 2.82	0.44
	T_{max} (h)	0.5	0.5	N/C	1.0 ± 0.87	N/C
	C_{max} (μg mg^{-1})	0.31 ± 0.06	0.45 ± 0.09	0.09	0.25 ± 0.08	0.31
	AUC_{0-t} (μg/mg*h)	0.89 ± 0.23	1.06 ± 0.14	0.32	0.67 ± 0.08	0.21
Kidney	$t_{1/2}$ (h)	1.61 ± 0.37	1.94 ± 0.25	0.27	2.18 ± 0.17	0.092
	T_{max} (h)	0.5	0.5		0.67 ± 0.29	
	C_{max} (μg mg^{-1})	1.5 ± 0.2	1.34 ± 0.08	0.27	0.93 ± 0.29	0.067
	AUC_{0-t} (μg/mg*h)	3.59 ± 0.26	3.02 ± 0.2	0.04*	2.42 ± 0.62	0.067
Liver	$t_{1/2}$ (h)	1.5 ± 0.12	1.71 ± 0.32	0.38	2.01 ± 0.11	0.006**
	T_{max} (h)	0.5	0.5	N/C	0.5	N/C
	C_{max} (μg mg^{-1})	4.16 ± 0.51	4.61 ± 0.98	0.54	2.71 ± 0.43	0.019*
	AUC_{0-t} (μg/mg*h)	9.34 ± 0.53	9.25 ± 2.01	0.86	6.25 ± 1.2	0.028*

Table 4.7 Tissue pharmacokinetic parameters with standard deviation for oral administration of PRD and PRD SDNs to CD1 mice. $T_{1/2}$: half-life, T_{max}: time to maximum concentration, C_{max}: maximum concentration, AUC_{0-t}: area under curve. P values compared to aqueous PRD (control), * significant *P*-value ($P < 0.05$). N/C: not calculable or no variation.

Tissue		**Aqueous PRD**	**SDN1**	***P*-value**	**SDN2**	***P*-value**
Brain	$t_{1/2}$ (h)	N/C	N/C	N/C	N/C	N/C
	T_{max} (h)	2.0	4	N/C	2.17 ± 1.76	N/C
	C_{max} (μg mg^{-1})	0.12 ± 0.03	0.12 ± 0.01	0.93	0.09 ± 0.01	0.27
	AUC_{0-t} (μg/mg*h)	0.29 ± 0.14	0.29 ± 0.05	0.79	0.28 ± 0.02	0.83
Heart	$t_{1/2}$ (h)	2.77 ± 0.09	3.8 ± 1.23	0.2	9.39 ± 4.38	0.029*
	T_{max} (h)	0.67 ± 0.29	0.5	N/C	0.5	N/C
	C_{max} (μg mg^{-1})	0.31 ± 0.05	0.37 ± 0.08	0.28	0.34 ± 0.05	0.5
	AUC_{0-t} (μg/mg*h)	0.67 ± 0.25	0.8 ± 0.11	0.42	0.88 ± 0.13	0.28
Lung	$t_{1/2}$ (h)	1.97 ± 0.55	4.7 ± 2.32	0.099	13.76 ± 16.87	0.13
	T_{max} (h)	0.5	0.5	N/C	0.5	N/C
	C_{max} (μg mg^{-1})	0.38 ± 0.04	0.3 ± 0.07	0.17	0.31 ± 0.03	0.08
	AUC_{0-t} (μg/mg*h)	0.7 ± 0.25	0.67 ± 0.09	1.0	0.75 ± 0.15	0.72
Intestine	$t_{1/2}$ (h)	N/C	0.82 ± 0.33	N/C	N/C	N/C
	T_{max} (h)	1.33 ± 0.58	0.67 ± 0.29	N/C	1.67 ± 0.58	N/C
	C_{max} (μg mg^{-1})	6.43 ±0.45	5.49 ± 2.67	0.49	6.53 ± 0.5	0.82
	AUC_{0-t} (μg/mg*h)	11.52 ± 5.48	8.1 ± 2.27	0.42	12.86 ± 4.21	0.7
Spleen	$t_{1/2}$ (h)	1.53 ± 0.25	2.29 ±1.88	0.79	N/C	N/C
	T_{max} (h)	1.17 ± 0.76	0.67 ± 0.29	N/C	1.0 ± 0.87	N/C
	C_{max} (μg mg^{-1})	0.62 ± 0.47	0.63 ± 0.46	0.95	0.29 ± 0.07	0.24
	AUC_{0-t} (μg/mg*h)	1.2 ± 1.13	0.9 ± 0.39	0.95	0.8 ± 0.1	0.87
Kidney	$t_{1/2}$ (h)	1.32 ± 0.14	1.98 ± 0.28	0.035*	2.22 ± 0.71	0.063
	T_{max} (h)	0.5	0.83 ± 0.29	N/C	0.67 ± 0.29	N/C
	C_{max} (μg mg^{-1})	1.01 ± 0.27	1.05 ± 0.18	0.8	1.18 ± 0.13	0.35
	AUC_{0-t} (μg/mg*h)	1.34 ± 0.45	2.31 ± 0.31	0.62	2.31 ± 0.18	0.56
Liver	$t_{1/2}$ (h)	1.42 ± 0.18	1.57 ± 0.34	0.56	2.1 ± 0.61	0.11
	T_{max} (h)	0.5	0.67 ± 0.29	N/C	0.5	N/C
	C_{max} (μg mg^{-1})	2.54 ± 0.6	3.34 ± 0.6	0.17	3.12 ± 0.29	0.19
	AUC_{0-t} (μg/mg*h)	4.71 ± 1.82	5.83 ± 0.86	0.38	5.77 ± 0.92	0.4

4.4 Discussion

A method of measuring PRD in mouse plasma and tissues by administering IV and oral radiolabelled (^{3}H) PRD SDNs was developed and successfully employed. Using this method, the *in vivo* PK of SDNs 1 and 2 were compared with unformulated PRD following IV and oral administration to CD-1 mice. For oral administered PRD, the plasma T_{max} was calculated to be 0.5 hours for unformulated PRD and 0.67 hours for SDNs 1 and 2, but due to limited sampling time points it is not known if the true plasma C_{max} following oral dosing were before, exactly at 0.5 hours, or between 0.5 and 1 hours. In a previous study in mice, the maximum observed plasma concentration was measured 15 minutes post-IV dose, although this dose was much higher at 20 mg kg^{-1} [153]. In humans, maximum plasma concentration occurs between 1 and 2 hours following oral dose [13, 154].

When orally dosed, both SDNs 1 and 2 retained higher plasma concentrations than unformulated PRD, with SDN2 reaching significantly higher concentration at two hours ($p < 0.05$, Fig. 4.1) and a significantly longer half-life (Table 4.5, $P = 0.049$). This difference in plasma PK between SDNs and unformulated PRD is not observed following IV administration, implying that the behaviour of PRD when formulated as an SDN is altered during passage through the GI system and into the circulatory system. This is likely due to particle-specific effects allowing more extensive absorption and therefore higher bioavailability. There are several possible mechanisms by which SDNs may enhance PRD absorption following oral administration. Particle hydrophobicity can improve mucoadhesion, a property which improves penetration of the mucous layer to

reach the epithelial cells and increases residence time of particles in the intestine, therefore allowing more extensive absorption [155]. However, SDNs 1 and 2 are more hydrophilic in nature as they are surface stabilised by neutral charged surfactants, and are therefore more likely to interact with M cells [156]. M cells are intestinal cells around which the mucous layer is less dense and mediate uptake of particles from the intestine into the lymphatic system. The presence of surface stabilisers including PVA, vitamin E and PEG increases particle absorption via improved adhesion and affinity to, and consequent uptake by epithelial cells [157]. This effect may be evident in PRD SDNs 1 and 2 which both contain kollicoat, a graft co-polymer of PVA and PEG; additionally SDN1 contains TPGS, a conjugate of vitamin E and PEG (see Chapter 2, Fig. 2.14). Another potential consideration is the slower clearance of SDNs 1 and 2 from the plasma following oral administration compared to unformulated PRD. All three preparations show a relatively rapid decrease in plasma concentration between 0.5 and 1 hour post-dose then a slower decrease between 1 and 4 hours, however the concentration of both SDNs 1 and 2 almost plateaus while unformulated PRD continues to decrease. This may be a result of continued absorption of drug as a result of particle adhesion to epithelial cells prolonging GI transit as discussed above. An alternative mechanism could involve interactions with plasma proteins which may differ between unformulated PRD and SDNs. PRD is known to bind transcortin and albumin non-linearly, and only unbound PRD can enter tissues or undergo elimination [158]. If intact, PRD SDNs in the plasma will probably interact with plasma proteins to form a corona, a process which is not well understood and may have effects on plasma half-life, tissue distribution and immunogenicity [159]. The proportion of protein-bound or unbound PRD was

not differentiated in this study, as only total PRD was measured by radiation, and the small volume of plasma collected was not sufficient to conduct plasma protein binding assays. Additionally, the prolonged plasma concentration of SDNs 1 and 2 may be due to the presence of excipients in the SDN formulations, particularly BW which is hydrophobic. Other lipid-based nanoparticles such as liposomes have demonstrated slow-release of drugs to improve PK and efficacy [160]. Although these PRD SDNs are intended for oral administration, the prolonged plasma concentrations may provide a similar potential for reducing dose and allowing less frequent dosing of PRD which could be particularly useful for treating chronic inflammatory diseases. It would be interesting to repeat this study with an extended sampling period to determine how long PRD is present in the plasma, and to incorporate an analysis of free versus protein-bound drug concentration.

The second key observation was that distribution of both SDNs 1 and 2 to the kidney was increased following oral but not IV administration (Fig. 4.3 L). All three preparations were comparable at 0.5 hours but the concentration of unformulated PRD in kidney tissue decreased more rapidly than SDNs 1 and 2 between 0.5 and 4 hours (At 2 hours SDN1: $P = 0.016$, SDN2: $P = 0.0006$). Distribution to the other organs was comparable for all three preparations at all time points for both routes of administration, so this implies that the increased kidney distribution may be due to tissue-specific passive targeting of the SDNs. Such passive targeting may occur due to the size or presence of excipients in the SDN formulations. This effect may be evident in oral-dosed but not IV-dosed animals as the plasma concentration of SDNs 1 and 2 are higher than unformulated PRD and therefore a larger proportion of PRD is available for

distribution to the kidney. If the SDNs are intact when the reach the kidney, it is unlikely that they are able to permeate the glomerular filtration barrier as the particles are around 300 nm in diameter [107]. Methods such as mass spectrometry imaging could be employed to visualise the localisation of PRD or SDNs in kidney tissue slices in order to determine the mechanism of kidney accumulation [161].

Although the mechanism for the increased accumulation of the SDNs in the kidney is unknown, it offers a potential use for targeted treatment of kidney disorders which respond to PRD such as nephrotic syndrome [162]. Nephrotic syndrome is treated with 2 mg kg^{-1} (or 60 mg/m^2) of PRD, double the dose used in this study [163]. To investigate the potential of the SDNs as targeted therapy for nephrotic syndrome the study would need to be repeated with an increased dose of 2 mg $kg^{-1}$of PRD to determine if the enhanced kidney distribution is retained. A suitable animal model to investigate the efficacy of PRD SDNs against kidney injury would be the adriamycin-induced nephropathy model, which can be induced in rats and mice [164, 165] or immune-mediated models such as induced Heymann's nephritis in rodents [166]. Using such a model is also important to determine how pathological conditions may affect PK and biodistribution of PRD SDNs. As the glomerular barrier may be compromised in nephrotic syndrome, there may be altered accumulation of PRD [107]. During inflammation, vascular permeability is altered which can affect distribution of nanoparticles [167].

The aims of this chapter were achieved through the investigation of PRD SDN PK and biodistribution in mice, and there is much potential for progression of

this investigation through further studies. Primarily, the reported study should be repeated to confirm these results, with larger groups of animals to better determine statistical significance for the observed differences. The nephropathy model mentioned above could provide a methodology to assess the potential use of PRD SDNs for the treatment of kidney diseases and is worth investigating. Finally, the PK of PRD SDNs may be beneficial in terms of reducing PRD dose or prolonging effective plasma concentrations between doses.

Acknowledgements

Administration of drug to animals and sample collection were assisted by J. Sharp and A. Jimenez-Valverde.

CHAPTER 5

GENERAL DISCUSSION

The research presented in this thesis has demonstrated that the application of nanomedicine technology can produce improved formulations of prednisolone for potential therapeutic use. By following a strategic process of screening, optimisation and assessment the aims of the thesis have been fulfilled, achieving the development of two novel formulations of prednisolone and determining their suitability for progression as oral therapeutics. This work has shown that prednisolone can be formulated as SDNs and through this modification may improve the limitations of this otherwise effective and widely useful drug.

A rational plan was followed to ensure efficiency and direction from the beginning of the project. Screening of excipients taken from the FDA Inactive Ingredient Database together with a miniaturised approach provided an efficient method of assessing large numbers of PRD SDN candidates. Single screens capable of producing up to 130 individual SDN formulations produced data to enable selection of candidates based on size, quality of particle dispersion and reproducibility between batches. Although this existing method was productive as a high-throughput screening process and had previously been successful in generating nanoparticles of other drugs, in the case of PRD only large particles several microns in size were formed. In order to accomplish the production of nanoscale PRD SDNs, considerable effort went into adapting the method, which required the inclusion of beeswax as an additional hydrophobic excipient. The investigation of how SDNs are formed, which factors determine particle size and how different drugs affect or behave in the process would itself be an enormous undertaking so could not be substantially explored within this project.

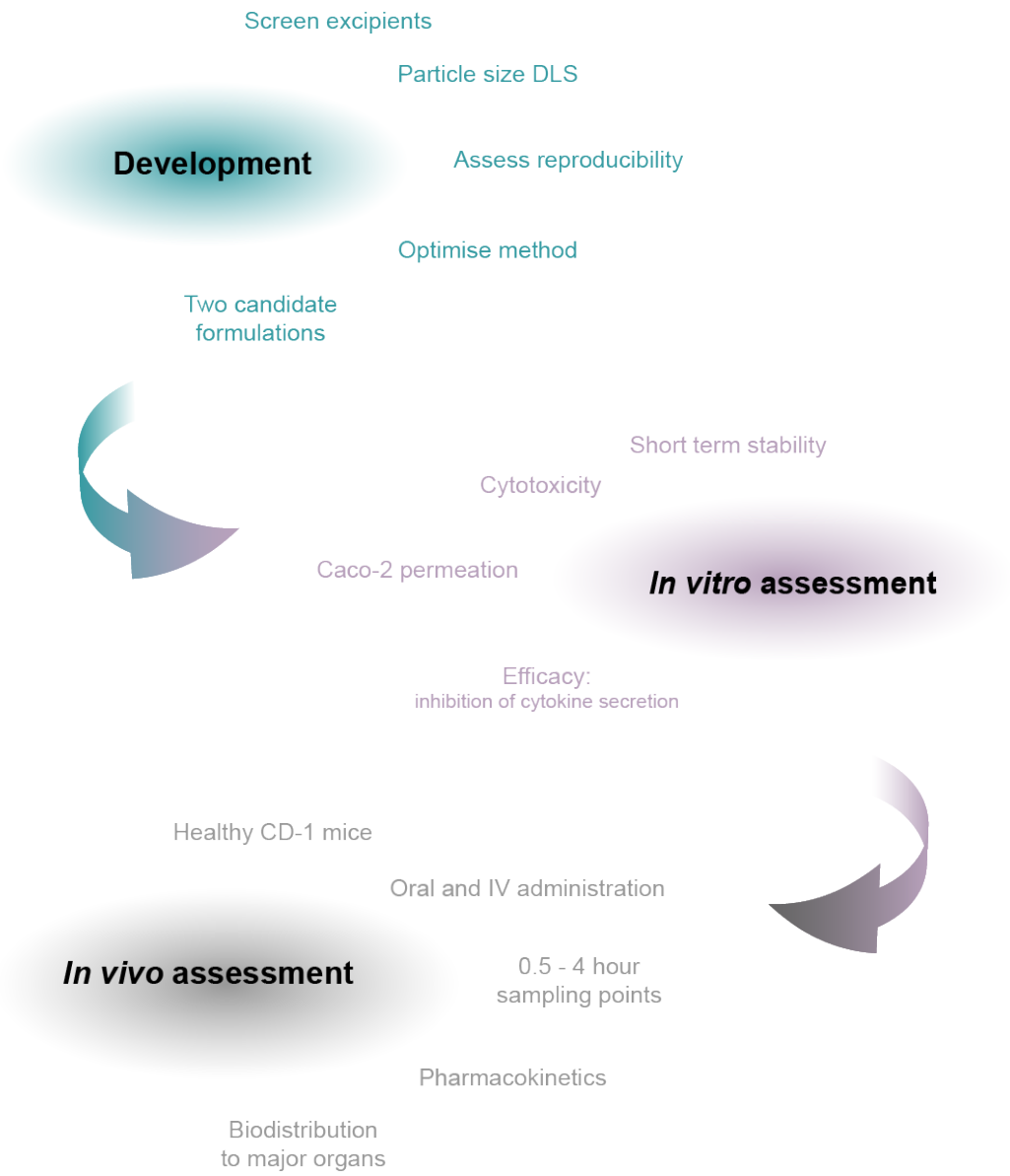

Figure 5.1 Overview of development and assessment process for prednisolone solid drug nanoparticles

Progression from the optimisation of this method began with *in vitro* tests of stability, cytotoxicity, permeation and therapeutic efficacy, all of which were selected to predict the effectiveness of the SDNs as oral therapeutic formulations. Stability of SDN dispersions were assessed in a range of simulated bio-relevant fluids including cell culture media and PBS in which the SDNs were dispersed in for *in vitro* and *in vivo* experiments to follow, and also simulated GI fluids to

predict compatibility with the oral route of administration. By measuring the particle size of SDN dispersions in these fluids over a 6 hour period, an indication of short term stability of the formulations primarily provided reasonable confidence that planned experiments would indeed be measuring effects of intact particles rather than dissolved PRD. Additionally, the data suggests that the GI environment may not physically alter the SDNs either by degradation or aggregation and therefore retain any advantages the nanoparticulate form may provide towards improved absorption from the intestine. Use of simulated GI fluids is not completely representative of an actual GI system, as it does not encompass other factors such as motility, functioning GI tract tissues, inter-individual variation or the constantly changing composition of GI contents although the published formulae used in this work have been closely matched in terms of pH, bile salts concentration and fed or fasted states [168]. For this study which is not predominantly focused on drug-GI interactions, the simulated fluids provide a simplified, standardised and replicable alternative to freshly obtained GI fluid which would introduce variability and complicate DLS measurements of particle size due to the presence of biomolecules of similar sizes. Further stability studies would be recommended for dispersions over longer time periods and for long-term storage stability of the freeze-dried monoliths, to determine if the drug degrades over time and if the material can still be dispersed weeks or months after production. This information is important when considering the potential clinical use of SDNs as the materials will need to be transported and stored between manufacture and use in the clinic.

As with any *in vitro* setting, these tests only provide a limited simulation of *in vivo* conditions, but were chosen from established and widely used models and assays such as the Caco-2 monolayer and lymphocyte activation [129, 169]. The MTT and CellTiter-Glo assays were chosen from a wide range of available cytotoxicity assays to give an overview of SDN effects on cell health, rather than an in depth assessment of toxicity mechanisms. In addition to unformulated PRD and the two SDN formulations, cytotoxicity of the excipients, singularly and in combination with PRD and the other excipients, was also determined to provide a comprehensive impression of material effects on cell viability. These studies were restricted to two cell lines, but in further work SDN cytotoxicity in additional cell lines and primary cells could be investigated, particularly in kidney derived cell types to determine if the enhanced kidney accumulation observed *in vivo* may lead to increased toxicity [170]. Similarly, a select number of immunological assays were chosen to give an overview of SDN efficacy on some of the main cell types involved in PRD anti-inflammatory mechanisms. As discussed in Chapter 3, there was not sufficient time for the third planned experiment with RBL cells as a model of mast cell activation, so this would be a priority in future work [143]. Regarding drug permeation models, the use of a multiple culture system encompassing other intestinal cell types would be more realistic and given more time to set up and optimise, would have been a valuable enhancement to the basic Caco-2 monolayer system [171].

This limited selection of *in vitro* tests ensured there was sufficient time remaining within the project for an *in vivo* study. Perhaps the most crucial aspect of the project, the data from the animal study provided an insight into how the PRD SDNs behave in an entire functional mammalian system. Principally, the

study demonstrated that formulating PRD as an SDN does not prevent absorption following oral administration and was successful in measuring radiolabelled PRD from samples to determine PK and biodistribution. As well as showing the method was effective, the results indicated that PRD SDNs may proffer benefits compared to conventional PRD through both formulations' improved pharmacokinetic profile and enhanced distribution to the kidney when given orally. Quantifying radiolabelled drug from samples is relatively quick compared to the alternative of quantification by HPLC or MS. This was one of the main advantages of choosing to use radiation, as running samples through a scintillation counter is faster and more straightforward than a HPLC method. Although a HPLC method was developed to quantify PRD, and used to confirm drug loading from preparations in PBS, much additional time and work would have been necessary to optimise this for extraction and quantification of PRD from biological samples. Preparation of tissue samples is time-consuming for either quantification technique, but more extensive purification of samples would be required for chromatographic analysis. The drawback of quantification by radiation is that it is measuring the radiolabel and not the drug itself, and therefore does not distinguish between the drug and its metabolites. In future work, a HPLC or MS quantification method would be optimised for measuring PRD from tissue samples.

The next step in continuing this work would assess the efficacy of PRD SDNs in an animal model of kidney disease, such as the toxicity mediated adriamycin-induced nephropathy model or the immune mediated Heymann's nephritis model discussed in Chapter 4 [166, 172]. Therapeutic effect may be evaluated by measurement of disease markers such as proteins in urine and cytokines in

tissues, and compared between animals treated with PRD SDNs and unformulated PRD. Use of a disease model is also important to determine how PK and biodistribution of PRD SDNs differs in animals with altered kidney function and possible inflammatory conditions. If the increased kidney accumulation of PRD following SDN treatment observed in this work also occurs in nephropathic animals, this effect could improve treatment of nephropathy and similar kidney conditions by passive targeting of PRD to the site of action, potential dose reduction and avoidance of toxicity by decreasing distribution to other tissues.

Larger studies beyond animal models would require a scale-up of PRD SDN production to make larger quantities, by spray drying large volumes of emulsion. A spray drying method would require optimisation for each formulation and may not be suitable for low melting point excipients such as TPGS and solutol, but would facilitate production to GMP (good manufacturing practice) standards necessary for potential future human trials [173, 174].

In further work, it would be interesting to modify the PRD SDN formulations to enable prolonged release of drug. Our results showed that PRD plasma concentration remains higher than that of unformulated PRD between 2 and 4 hours post-oral dose. If the plasma concentration could be sustained for longer periods of time following a single oral dose, this could reduce dosing frequency and may reduce toxicity whilst maintaining therapeutic concentrations of PRD, offering an improved regime for treating chronic inflammatory conditions.

Another direction would be to investigate how SDN formulation, particularly inclusion of an additional hydrophobic excipient, affects the properties of other

hydrophobic drugs. Using the exact formulation method presented in this work with a drug such as dexamethasone would allow exploration into how a drug with a similar structure to PRD compares in terms of SDN formation, particle size and crystallinity.

In conclusion, all of the data from this project supports the potential use of PRD SDNs as a minimally cytotoxic, efficacious oral formulation as an alternative to conventional unformulated PRD. Additional studies will further explore this potential, primarily through the use of animal models of disease to determine the therapeutic effectiveness and any change in side effects of the PRD SDN formulations. This project has successfully demonstrated a cohesive programme of development, optimisation and biological assessment of drug nanoformulations enabled by a close interaction between aspects of chemistry, pharmacology and immunology.

Appendix I

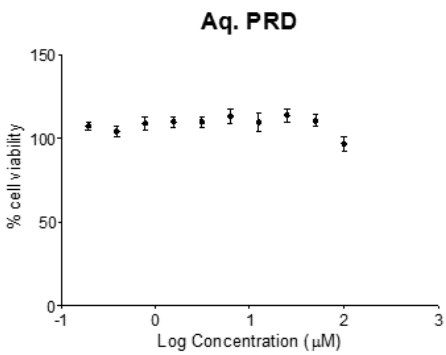
Aq. PRD
% cell viability
150
100
50
0
-1
0
1
2
3
Log Concentration (µM)

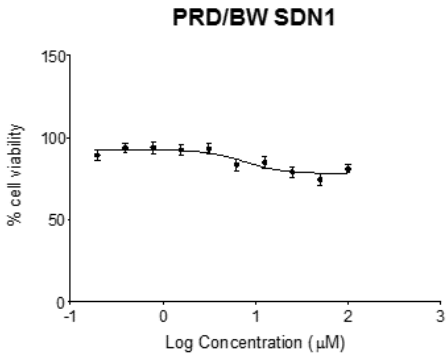
PRD/BW SDN1
% cell viability
150
100
50
0
-1
0
1
2
3
Log Concentration (µM)

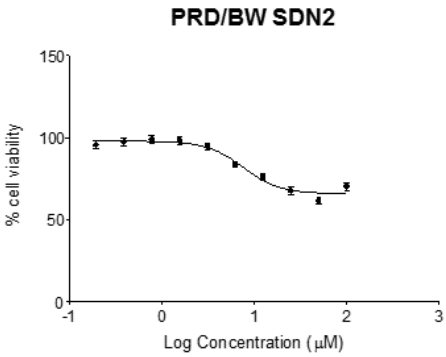
PRD/BW SDN2
% cell viability
150
100
50
0
-1
0
1
2
3
Log Concentration (µM)

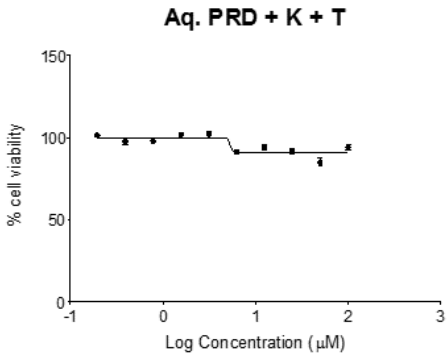
Aq. PRD + K + T
% cell viability
150
100
50
0
-1
0
1
2
3
Log Concentration (µM)

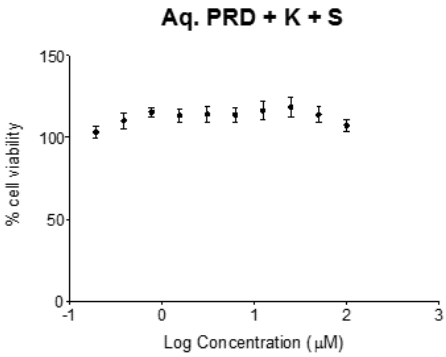
Aq. PRD + K + S
% cell viability
150
100
50
0
-1
0
1
2
3
Log Concentration (µM)

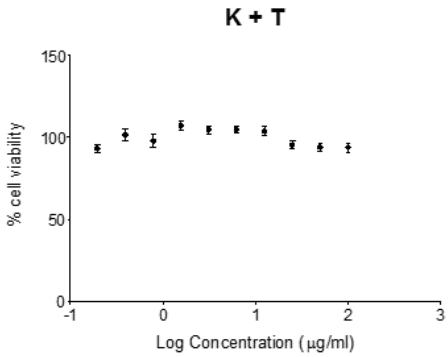
K + T
% cell viability
150
100
50
0
-1
0
1
2
3
Log Concentration (µg/ml)

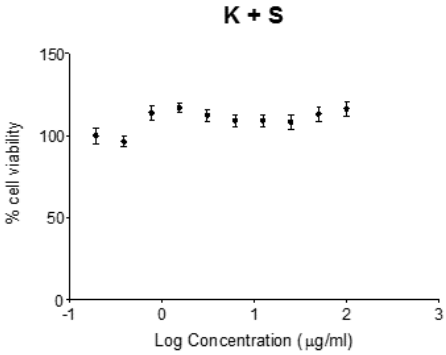
K + S
% cell viability
150
100
50
0
-1
0
1
2
3
Log Concentration (µg/ml)

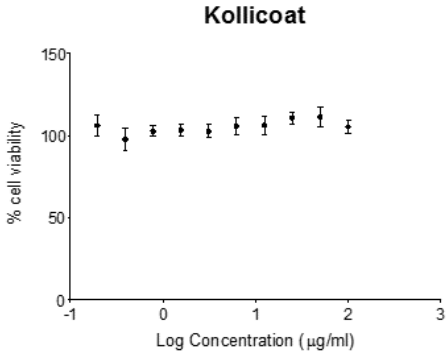
Kollicoat
% cell viability
150
100
50
0
-1
0
1
2
3
Log Concentration (µg/ml)

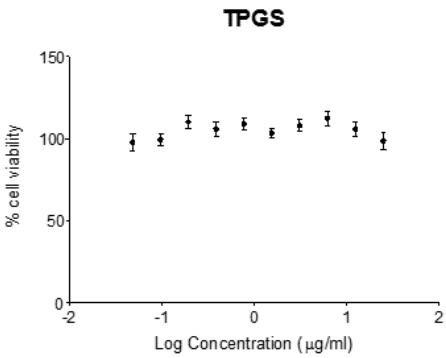
TPGS
% cell viability
150
100
50
0
-2
-1
0
1
2
Log Concentration (µg/ml)

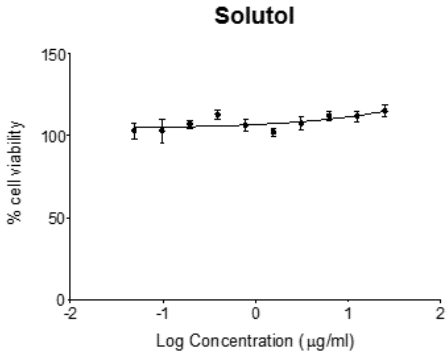
Solutol
% cell viability
150
100
50
0
-2
-1
0
1
2
Log Concentration (µg/ml)

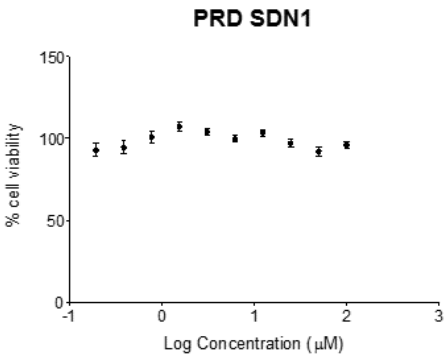
PRD SDN1
% cell viability
150
100
50
0
-1
0
1
2
3
Log Concentration (µM)

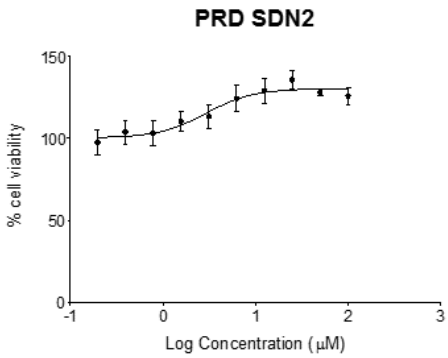
PRD SDN2
% cell viability
150
100
50
0
-1
0
1
2
3
Log Concentration (µM)

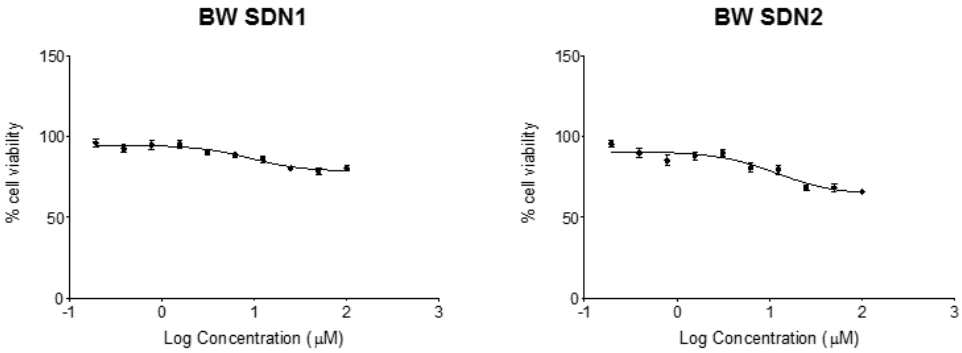

Figure AI.1: Percentage cell viability of Caco-2 cells determined by MTT assay following 24 hour incubation with aqueous PRD, PRD/BW SDN1, PRD/BW SDN2, [aqueous PRD + kollicoat + TPGS], [aqueous PRD + kollicoat + solutol], [kollicoat + TPGS], [kollicoat + solutol], kollicoat, TPGS, solutol, PRD-only SDN1, PRD-only SDN2, BW-only SDN1, BW-only SDN2. N = 8.

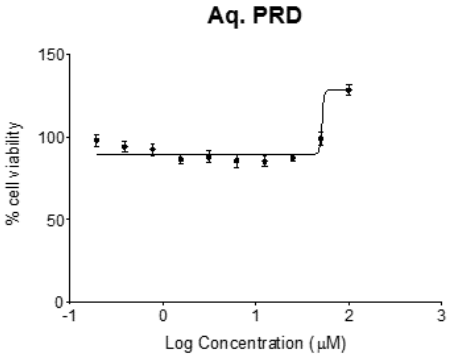
Aq. PRD
% cell viability
150
100
50
0
-1
0
1
2
3
Log Concentration (µM)

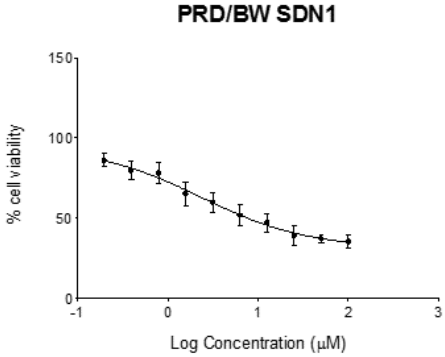
PRD/BW SDN1
% cell viability
150
100
50
0
-1
0
1
2
3
Log Concentration (µM)

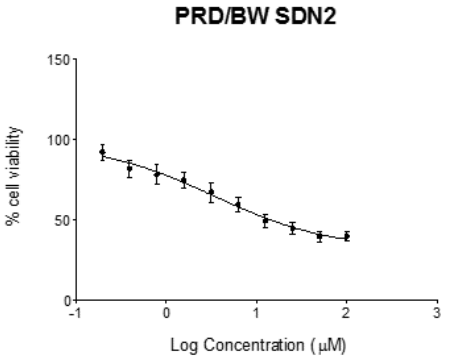
PRD/BW SDN2
% cell viability
150
100
50
0
-1
0
1
2
3
Log Concentration (µM)

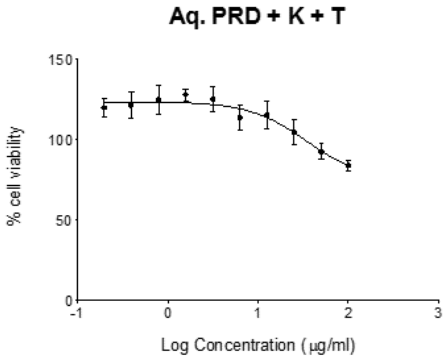
Aq. PRD + K + T
% cell viability
150
100
50
0
-1
0
1
2
3
Log Concentration (µg/ml)

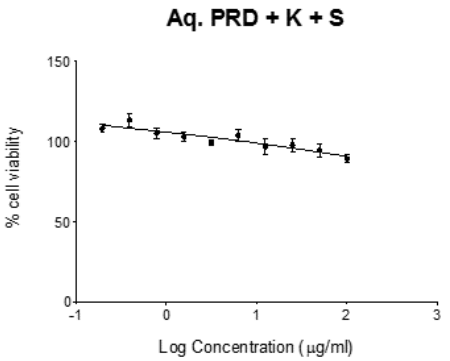
Aq. PRD + K + S
% cell viability
150
100
50
0
-1
0
1
2
3
Log Concentration (µg/ml)

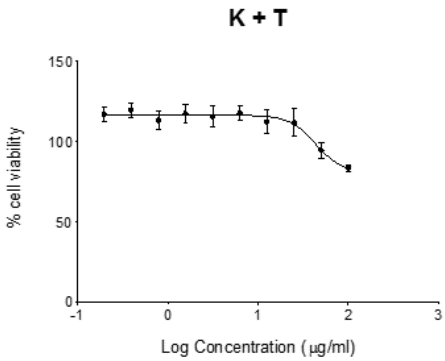
K + T
% cell viability
150
100
50
0
-1
0
1
2
3
Log Concentration (µg/ml)

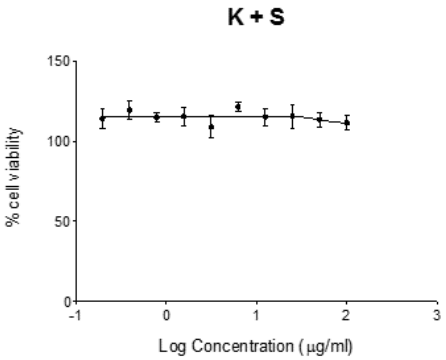
K + S
% cell viability
150
100
50
0
-1
0
1
2
3
Log Concentration (µg/ml)

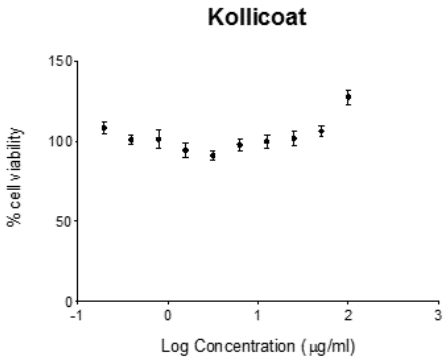
Kollicoat
% cell viability
150
100
50
0
-1
0
1
2
3
Log Concentration (µg/ml)

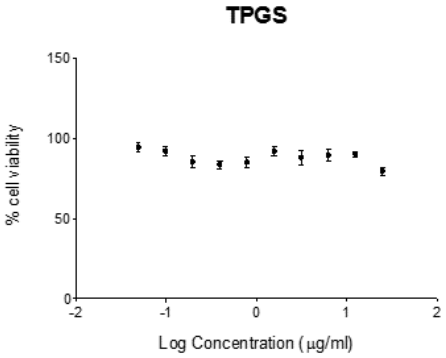
TPGS
% cell viability
150
100
50
0
-2
-1
0
1
2
Log Concentration (µg/ml)

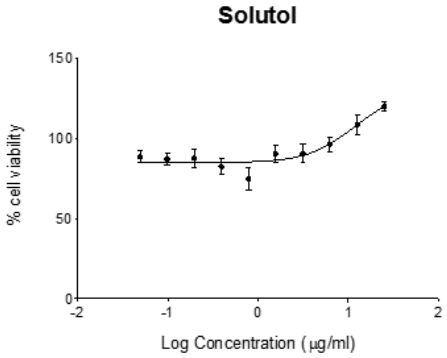
Solutol
% cell viability
150
100
50
0
-2
-1
0
1
2
Log Concentration (µg/ml)

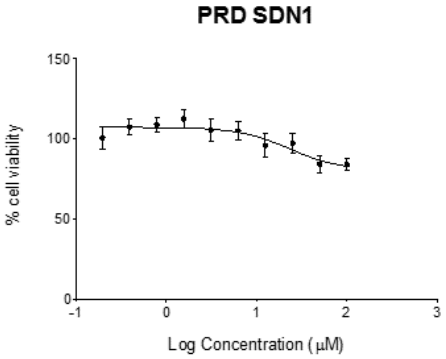
PRD SDN1
% cell viability
150
100
50
0
-1
0
1
2
3
Log Concentration (µM)

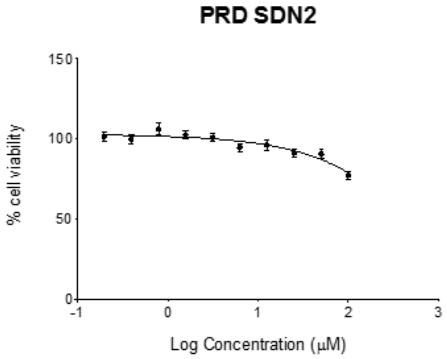
PRD SDN2
% cell viability
150
100
50
0
-1
0
1
2
3
Log Concentration (µM)

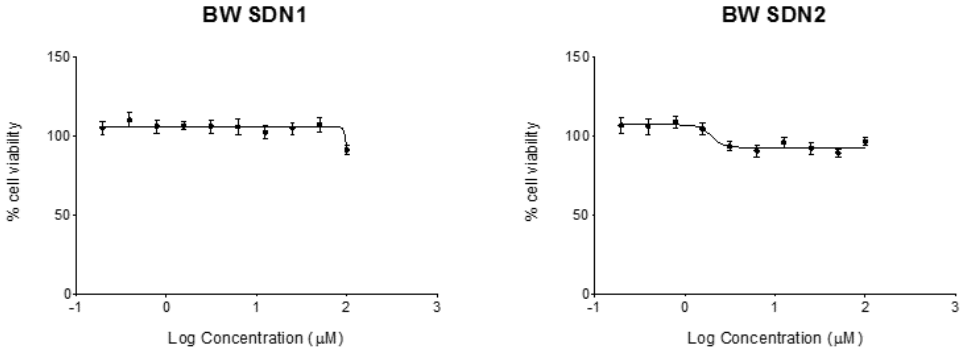

Figure AI.2: Percentage cell viability of Caco-2 cells determined by MTT assay following 120 hour incubation with aqueous PRD, PRD/BW SDN1, PRD/BW SDN2, [aqueous PRD + kollicoat + TPGS], [aqueous PRD + kollicoat + solutol], [kollicoat + TPGS], [kollicoat + solutol], kollicoat, TPGS, solutol, PRD-only SDN1, PRD-only SDN2, BW-only SDN1, BW-only SDN2. N = 8.

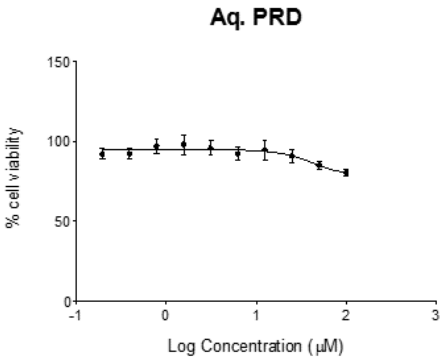
Aq. PRD
% cell viability
150
100
50
0
-1
0
1
2
3
Log Concentration (µM)

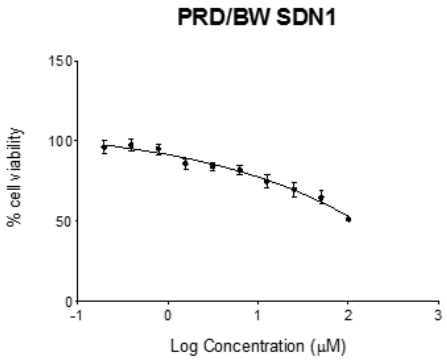
PRD/BW SDN1
% cell viability
150
100
50
0
-1
0
1
2
3
Log Concentration (µM)

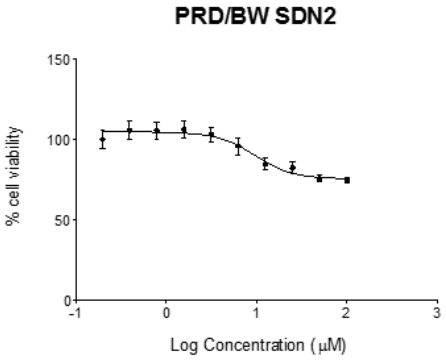
PRD/BW SDN2
% cell viability
150
100
50
0
-1
0
1
2
3
Log Concentration (µM)

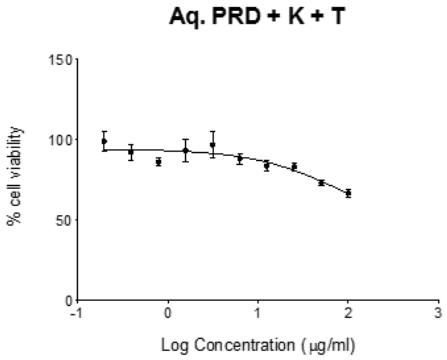
Aq. PRD + K + T
% cell viability
150
100
50
0
-1
0
1
2
3
Log Concentration (µg/ml)

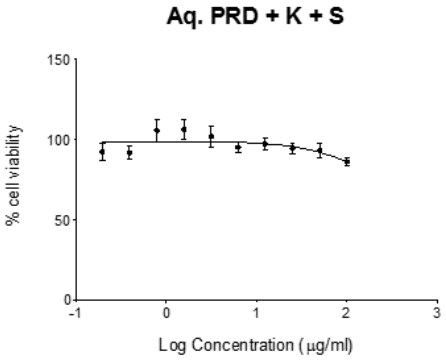
Aq. PRD + K + S
% cell viability
150
100
50
0
-1
0
1
2
3
Log Concentration (µg/ml)

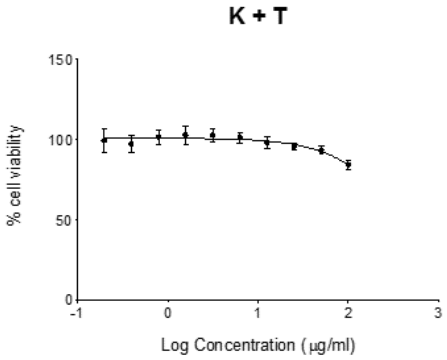
K + T
% cell viability
150
100
50
0
-1
0
1
2
3
Log Concentration (µg/ml)

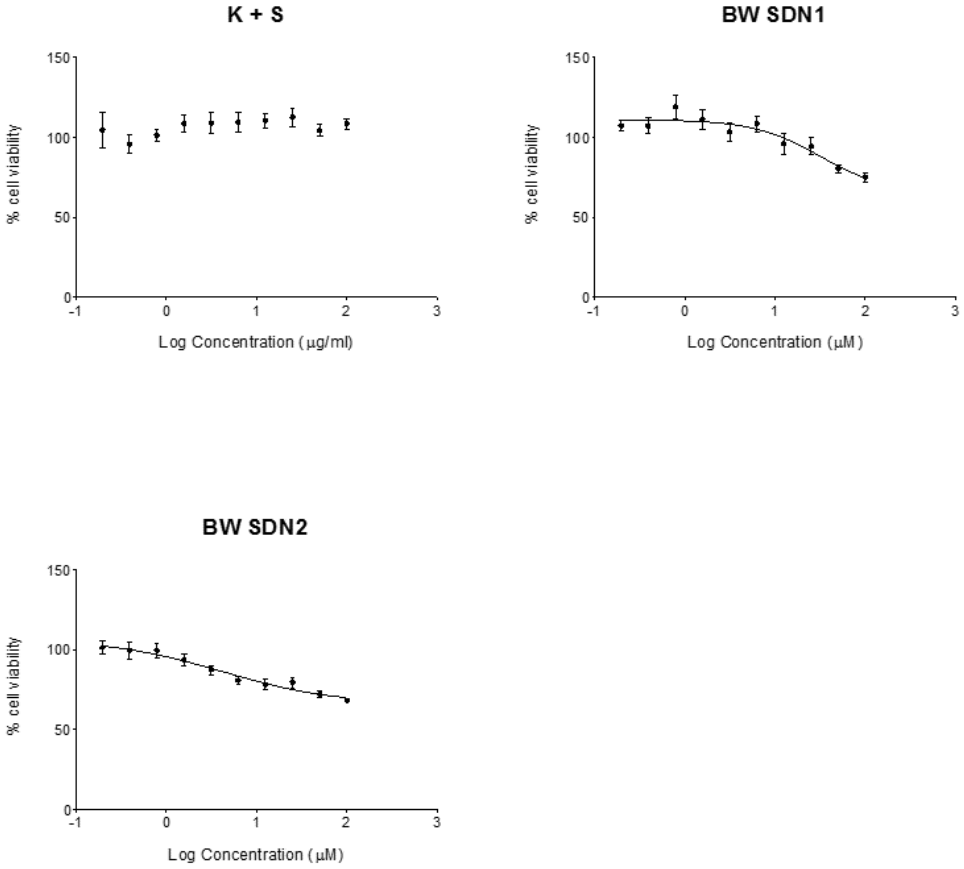

Figure AI.3: Percentage cell viability of A549 cells determined by MTT assay following 24 hour incubation with aqueous PRD, PRD/BW SDN1, PRD/BW SDN2, [aqueous PRD + kollicoat + TPGS], [aqueous PRD + kollicoat + solutol], [kollicoat + TPGS], [kollicoat + solutol], BW-only SDN1, BW-only SDN2. N = 8.

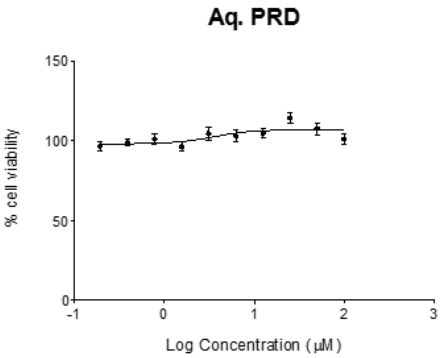
Aq. PRD
% cell viability
Log Concentration (µM)

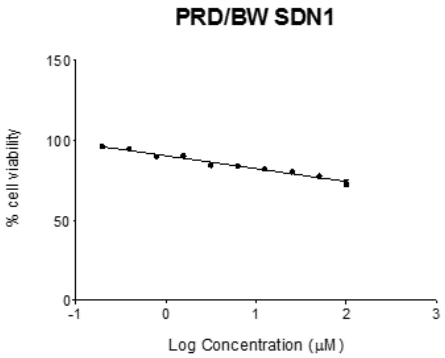
PRD/BW SDN1
% cell viability
Log Concentration (µM)

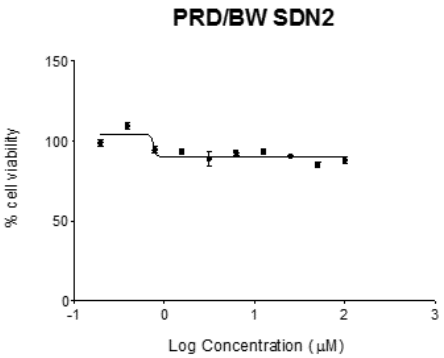
PRD/BW SDN2
% cell viability
Log Concentration (µM)

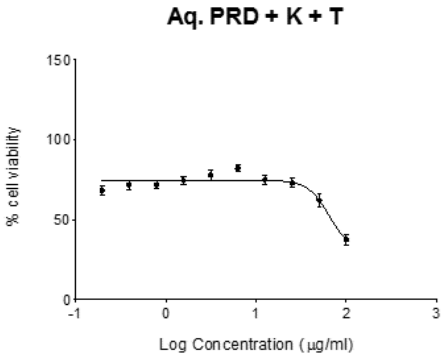
Aq. PRD + K + T
% cell viability
Log Concentration (µg/ml)

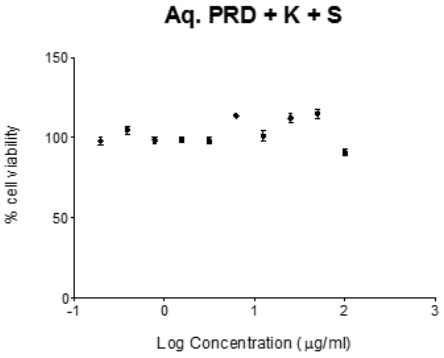
Aq. PRD + K + S
% cell viability
Log Concentration (µg/ml)

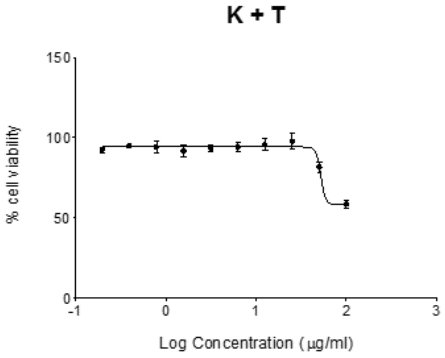
K + T
% cell viability
Log Concentration (µg/ml)

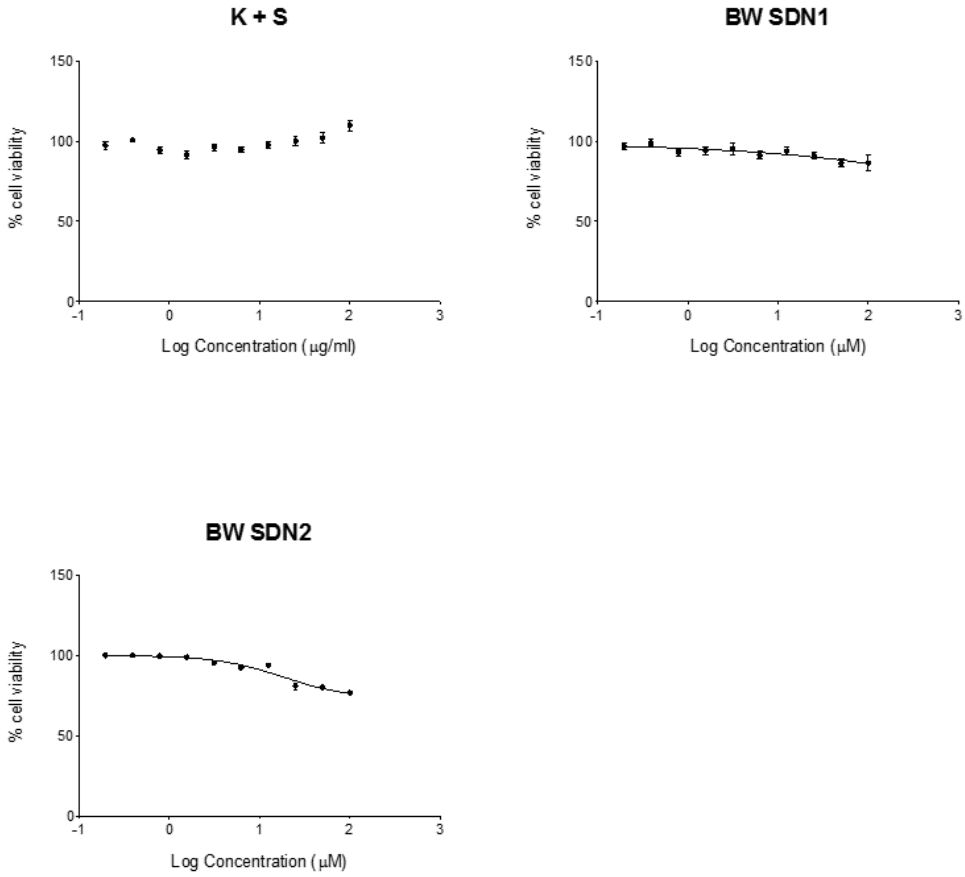

Figure AI.4: Percentage cell viability of A549 cells determined by MTT assay following 120 hour incubation with aqueous PRD, PRD/BW SDN1, PRD/BW SDN2, [aqueous PRD + kollicoat + TPGS], [aqueous PRD + kollicoat + solutol], [kollicoat + TPGS], [kollicoat + solutol], BW-only SDN1, BW-only SDN2. N = 8.

Appendix II

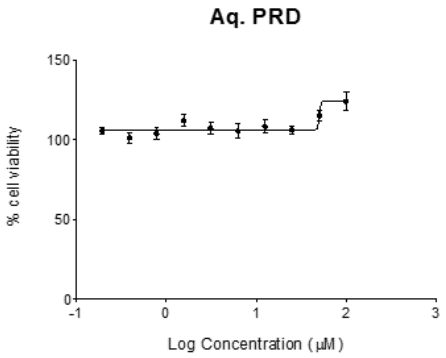
Aq. PRD
% cell viability
Log Concentration (µM)

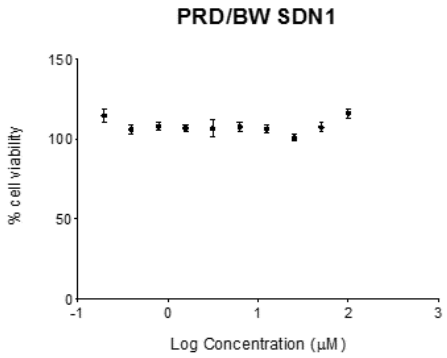
PRD/BW SDN1
% cell viability
Log Concentration (µM)

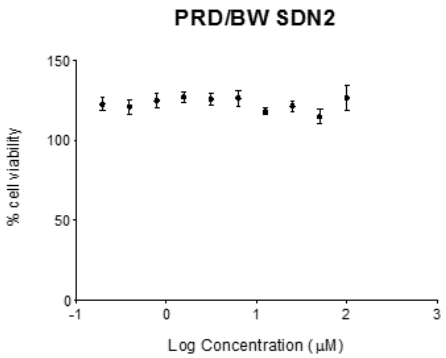
PRD/BW SDN2
% cell viability
Log Concentration (µM)

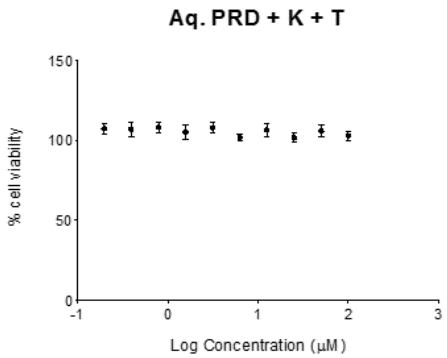
Aq. PRD + K + T
% cell viability
Log Concentration (µM)

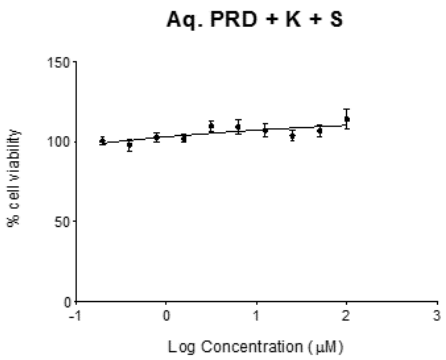
Aq. PRD + K + S
% cell viability
Log Concentration (µM)

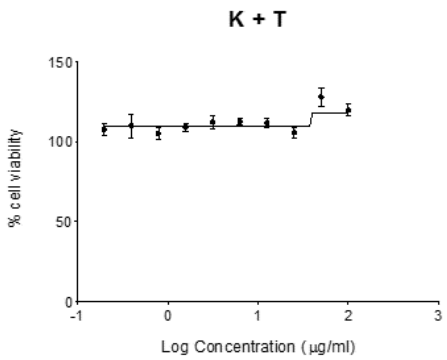
K + T
% cell viability
Log Concentration (µg/ml)

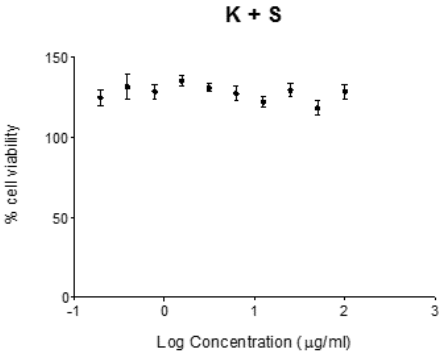
K + S
% cell viability
150
100
50
0
-1
0
1
2
3
Log Concentration (µg/ml)

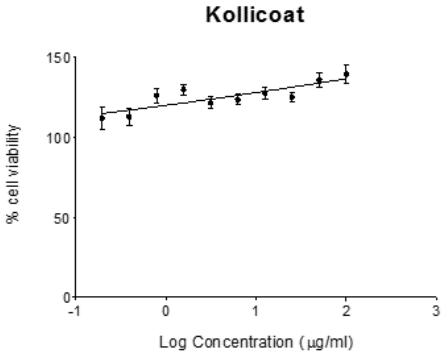
Kollicoat
% cell viability
150
100
50
0
-1
0
1
2
3
Log Concentration (µg/ml)

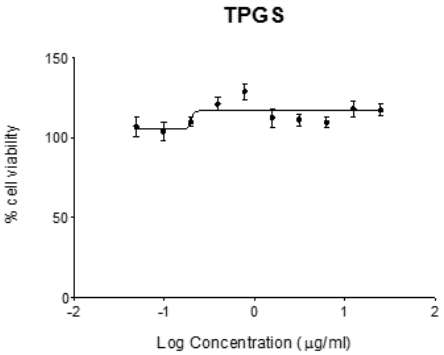
TPGS
% cell viability
150
100
50
0
-2
-1
0
1
2
Log Concentration (µg/ml)

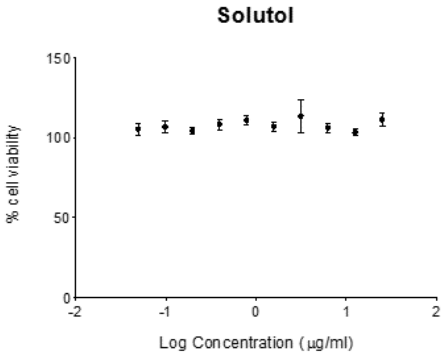
Solutol
% cell viability
150
100
50
0
-2
-1
0
1
2
Log Concentration (µg/ml)

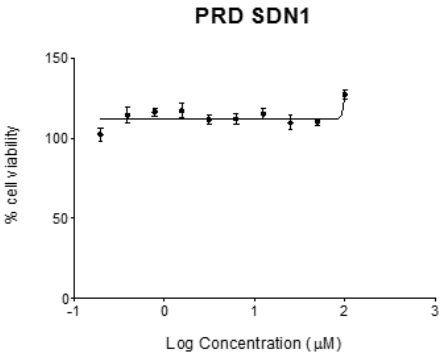
PRD SDN1
% cell viability
150
100
50
0
-1
0
1
2
3
Log Concentration (µM)

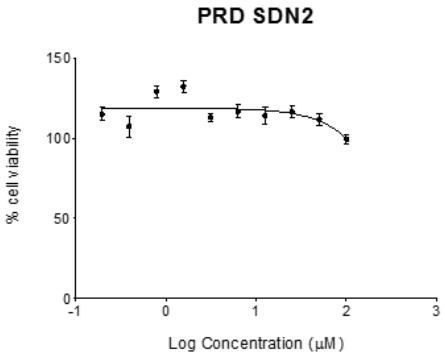
PRD SDN2
% cell viability
150
100
50
0
-1
0
1
2
3
Log Concentration (µM)

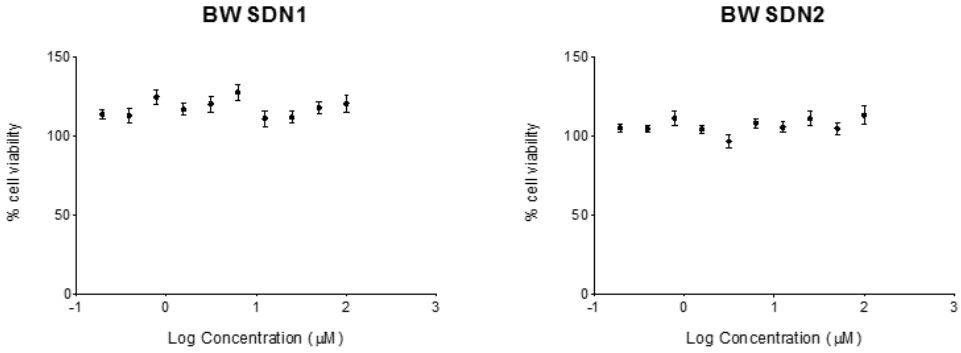

Figure AII.1: Percentage cell viability of Caco-2 cells determined by CellTiter-Glo assay following 24 hour incubation with aqueous PRD, PRD/BW SDN1, PRD/BW SDN2, [aqueous PRD + kollicoat + TPGS], [aqueous PRD + kollicoat + solutol], [kollicoat + TPGS], [kollicoat + solutol], kollicoat, TPGS, solutol, PRD-only SDN1, PRD-only SDN2, BW-only SDN1, BW-only SDN2. N = 8.

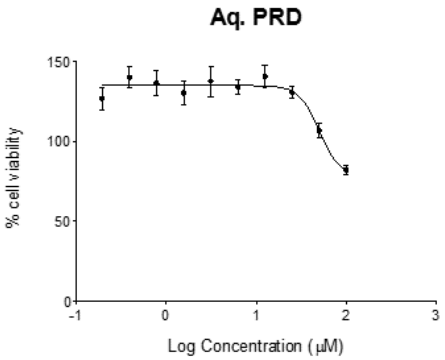
Aq. PRD
% cell viability
Log Concentration (µM)

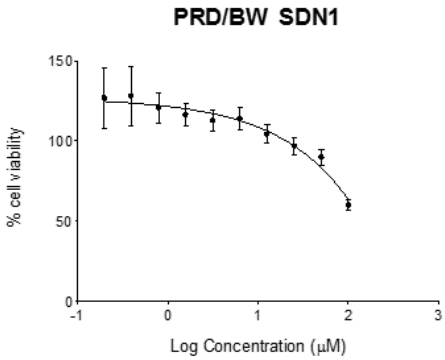
PRD/BW SDN1
% cell viability
Log Concentration (µM)

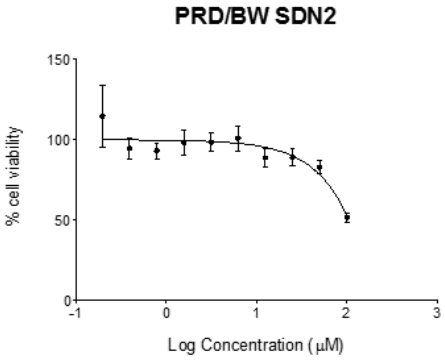
PRD/BW SDN2
% cell viability
Log Concentration (µM)

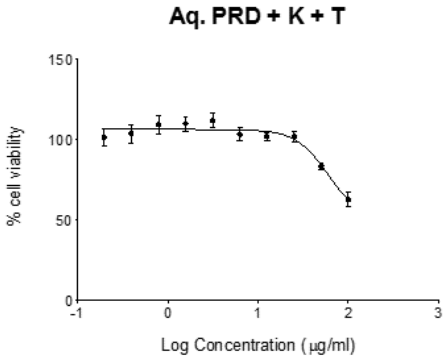
Aq. PRD + K + T
% cell viability
Log Concentration (µg/ml)

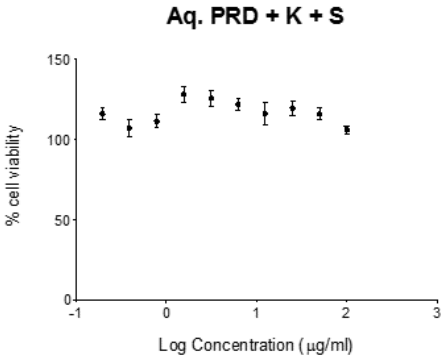
Aq. PRD + K + S
% cell viability
Log Concentration (µg/ml)

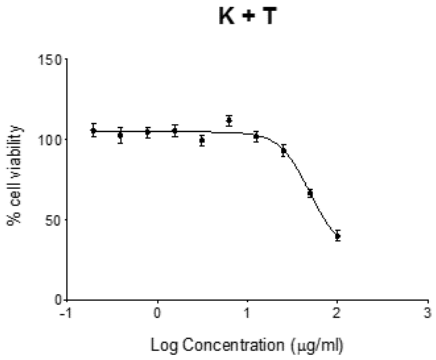
K + T
% cell viability
Log Concentration (µg/ml)

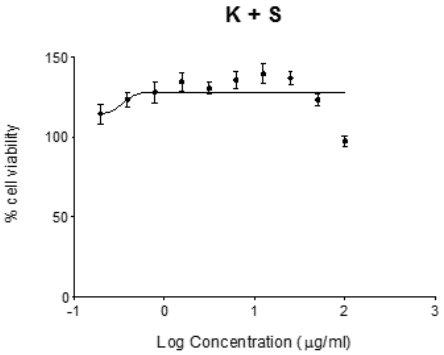
K + S
% cell viability
Log Concentration (µg/ml)

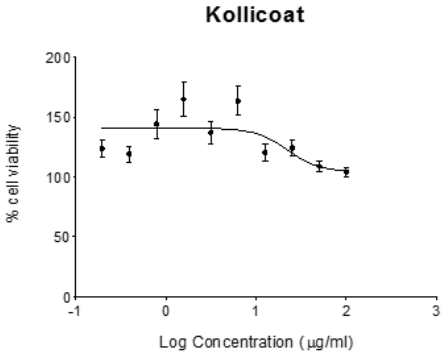
Kollicoat
% cell viability
Log Concentration (µg/ml)

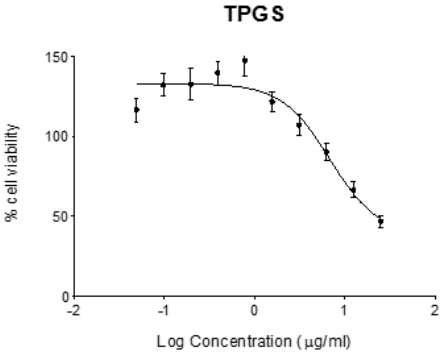
TPGS
% cell viability
Log Concentration (µg/ml)

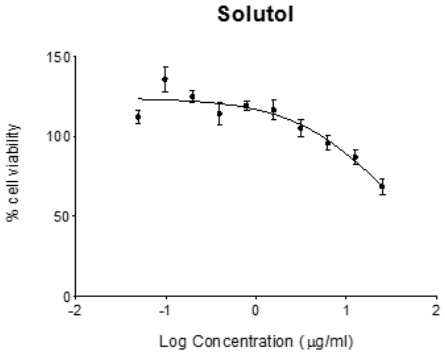
Solutol
% cell viability
Log Concentration (µg/ml)

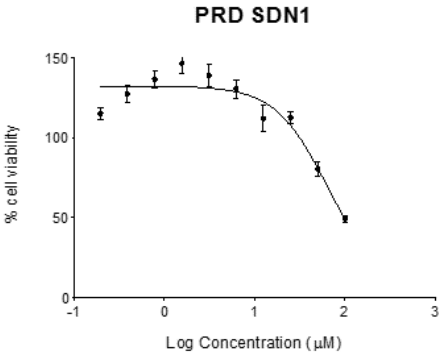
PRD SDN1
% cell viability
Log Concentration (µM)

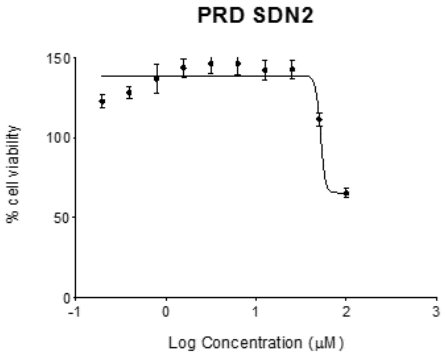
PRD SDN2
% cell viability
Log Concentration (µM)

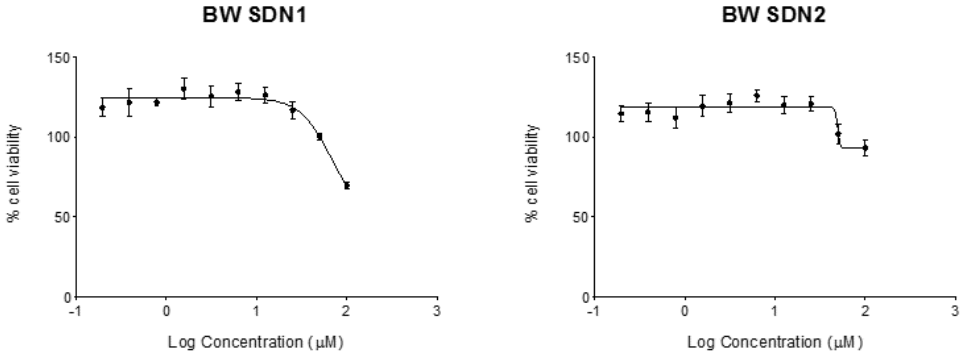

Figure AII.2: Percentage cell viability of Caco-2 cells determined by CellTiter-Glo assay following 120 hour incubation with aqueous PRD, PRD/BW SDN1, PRD/BW SDN2, [aqueous PRD + kollicoat + TPGS], [aqueous PRD + kollicoat + solutol], [kollicoat + TPGS], [kollicoat + solutol], kollicoat, TPGS, solutol, PRD-only SDN1, PRD-only SDN2, BW-only SDN1, BW-only SDN2. N = 8.

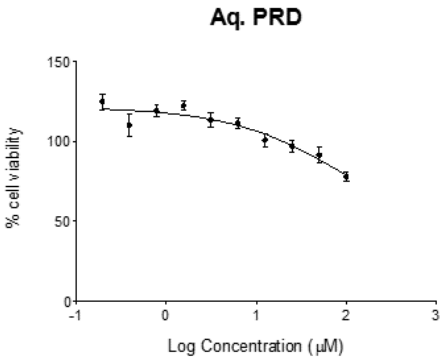
Aq. PRD
% cell viability
150
100
50
0
-1
0
1
2
3
Log Concentration (µM)

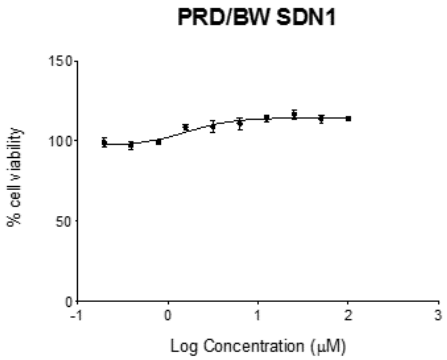
PRD/BW SDN1
% cell viability
150
100
50
0
-1
0
1
2
3
Log Concentration (µM)

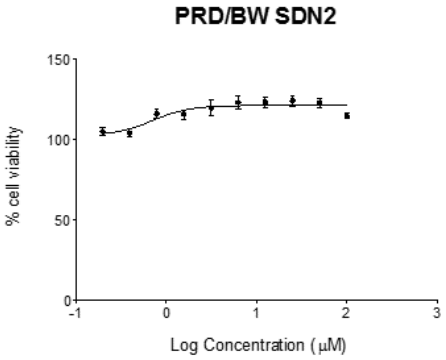
PRD/BW SDN2
% cell viability
150
100
50
0
-1
0
1
2
3
Log Concentration (µM)

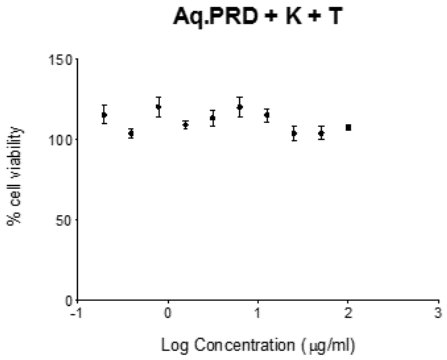
Aq.PRD + K + T
% cell viability
150
100
50
0
-1
0
1
2
3
Log Concentration (µg/ml)

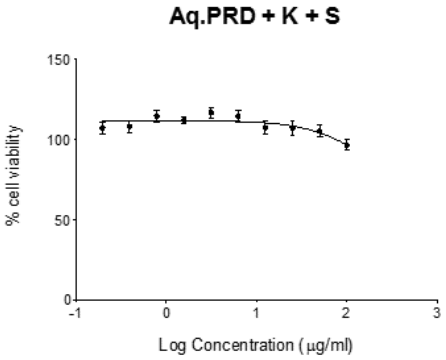
Aq.PRD + K + S
% cell viability
150
100
50
0
-1
0
1
2
3
Log Concentration (µg/ml)

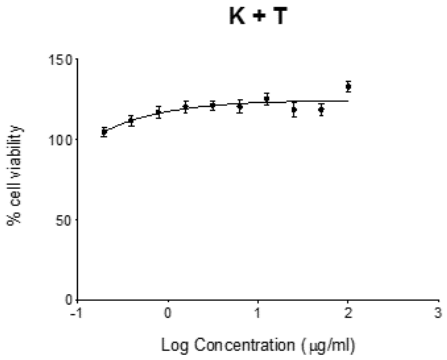
K + T
% cell viability
150
100
50
0
-1
0
1
2
3
Log Concentration (µg/ml)

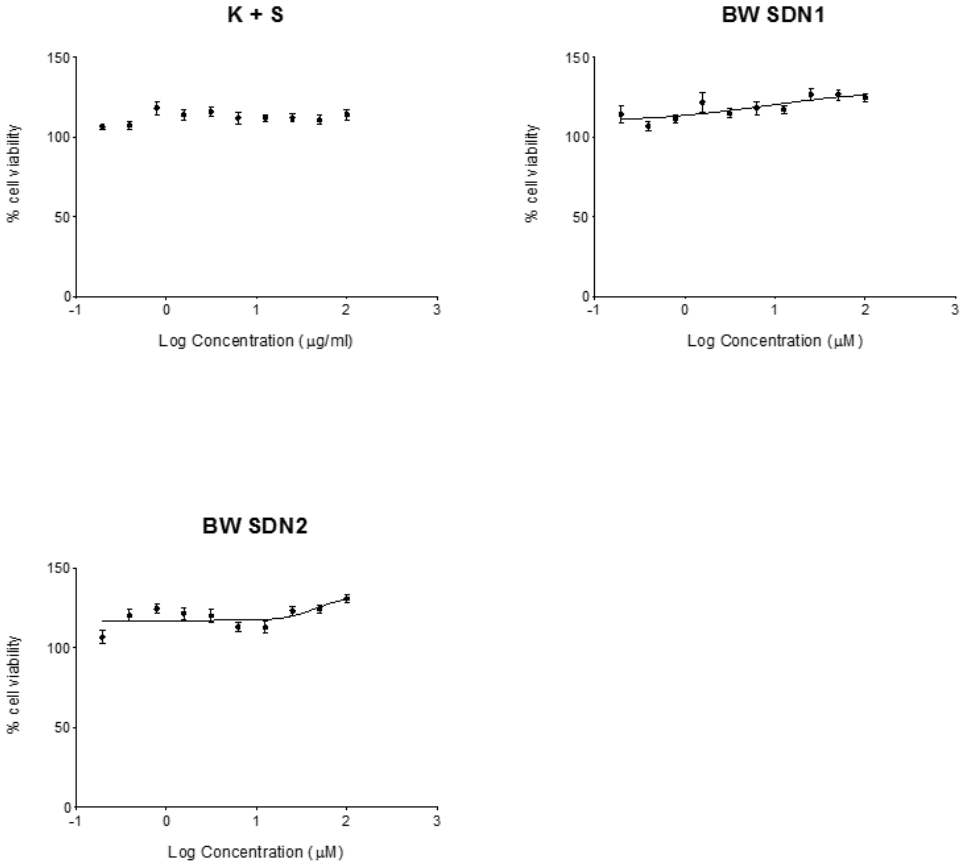

Figure AII.3: Percentage cell viability of A549 cells determined by CellTiter-Glo assay following 24 hour incubation with aqueous PRD, PRD/BW SDN1, PRD/BW SDN2, [aqueous PRD + kollicoat + TPGS], [aqueous PRD + kollicoat + solutol], [kollicoat + TPGS], [kollicoat + solutol], BW-only SDN1, BW-only SDN2. N = 8.

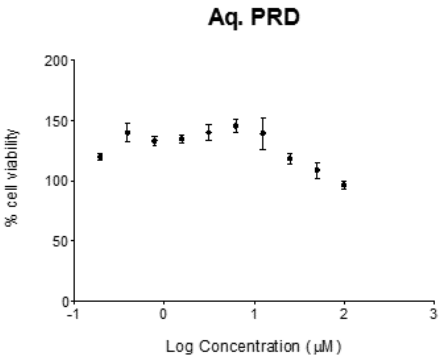
Aq. PRD
% cell viability
Log Concentration (µM)

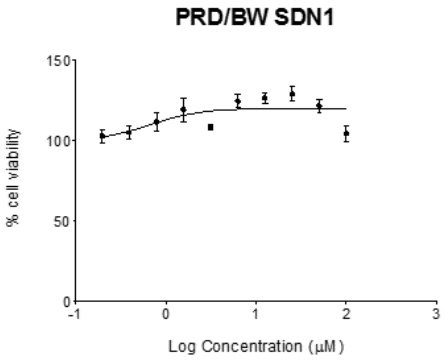
PRD/BW SDN1
% cell viability
Log Concentration (µM)

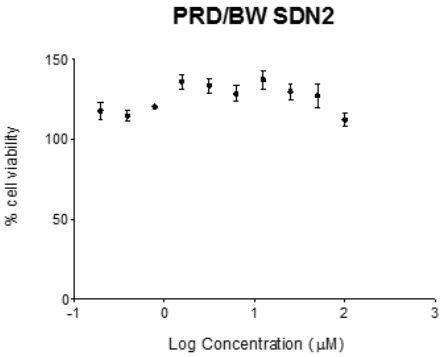
PRD/BW SDN2
% cell viability
Log Concentration (µM)

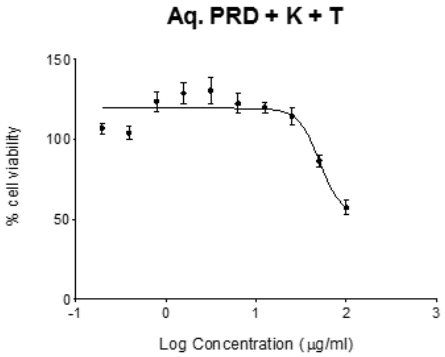
Aq. PRD + K + T
% cell viability
Log Concentration (µg/ml)

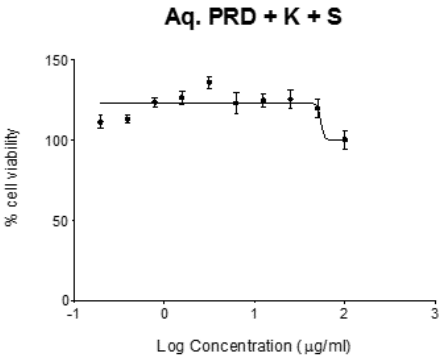
Aq. PRD + K + S
% cell viability
Log Concentration (µg/ml)

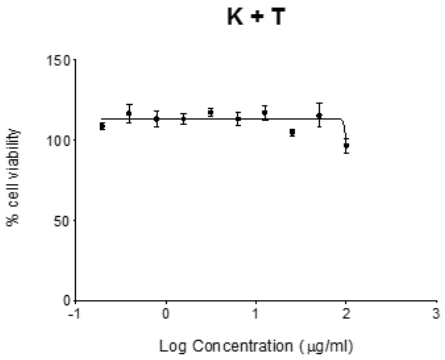
K + T
% cell viability
Log Concentration (µg/ml)

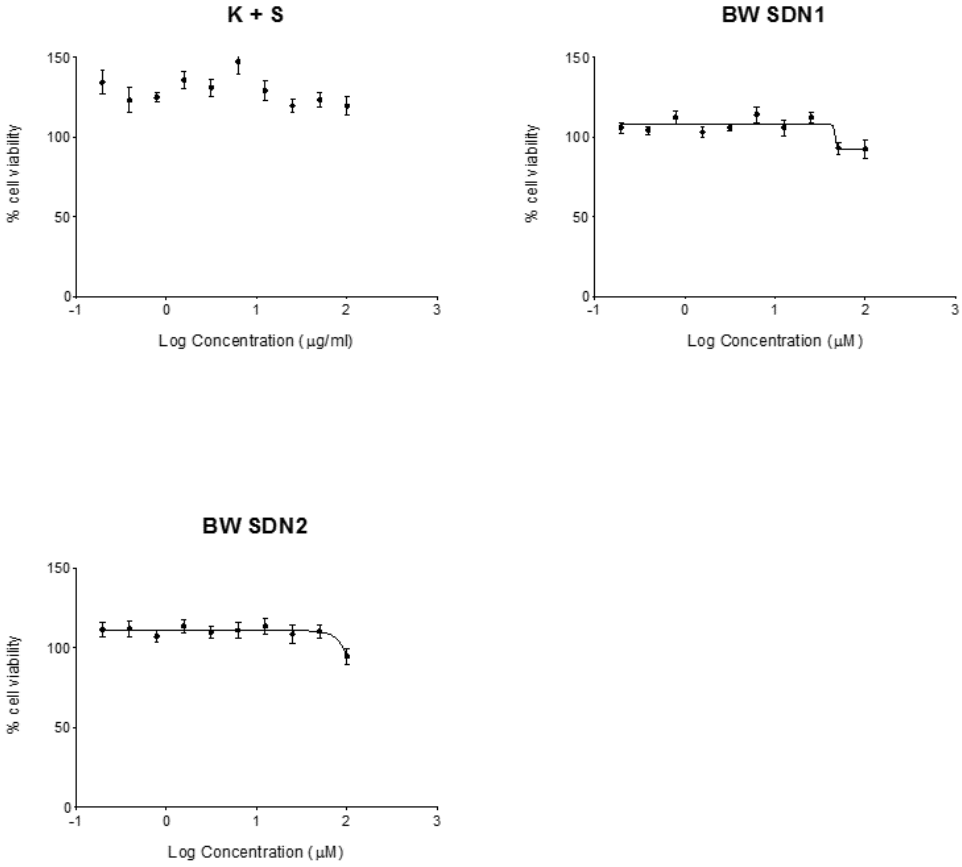

Figure AII.4: Percentage cell viability of A549 cells determined by CellTiter-Glo assay following 120 hour incubation with aqueous PRD, PRD/BW SDN1, PRD/BW SDN2, [aqueous PRD + kollicoat + TPGS], [aqueous PRD + kollicoat + solutol], [kollicoat + TPGS], [kollicoat + solutol], BW-only SDN1, BW-only SDN2. N = 8.

Bibliography

1. Freel, E.M., et al., *Endogenous corticosteroid biosynthesis in subjects after bilateral adrenalectomy.* Clinical Endocrinology, 2007. **66**(5): p. 659-665.
2. Zhou, J. and J.A. Cidlowski, *The human glucocorticoid receptor: One gene, multiple proteins and diverse responses.* Steroids, 2005. **70**(5): p. 407-417.
3. Funder, J.W., *Mineralocorticoid receptors: Distribution and activation.* Heart Failure Reviews, 2005. **10**(1): p. 15-22.
4. Braun, T.P. and D.L. Marks, *The regulation of muscle mass by endogenous glucocorticoids.* Frontiers in Physiology, 2015. **6**(FEB).
5. Weiser, M.J., C. Osterlund, and R.L. Spencer, *Inhibitory Effects of Corticosterone in the Hypothalamic Paraventricular Nucleus (PVN) on Stress-Induced Adrenocorticotrophic Hormone Secretion and Gene Expression in the PVN and Anterior Pituitary.* Journal of Neuroendocrinology, 2011. **23**(12): p. 1231-1240.
6. Hillier, S.G., *Diamonds are forever: The cortisone legacy.* Journal of Endocrinology, 2007. **195**(1): p. 1-6.
7. Barnes, P.J., *Corticosteroids: The drugs to beat.* European Journal of Pharmacology, 2006. **533**(1): p. 2-14.
8. Stahn, C., et al., *Molecular mechanisms of glucocorticoid action and selective glucocorticoid receptor agonists.* Molecular and Cellular Endocrinology, 2007. **275**(1-2): p. 71-78.
9. Rohatagi, S., et al., *Risk-Benefit Value of Inhaled Glucocorticoids: A Pharmacokinetic/ Pharmacodynamic Perspective.* The Journal of Clinical Pharmacology, 2004. **44**(1): p. 37-47.
10. Claahsen-van der Grinten, H.L., et al., *Congenital adrenal hyperplasia — Pharmacologic interventions from the prenatal phase to adulthood.* Pharmacology & Therapeutics, 2011. **132**(1): p. 1-14.
11. Buttgereit, F., H. Zhou, and M.J. Seibel, *Arthritis and endogenous glucocorticoids: The emerging role of the 11β-HSD enzymes.* Annals of the Rheumatic Diseases, 2008. **67**(9): p. 1201-1203.
12. Bergmann, T.K., et al., *Clinical pharmacokinetics and pharmacodynamics of prednisolone and prednisone in solid organ transplantation.* Clinical Pharmacokinetics, 2012. **51**(11): p. 711-741.
13. Vogt, M., et al., *Biowaiver monographs for immediate release solid oral dosage forms: Prednisolone.* Journal of Pharmaceutical Sciences, 2007. **96**(1): p. 27-37.
14. Xu, J., J. Winkler, and H. Derendorf, *A pharmacokinetic/pharmacodynamic approach to predict total prednisolone concentrations in human plasma.* Journal of Pharmacokinetics and Pharmacodynamics, 2007. **34**(3): p. 355-372.
15. Czock, D., et al., *Pharmacokinetics and pharmacodynamics of systemically administered glucocorticoids.* Clinical Pharmacokinetics, 2005. **44**(1): p. 61-98.

16. Napier, C. and S.H.S. Pearce, *Current and emerging therapies for Addison's disease.* Current Opinion in Endocrinology, Diabetes and Obesity, 2014. **21**(3): p. 147-153.
17. British Thoracic Society, S.I.G.N., *British guideline on the management of asthma*. 2016.
18. Bush, A., et al., *Pharmacological treatment of severe, therapy-resistant asthma in children: what can we learn from where?* European Respiratory Journal, 2011. **38**(4): p. 947.
19. Van Der Goes, M.C., J.W.G. Jacobs, and J.W.J. Bijlsma, *Rediscovering the therapeutic use of glucocorticoids in rheumatoid arthritis.* Current Opinion in Rheumatology, 2016. **28**(3): p. 289-296.
20. Simic, I., M. Tabatabaeifar, and F. Schaefer, *Animal models of nephrotic syndrome.* Pediatric Nephrology (Berlin, Germany), 2013. **28**(11): p. 2079-2088.
21. Zolotas, E. and R.G. Krishnan, *Nephrotic syndrome.* Paediatrics and Child Health, 2016. **26**(8): p. 349-352.
22. Palmer, S.C., K. Nand, and G.F. Strippoli, *Interventions for minimal change disease in adults with nephrotic syndrome.* Cochrane database of systematic reviews (Online), 2008(1).
23. Lombel, R.M., D.S. Gipson, and E.M. Hodson, *Treatment of steroid-sensitive nephrotic syndrome: new guidelines from KDIGO.* Pediatric Nephrology (Berlin, Germany), 2013. **28**(3): p. 415-426.
24. Hunter, R.W., J.R. Ivy, and M.A. Bailey, *Glucocorticoids and renal Na+ transport: Implications for hypertension and salt sensitivity.* Journal of Physiology, 2014. **592**(8): p. 1731-1744.
25. Wikstrom, A.C., *Glucocorticoid action and novel mechanisms of steroid resistance: role of glucocorticoid receptor-interacting proteins for glucocorticoid responsiveness.* Journal of Endocrinology, 2003. **178**(3): p. 331-337.
26. Htun, H., et al., *Visualization of glucocorticoid receptor translocation and intranuclear organization in living cells with a green fluorescent protein chimera.* Proceedings of the National Academy of Sciences of the United States of America, 1996. **93**(10): p. 4845-4850.
27. Rhen, T. and J.A. Cidlowski, *Antiinflammatory action of glucocorticoids - New mechanisms for old drugs.* New England Journal of Medicine, 2005. **353**(16).
28. Murray, P.J., *Understanding and exploiting the endogenous interleukin-10/STAT3-mediated anti-inflammatory response.* Current Opinion in Pharmacology, 2006. **6**(4): p. 379-386.
29. Ouyang, W., et al., *Regulation and functions of the IL-10 family of cytokines in inflammation and disease*, in *Annual Review of Immunology*. 2011. p. 71-109.
30. Kim, S.W., et al., *Inhibition of cytosolic phospholipase A<inf>2</inf> by annexin I: Specific interaction model and mapping of the interaction site.* Journal of Biological Chemistry, 2001. **276**(19): p. 15712-15719.
31. Hayashi, R., et al., *Effects of glucocorticoids on gene transcription.* European Journal of Pharmacology, 2004. **500**(1–3): p. 51-62.
32. Barnes, P.J., *Allergy review series VII: Intracellular signaling and regulation of allergic reactions: Molecular mechanisms of*

corticosteroids in allergic diseases. Allergy: European Journal of Allergy and Clinical Immunology, 2001. **56**(10): p. 928-936.
33. Busillo, J.M., K.M. Azzam, and J.A. Cidlowski, *Glucocorticoids Sensitize the Innate Immune System through Regulation of the NLRP3 Inflammasome.* Journal of Biological Chemistry, 2011. **286**(44): p. 38703-38713.
34. Reichardt, H.M. and G. Schütz, *Glucocorticoid signalling - Multiple variations of a common theme.* Molecular and Cellular Endocrinology, 1998. **146**(1-2): p. 1-6.
35. Zhou, H., et al., *Osteoblasts directly control lineage commitment of mesenchymal progenitor cells through Wnt signaling.* Journal of Biological Chemistry, 2008. **283**(4): p. 1936-1945.
36. Van Staa, T.P., et al., *Use of Oral Corticosteroids and Risk of Fractures.* Journal of Bone and Mineral Research, 2000. **15**(6): p. 993-1000.
37. Ohnaka, K., et al., *Glucocorticoid suppresses the canonical Wnt signal in cultured human osteoblasts.* Biochemical and Biophysical Research Communications, 2005. **329**(1): p. 177-181.
38. O'Brien, C.A., et al., *Glucocorticoids act directly on osteoblasts and osteocytes to induce their apoptosis and reduce bone formation and strength.* Endocrinology, 2004. **145**(4): p. 1835-1841.
39. Canalis, E., et al., *Glucocorticoid-induced osteoporosis: pathophysiology and therapy.* Osteoporosis International: A Journal Established As Result Of Cooperation Between The European Foundation For Osteoporosis And The National Osteoporosis Foundation Of The USA, 2007. **18**(10): p. 1319-1328.
40. Amin, S., et al., *The comparative efficacy of drug therapies used for the management of corticosteroid-induced osteoporosis: A meta-regression.* Journal of Bone and Mineral Research, 2002. **17**(8): p. 1512-1526.
41. Rafacho, A., et al., *Glucocorticoid treatment and endocrine pancreas function: implications for glucose homeostasis, insulin resistance and diabetes.* Journal of Endocrinology, 2014. **223**(3): p. R49-R62.
42. Ruzzin, J., A.S. Wagman, and J. Jensen, *Glucocorticoid-induced insulin resistance in skeletal muscles: Defects in insulin signalling and the effects of a selective glycogen synthase kinase-3 inhibitor.* Diabetologia, 2005. **48**(10): p. 2119-2130.
43. Schakman, O., H. Gilson, and J.P. Thissen, *Mechanisms of glucocorticoid-induced myopathy.* Journal of Endocrinology, 2008. **197**(1): p. 1-10.
44. Van Raalte, D.H., D.M. Ouwens, and M. Diamant, *Novel insights into glucocorticoid-mediated diabetogenic effects: Towards expansion of therapeutic options?* European Journal of Clinical Investigation, 2009. **39**(2): p. 81-93.
45. Vander Kooi, B.T., et al., *The glucose-6-phosphatase catalytic subunit gene promoter contains both positive and negative glucocorticoid response elements.* Molecular Endocrinology, 2005. **19**(12): p. 3001-3022.
46. van Raalte, D.H., et al., *Acute and 2-week exposure to prednisolone impair different aspects of β-cell function in healthy men.* European Journal of Endocrinology, 2010. **162**(4): p. 729-735.

47. Ahrén, B., *Evidence that autonomic mechanisms contribute to the adaptive increase in insulin secretion during dexamethasone-induced insulin resistance in humans.* Diabetologia, 2008. **51**(6): p. 1018-1024.
48. Soliday, E., S. Grey, and M.B. Lande, *Behavioral Effects of Corticosteroids in Steroid-sensitive Nephrotic Syndrome.* Pediatrics, 1999. **104**(4): p. e51.
49. Bolanos, S.H., et al., *Assessment of mood states in patients receiving long-term corticosteroid therapy and in controls with patient-rated and clinician-rated scales.* Annals of Allergy, Asthma & Immunology, 2004. **92**(5): p. 500-505.
50. Fietta, P., P. Fietta, and G. Delsante, *Central nervous system effects of natural and synthetic glucocorticoids.* Psychiatry and Clinical Neurosciences, 2009. **63**(5): p. 613-622.
51. Brown, E.S., et al., *Hippocampal volume, spectroscopy, cognition, and mood in patients receiving corticosteroid therapy.* Biological Psychiatry, 2004. **55**(5): p. 538-545.
52. Schoepe, S., et al., *Glucocorticoid therapy-induced skin atrophy.* Experimental Dermatology, 2006. **15**(6): p. 406-420.
53. Wang, C., et al., *Dexamethasone influences FGF-induced responses in lens epithelial explants and promotes the posterior capsule coverage that is a feature of glucocorticoid-induced cataract.* Experimental Eye Research, 2013. **111**: p. 79-87.
54. Jobling, A.I. and R.C. Augusteyn, *What causes steroid cataracts? A review of steroid-induced posterior subcapsular cataracts.* Clinical and Experimental Optometry, 2002. **85**(2): p. 61-75.
55. Kersey, J.P. and D.C. Broadway, *Corticosteroid-induced glaucoma: a review of the literature.* Eye, 2006. **20**(4): p. 407-416.
56. Clark, A.R. and M.G. Belvisi, *Maps and legends: The quest for dissociated ligands of the glucocorticoid receptor.* Pharmacology and Therapeutics, 2012. **134**(1): p. 54-67.
57. Clark, A.R., *Anti-inflammatory functions of glucocorticoid-induced genes.* Molecular and Cellular Endocrinology, 2007. **275**(1-2): p. 79-97.
58. Shah, S., et al., *Roles for the Mitogen-activated Protein Kinase (MAPK) Phosphatase, DUSP1, in Feedback Control of Inflammatory Gene Expression and Repression by Dexamethasone.* Journal of Biological Chemistry, 2014. **289**(19): p. 13667-13679.
59. Ronchetti, S., G. Migliorati, and C. Riccardi, *GILZ as a Mediator of the Anti-Inflammatory Effects of Glucocorticoids.* Frontiers in Endocrinology, 2015. **6**(170).
60. Liu, X., et al., *Prednisolone-glucose derivative conjugate: Synthesis, biodistribution and pharmacodynamics evaluation.* Archiv der Pharmazie, 2012. **345**(12): p. 925-933.
61. Schiffelers, R.M., et al., *Liposome-encapsulated prednisolone phosphate inhibits growth of established tumors in mice.* Neoplasia, 2005. **7**(2): p. 118-127.
62. Anselmo, A.C., et al., *Exploiting shape, cellular-hitchhiking and antibodies to target nanoparticles to lung endothelium: Synergy between physical, chemical and biological approaches.* Biomaterials, 2015. **68**: p. 1-8.

63. NNI. [cited 2017 4 August]; Available from: https://www.nano.gov//nanotech-101/nanotechnology-facts.
64. ETPN. [cited 2017 4 August]; Available from: https://www.etp-nanomedicine.eu/public/about-nanomedicine/what-is-nanomedicine.
65. Hernán Pérez de la Ossa, D. *Nanomedicines: EMA experience and perspective*. in *EuroNanoForum* 2015.
66. Dolez, P.I., *Nanoengineering: Global Approaches to Health and Safety Issues*. Nanoengineering: Global Approaches to Health and Safety Issues. 2015. 1-706.
67. Thomas, R., et al., *Electrospun Polycaprolactone Membrane Incorporated with Biosynthesized Silver Nanoparticles as Effective Wound Dressing Material.* Applied Biochemistry and Biotechnology, 2015. **176**(8): p. 2213-2224.
68. Dreaden, E.C., et al., *The golden age: gold nanoparticles for biomedicine.* Chemical Society Reviews, 2012. **41**(7): p. 2740-2779.
69. Lohse, S.E. and C.J. Murphy, *Applications of Colloidal Inorganic Nanoparticles: From Medicine to Energy.* Journal of the American Chemical Society, 2012. **134**(38): p. 15607-15620.
70. Colilla, M., B. Gonzalez, and M. Vallet-Regi, *Mesoporous silica nanoparticles for the design of smart delivery nanodevices.* Biomaterials Science, 2013. **1**(2): p. 114-134.
71. Fernando, I.R., et al., *Esterase- and pH-responsive poly([small beta]-amino ester)-capped mesoporous silica nanoparticles for drug delivery.* Nanoscale, 2015. **7**(16): p. 7178-7183.
72. Tarn, D., et al., *Mesoporous Silica Nanoparticle Nanocarriers: Biofunctionality and Biocompatibility.* Accounts of Chemical Research, 2013. **46**(3): p. 792-801.
73. Gómez, D.M., S. Urcuqui-Inchima, and J.C. Hernandez, *Silica nanoparticles induce NLRP3 inflammasome activation in human primary immune cells.* Innate Immunity, 2017. **23**(8): p. 697-708.
74. Kiriyama, A., K. Iga, and N. Shibata, *Availability of polymeric nanoparticles for specific enhanced and targeted drug delivery.* Therapeutic Delivery, 2013. **4**(10): p. 1261-1278.
75. Crucho, C.I.C., *Stimuli-responsive polymeric nanoparticles for nanomedicine.* ChemMedChem, 2015. **10**(1): p. 24-38.
76. Deng, C., et al., *Biodegradable polymeric micelles for targeted and controlled anticancer drug delivery: Promises, progress and prospects.* Nano Today, 2012. **7**(5): p. 467-480.
77. Gref, R., et al., *The controlled intravenous delivery of drugs using PEG-coated sterically stabilized nanospheres.* Advanced Drug Delivery Reviews, 2012. **64**: p. 316-326.
78. Tomalia, D.A., A.M. Naylor, and W.A. Goddard Iii, *Starbust dendrimers: Molecular-level control of size, shape, surface chemistry, topology, and flexibility from atoms to macroscopic matter.* Angewandte Chemie - International Edition in English, 1990. **29**(2): p. 138-175.
79. Jang, W.-D., et al., *Bioinspired application of dendrimers: From bio-mimicry to biomedical applications.* Progress in Polymer Science, 2009. **34**(1): p. 1-23.

80. Crampton, H.L. and E.E. Simanek, *Dendrimers as drug delivery vehicles: non-covalent interactions of bioactive compounds with dendrimers.* Polymer International, 2007. **56**(4): p. 489-496.
81. Kolhar, P., et al., *Using shape effects to target antibody-coated nanoparticles to lung and brain endothelium.* Proceedings of the National Academy of Sciences of the United States of America, 2013. **110**(26): p. 10753-10758.
82. Duncan, R., S. Dimitrijevic, and E.G. Evagorou, *The role of polymer conjugates in the diagnosis and treatment of cancer.* S.T.P. Pharma Sciences, 1996. **6**(4): p. 237-263.
83. Bhadra, D., et al., *A PEGylated dendritic nanoparticulate carrier of fluorouracil.* International Journal of Pharmaceutics, 2003. **257**(1-2): p. 111-124.
84. Jevprasesphant, R., et al., *The influence of surface modification on the cytotoxicity of PAMAM dendrimers.* International Journal of Pharmaceutics, 2003. **252**(1-2): p. 263-266.
85. Kobayashi, H., et al., *Micro-MR angiography of normal and intratumoral vessels in mice using dedicated intravascular MR contrast agents with high generation of polyamidoamine dendrimer core: Reference to pharmacokinetic properties of dendrimer-based MR contrast agents.* Journal of Magnetic Resonance Imaging, 2001. **14**(6): p. 705-713.
86. Liu, Y., et al., *A double antigen bridging immunogenicity ELISA for the detection of antibodies to polyethylene glycol polymers.* Journal of Pharmacological and Toxicological Methods, 2011. **64**(3): p. 238-245.
87. Wan, X., et al., *Effect of protein immunogenicity and PEG size and branching on the anti-PEG immune response to PEGylated proteins.* Process Biochemistry, 2017. **52**(Supplement C): p. 183-191.
88. Date, A.A. and C.J. Destache, *A review of nanotechnological approaches for the prophylaxis of HIV/AIDS.* Biomaterials, 2013. **34**(26): p. 6202-6228.
89. Yoon, G., J.W. Park, and I.-S. Yoon, *Solid lipid nanoparticles (SLNs) and nanostructured lipid carriers (NLCs): recent advances in drug delivery.* Journal of Pharmaceutical Investigation, 2013. **43**(5): p. 353-362.
90. Beloqui, A., et al., *Nanostructured lipid carriers: Promising drug delivery systems for future clinics.* Nanomedicine: Nanotechnology, Biology and Medicine, 2016. **12**(1): p. 143-161.
91. Kraft, J.C., et al., *Emerging research and clinical development trends of liposome and lipid nanoparticle drug delivery systems.* Journal Of Pharmaceutical Sciences, 2014. **103**(1): p. 29-52.
92. Barenholz, Y., *Doxil® — The first FDA-approved nano-drug: Lessons learned.* Journal of Controlled Release, 2012. **160**(2): p. 117-134.
93. Moallem, E., et al., *A liposomal steroid nano-drug for treating systemic lupus erythematosus.* Lupus, 2016. **25**(11): p. 1209-1216.
94. Lobatto, M.E., et al., *Multimodal clinical imaging to longitudinally assess a nanomedical anti-inflammatory treatment in experimental atherosclerosis.* Mol Pharm, 2010. **7**(6): p. 2020-9.
95. McClements, D.J., *Nanoemulsion-based oral delivery systems for lipophilic bioactive components: Nutraceuticals and pharmaceuticals.* Therapeutic Delivery, 2013. **4**(7): p. 841-857.

96. Chuan, Y.P., et al., *Co-delivery of antigen and a lipophilic anti-inflammatory drug to cells via a tailorable nanocarrier emulsion.* Journal of Colloid and Interface Science, 2012. **368**(1): p. 616-624.
97. Tatham, L.M., S.P. Rannard, and A. Owen, *Nanoformulation strategies for the enhanced oral bioavailability of antiretroviral therapeutics.* Therapeutic Delivery, 2015. **6**(4): p. 469-490.
98. Schütz, C.A., et al., *Therapeutic nanoparticles in clinics and under clinical evaluation.* Nanomedicine, 2013. **8**(3): p. 449-467.
99. Benet, L.Z., *The role of BCS (biopharmaceutics classification system) and BDDCS (biopharmaceutics drug disposition classification system) in drug development.* Journal of Pharmaceutical Sciences, 2013. **102**(1): p. 34-42.
100. Junghanns, J.-U.A.H. and R.H. Müller, *Nanocrystal technology, drug delivery and clinical applications.* International Journal of Nanomedicine, 2008. **3**(3): p. 295-310.
101. Zhang, H., et al., *Formation and enhanced biocidal activity of water-dispersable organic nanoparticles.* Nature Nanotechnology, 2008. **3**(8): p. 506-511.
102. McDonald, T.O., et al., *Antiretroviral Solid Drug Nanoparticles with Enhanced Oral Bioavailability: Production, Characterization, and In Vitro-In Vivo Correlation.* Advanced Healthcare Materials, 2014. **3**(3): p. 400-411.
103. Giardiello, M., et al., *Accelerated oral nanomedicine discovery from miniaturized screening to clinical production exemplified by paediatric HIV nanotherapies.* Nature Communications, 2016. **7**.
104. McDonald, T.O., et al., *Multicomponent organic nanoparticles for fluorescence studies in biological systems.* Advanced Functional Materials, 2012. **22**(12): p. 2469-2478.
105. Katzer, T., et al., *Prednisolone-loaded nanocapsules as ocular drug delivery system: Development, in vitro drug release and eye toxicity.* Journal of Microencapsulation, 2014. **31**(6): p. 519-528.
106. Martin-Saldana, S., et al., *Otoprotective properties of 6alpha-methylprednisolone-loaded nanoparticles against cisplatin: In vitro and in vivo correlation.* Nanomedicine, 2016. **12**(4): p. 965-76.
107. Bruni, R., et al., *Ultrasmall polymeric nanocarriers for drug delivery to podocytes in kidney glomerulus.* Journal of Controlled Release, 2017. **255**: p. 94-107.
108. Hwang, J., et al., *Alpha-methylprednisolone conjugated cyclodextrin polymer-based nanoparticles for rheumatoid arthritis therapy.* Int J Nanomedicine, 2008. **3**(3): p. 359-71.
109. Banciu, M., et al., *Liposomal glucocorticoids as tumor-targeted anti-angiogenic nanomedicine in B16 melanoma-bearing mice.* J Steroid Biochem Mol Biol, 2008. **111**(1-2): p. 101-10.
110. Cittadino, E., et al., *MRI evaluation of the antitumor activity of paramagnetic liposomes loaded with prednisolone phosphate.* Eur J Pharm Sci, 2012. **45**(4): p. 436-41.
111. van der Valk, F.M., et al., *Prednisolone-containing liposomes accumulate in human atherosclerotic macrophages upon intravenous administration.* Nanomedicine, 2015. **11**(5): p. 1039-46.

112. van der Valk, F.M., et al., *Liposomal prednisolone promotes macrophage lipotoxicity in experimental atherosclerosis.* Nanomedicine, 2016. **12**(6): p. 1463-70.
113. FDA. *Inactive Ingredients Database*. 2017 [cited 2017 10 July]; Available from: https://www.fda.gov/Drugs/InformationOnDrugs/ucm113978.htm.
114. EMA. *ICH guideline Q3C (R6) on impurities: guideline for residual solvents*. 2016 [cited 2017 10 July]; Available from: http://www.ich.org/products/guidelines/quality/quality-single/article/impurities-guideline-for-residual-solvents.html.
115. Dressman, J.B., et al., *Dissolution testing as a prognostic tool for oral drug absorption: Immediate release dosage forms.* Pharmaceutical Research, 1998. **15**(1): p. 11-22.
116. Marques, M.R.C., R. Loebenberg, and M. Almukainzi, *Simulated biological fluids with possible application in dissolution testing.* Dissolution Technologies, 2011. **18**(3): p. 15-28.
117. Hanke, U., et al., *Commonly used nonionic surfactants interact differently with the human efflux transporters ABCB1 (p-glycoprotein) and ABCC2 (MRP2).* European Journal of Pharmaceutics and Biopharmaceutics, 2010. **76**(2): p. 260-268.
118. Crowe, A. and A.M. Tan, *Oral and inhaled corticosteroids: Differences in P-glycoprotein (ABCB1) mediated efflux.* Toxicology and Applied Pharmacology, 2012. **260**(3): p. 294-302.
119. Karssen, A.M., et al., *The role of the efflux transporter P-glycoprotein in brain penetration of prednisolone.* J Endocrinol, 2002. **175**(1): p. 251-60.
120. Junghanns, J.U.A.H. and R.H. Müller, *Nanocrystal technology, drug delivery and clinical applications.* International Journal of Nanomedicine, 2008. **3**(3): p. 295-309.
121. Kendall, R.A., et al., *Fabrication and in vivo evaluation of highly pH-responsive acrylic microparticles for targeted gastrointestinal delivery.* European Journal of Pharmaceutical Sciences, 2009. **37**(3–4): p. 284-290.
122. Kawakami, K., *Miscibility analysis of particulate solid dispersions prepared by electrospray deposition.* International Journal of Pharmaceutics, 2012. **433**(1–2): p. 71-78.
123. Van Den Hoven, J.M., et al., *Cyclodextrin as membrane protectant in spray-drying and freeze-drying of PEGylated liposomes.* International Journal of Pharmaceutics, 2012. **438**(1-2): p. 209-216.
124. Guada, M., et al., *Lipid nanoparticles enhance the absorption of cyclosporine A through the gastrointestinal barrier: In vitro and in vivo studies.* International Journal of Pharmaceutics, 2016. **500**(1–2): p. 154-161.
125. Wolfram, J., et al., *Safety of nanoparticles in medicine.* Current drug targets, 2015. **16**(14): p. 1671-1681.
126. Panariti, A., G. Miserocchi, and I. Rivolta, *The effect of nanoparticle uptake on cellular behavior: disrupting or enabling functions?* Nanotechnology, Science and Applications, 2012. **5**: p. 87-100.
127. Berridge, M.V., P.M. Herst, and A.S. Tan, *Tetrazolium dyes as tools in cell biology: New insights into their cellular reduction*, in *Biotechnology Annual Review*. 2005, Elsevier. p. 127-152.

128. Lee, M.-S., et al., *Intracellular ATP Assay of Live Cells Using PTD-Conjugated Luciferase.* Sensors (Basel, Switzerland), 2012. **12**(11): p. 15628-15637.
129. Hubatsch, I., E.G.E. Ragnarsson, and P. Artursson, *Determination of drug permeability and prediction of drug absorption in Caco-2 monolayers.* Nature Protocols, 2007. **2**(9): p. 2111-2119.
130. Kauffman, A., et al., *Alternative functional in vitro models of human intestinal epithelia.* Frontiers in Pharmacology, 2013. **4**(79).
131. Gohy, S.T., et al., *Chronic inflammatory airway diseases: The central role of the epithelium revisited.* Clinical and Experimental Allergy, 2016. **46**(4): p. 529-542.
132. Zhu, J. and W.E. Paul, *CD4 T cells: fates, functions, and faults.* Blood, 2008. **112**(5): p. 1557-1569.
133. Luzina, I.G., et al., *Regulation of inflammation by interleukin-4: A review of "alternatives".* Journal of Leukocyte Biology, 2012. **92**(4): p. 753-764.
134. Nelms, K., et al., *The IL-4 receptor: Signaling mechanisms and biologic functions*, in *Annual Review of Immunology*. 1999. p. 701-738.
135. Mahto, S.K., P. Chandra, and S.W. Rhee, *In vitro models, endpoints and assessment methods for the measurement of cytotoxicity.* Toxicology and Environmental Health Sciences, 2010. **2**(2): p. 87-93.
136. Schimpel, C., et al., *Development of an advanced intestinal in vitro triple culture permeability model to study transport of nanoparticles.* Molecular Pharmaceutics, 2014. **11**(3): p. 808-818.
137. Hillegass, J.M., et al., *Assessing nanotoxicity in cells in vitro.* Wiley interdisciplinary reviews. Nanomedicine and nanobiotechnology, 2010. **2**(3): p. 219-231.
138. Shen, Q., et al., *Modulating effect of polyethylene glycol on the intestinal transport and absorption of prednisolone, methylprednisolone and quinidine in rats by in-vitro and in-situ absorption studies.* Journal of Pharmacy and Pharmacology, 2008. **60**(12): p. 1633-1641.
139. Lin, I.C., et al., *Cellular transport pathways of polymer coated gold nanoparticles.* Nanomedicine: Nanotechnology, Biology and Medicine, 2012. **8**(1): p. 8-11.
140. Costanzo, M., et al., *Fluorescence and electron microscopy to visualize the intracellular fate of nanoparticles for drug delivery.* European Journal of Histochemistry, 2016. **60**(2): p. 107-115.
141. Zhao, F., et al., *Cellular uptake, intracellular trafficking, and cytotoxicity of nanomaterials.* Small, 2011. **7**(10): p. 1322-1337.
142. Wang, L., et al., *Nanomaterial induction of oxidative stress in lung epithelial cells and macrophages.* Journal of Nanoparticle Research, 2014. **16**(9).
143. Koranteng, R.D., et al., *Differential regulation of mast cell cytokines by both dexamethasone and the p38 mitogen-activated protein kinase (MAPK) inhibitor SB203580.* Clinical and Experimental Immunology, 2004. **137**(1): p. 81-87.
144. Min, B. and W.E. Paul, *Basophils and type 2 immunity.* Current Opinion in Hematology, 2008. **15**(1): p. 59-63.
145. Wolfram, J., et al., *The nano-plasma interface: Implications of the protein corona.* Colloids and Surfaces B: Biointerfaces, 2014. **124**: p. 17-24.

146. Dutta, D., et al., *Adsorbed proteins influence the biological activity and molecular targeting of nanomaterials.* Toxicological Sciences, 2007. **100**(1): p. 303-315.
147. Liptrott, N.J., et al., *Flow cytometric analysis of the physical and protein-binding characteristics of solid drug nanoparticle suspensions.* Nanomedicine, 2015. **10**(9): p. 1407-1421.
148. Wang, Y., et al., *Stability of nanosuspensions in drug delivery.* Journal of Controlled Release, 2013. **172**(3): p. 1126-1141.
149. Kroll, A., et al., *Interference of engineered nanoparticles with in vitro toxicity assays.* Archives of Toxicology, 2012. **86**(7): p. 1123-1136.
150. Siccardi, M., et al., *Towards a rational design of solid drug nanoparticles with optimised pharmacological properties.* J Interdiscip Nanomed, 2016. **1**(3): p. 110-123.
151. Martin, P., et al., *Mediation of in vitro cytochrome P450 activity by common pharmaceutical excipients.* Molecular Pharmaceutics, 2013. **10**(7): p. 2739-2748.
152. Hofkens, W., et al., *Safety of glucocorticoids can be improved by lower yet still effective dosages of liposomal steroid formulations in murine antigen-induced arthritis: Comparison of prednisolone with budesonide.* International Journal of Pharmaceutics, 2011. **416**(2): p. 493-498.
153. Ulrich, B., et al., *Pharmacokinetics/pharmacodynamics of ketoconazole-prednisolone interaction.* Journal of Pharmacology and Experimental Therapeutics, 1992. **260**(2): p. 487-490.
154. English, J., M. Dunne, and V. Marks, *Diurnal variation in prednisolone kinetics.* Clinical Pharmacology and Therapeutics, 1983. **33**(3): p. 381-385.
155. Lai, S.K., Y.Y. Wang, and J. Hanes, *Mucus-penetrating nanoparticles for drug and gene delivery to mucosal tissues.* Adv Drug Deliv Rev, 2009. **61**(2): p. 158-71.
156. Shahbazi, M.A. and H.A. Santos, *Improving oral absorption via drug-loaded nanocarriers: absorption mechanisms, intestinal models and rational fabrication.* Curr Drug Metab, 2013. **14**(1): p. 28-56.
157. Tatham, L.M., S.P. Rannard, and A. Owen, *Nanoformulation strategies for the enhanced oral bioavailability of antiretroviral therapeutics.* Ther Deliv, 2015. **6**(4): p. 469-90.
158. Shibasaki, H., et al., *Simultaneous determination of prednisolone, prednisone, cortisol, and cortisone in plasma by GC–MS: Estimating unbound prednisolone concentration in patients with nephrotic syndrome during oral prednisolone therapy.* Journal of Chromatography B, 2008. **870**(2): p. 164-169.
159. David, C.A.W., A. Owen, and N.J. Liptrott, *Determining the relationship between nanoparticle characteristics and immunotoxicity: Key challenges and approaches.* Nanomedicine, 2016. **11**(11): p. 1447-1464.
160. Lobatto, M.E., et al., *Pharmaceutical development and preclinical evaluation of a GMP-grade anti-inflammatory nanotherapy.* Nanomedicine: Nanotechnology, Biology, and Medicine, 2015. **11**(5): p. 1133-1140.
161. Bruinen, A.L., et al., *Mass Spectrometry Imaging of Drug Related Crystal-Like Structures in Formalin-Fixed Frozen and Paraffin-*

Embedded Rabbit Kidney Tissue Sections. Journal of The American Society for Mass Spectrometry, 2016. **27**(1): p. 117-123.
162. Baris, H.E., et al., *The effect of systemic corticosteroids on the innate and adaptive immune system in children with steroid responsive nephrotic syndrome.* European Journal of Pediatrics, 2016. **175**(5): p. 685-693.
163. Raja, K., et al., *Use of a low-dose prednisolone regimen to treat a relapse of steroid-sensitive nephrotic syndrome in children.* Pediatric Nephrology, 2017. **32**(1): p. 99-105.
164. Lee, V.W., et al., *Adriamycin nephropathy in severe combined immunodeficient (SCID) mice.* Nephrol Dial Transplant, 2006. **21**(11): p. 3293-8.
165. Guo, J., et al., *Protective effects of mesenchymal stromal cells on adriamycin-induced minimal change nephrotic syndrome in rats and possible mechanisms.* Cytotherapy, 2014. **16**(4): p. 471-84.
166. Simic, I., M. Tabatabaeifar, and F. Schaefer, *Animal models of nephrotic syndrome.* Pediatric Nephrology, 2013. **28**(11): p. 2079-2088.
167. Chen, K.H., et al., *Nanoparticle distribution during systemic inflammation is size-dependent and organ-specific.* Nanoscale, 2015. **7**(38): p. 15863-15872.
168. Gamboa, J.M. and K.W. Leong, *In vitro and in vivo models for the study of oral delivery of nanoparticles.* Advanced Drug Delivery Reviews, 2013. **65**(6): p. 800-810.
169. Machhar, B.K., et al., *Biological, pharmaceutical and analytical considerations of caco-2 monolayer.* Research Journal of Pharmacy and Technology, 2013. **6**(4): p. 336-344.
170. Paget, V., J.A. Sergent, and S. Chevillard, *Nano-silicon dioxide toxicological characterization on two human kidney cell lines.* Journal of Physics: Conference Series, 2011. **304**(1).
171. Schimpel, C., et al., *Development of an advanced intestinal in vitro triple culture permeability model to study transport of nanoparticles.* Mol Pharm, 2014. **11**(3): p. 808-18.
172. Lee, V.W.S., et al., *Adriamycin nephropathy in severe combined immunodeficient (SCID) mice.* Nephrology Dialysis Transplantation, 2006. **21**(11): p. 3293-3298.
173. Lobatto, M.E., et al., *Pharmaceutical development and preclinical evaluation of a GMP-grade anti-inflammatory nanotherapy.* Nanomedicine: Nanotechnology, Biology and Medicine, 2015. **11**(5): p. 1133-1140.
174. Wicki, A., et al., *Large-scale manufacturing of GMP-compliant anti-EGFR targeted nanocarriers: Production of doxorubicin-loaded anti-EGFR-immunoliposomes for a first-in-man clinical trial.* International Journal of Pharmaceutics, 2015. **484**(1): p. 8-15.